



January 2023

Spacesuit Hard Upper Torso Assembly: Development Of Fit Metrics And Customized Design Frameworks

Will J. Green

[How does access to this work benefit you? Let us know!](#)

Follow this and additional works at: <https://commons.und.edu/theses>

Recommended Citation

Green, Will J., "Spacesuit Hard Upper Torso Assembly: Development Of Fit Metrics And Customized Design Frameworks" (2023). *Theses and Dissertations*. 5301.
<https://commons.und.edu/theses/5301>

This Dissertation is brought to you for free and open access by the Theses, Dissertations, and Senior Projects at UND Scholarly Commons. It has been accepted for inclusion in Theses and Dissertations by an authorized administrator of UND Scholarly Commons. For more information, please contact und.common@library.und.edu.

**Spacesuit Hard Upper Torso Assembly:
Development of Fit Metrics and Customized Design Frameworks**

By

Will J Green

B.S., Mechanical Engineering, Drexel University (2017)
M.S., Mechanical Engineering, University of Delaware (2019)

A Dissertation

Submitted to the Department of Aerospace Sciences
in partial fulfillment of the requirements
for the Degree of

DOCTOR OF PHILOSOPHY IN AEROSPACE SCIENCES

At the

UNIVERSITY OF NORTH DAKOTA

Grand Forks, North Dakota

August 4

2023

Copyright Page

APPROVAL

This dissertation, submitted by Will J. Green in partial fulfillment of the requirements for the Degree of Philosophy in Aerospace Science from the University of North Dakota, has been read by the Faculty Advisory Committee under whom the work has been done and is hereby approved.

Dr. Pablo de León,
Professor in Department of Aerospace Sciences, UND
Ph.D. Committee Chair

Dr. Keith Crisman,
Professor in Department of Aerospace Sciences, UND
Member, Ph.D. Committee

Dr. Kavya Manyapu
Professor in Department of Aerospace Sciences, UND
Member, Ph.D. Committee

Dr. Jesse Rhoades
Professor in Department of Biomedical Sciences, UND
Member, Ph.D. Committee

Dr. Han Kim
Research Scientist, NASA Johnson Space Center
Member, Ph.D. Committee

This dissertation is being submitted by the appointed advisory committee as having met all of the requirements of the School of Graduate Studies at the University of North Dakota and is hereby approved.

Grant McGimpsey, Dean of the School of Graduate Studies

Date

PERMISSION

Title Spacesuit Hard Upper Torso Assembly:
 Development of Fit Metrics and Customized Design Frameworks

Department Aerospace Science

Degree Doctor of Philosophy

In presenting this or dissertation in partial fulfillment of the requirements for a graduate degree from the University of North Dakota, I agree that the library of this University shall make it freely available for inspection. I further agree that permission for extensive copying for scholarly purposes may be granted by the professor who supervised my dissertation work or, in his absence, by the Chairperson of the department or the dean of the School of Graduate Studies. It is understood that any copying or publication or other use of this dissertation or part thereof for financial gain shall not be allowed without my written permission. It is also understood that due recognition shall be given to me and to the University of North Dakota in any scholarly use which may be made of any material in my dissertation.

Will Green
August 4th, 2023

ABSTRACT

The Hard Upper Torso (HUT) of the spacesuit pressure garment is a central component of a spacesuit, enclosing the upper body and connecting with the shoulder joints, bearings, helmet, hatch, and waist-brief-hip components. The shape and positioning of the HUT and its connected components are critical for ensuring comfort, range of motion, field of view, and minimizing astronaut injury risk.

This dissertation aims to build upon previous work on spacesuit sizing and develop new spacesuit fit metrics. Motion-tracking technology has been utilized to define the reach envelope and range of motion for test subjects wearing a HUT. Subjective surveys have also been conducted to evaluate suit mobility, feature alignment, indexing, and discomfort. These tools can be adapted to investigate the effects of HUT sizing, leading to the proposal of new metrics ideal for the fit and mobility of HUT based on these technologies.

Additive manufacturing can be employed to create custom spacesuit hardware with minimal additional manufacturing steps. This technique enables efficient testing and benchmarking of a wide variety of HUT prototypes. With the development of fit and performance metrics, it becomes logical to utilize these metrics to design optimally sized HUT geometry.

The above goals were pursued through the following activities:

1. Define two separate HUT design frameworks: The first framework will result in an optimally distributed discreet HUT sizing system, while the second will establish a framework for the rapid prediction and design of customized HUTs.
2. Investigate the subjective effect of HUT customization on HUT fitment using a subjective fit survey, demonstrating the benefits of HUT customization.
3. Explore the effect of HUT customization using human in-the-loop testing, including range of motion and reach envelope analyses, highlighting the benefits of HUT customization on suited mobility.
4. Confirm the preliminary feasibility of 3D printed HUTs through stress analysis of virtual HUT prototypes using a range of pressures, shell thicknesses, and candidate materials.

ACKNOWLEDGEMENTS

Funding for this research was partially provided by NASA EPSCoR Grant ND-80NSSC20M0230 "Development of an Advanced Planetary Mobility Spacesuit using Advanced Additive Manufacturing Design and Techniques" Warren Ruemmele, NASA Technical Monitor.

Lab assistance provided by UND's High-Performance Computing Lab and the Bi-PED Lab

Informal assistance provided by JSC's Anthropometry and Biomechanics Facility

Dedication:

I dedicate this dissertation to the individuals whose unwavering support and invaluable contributions made this journey possible:

To the extraordinary friends and the nurturing community at the University of North Dakota's Human Spaceflight Laboratory, your camaraderie and encouragement time at UND beyond measure. The moments of collaboration and shared passion for exploration will forever hold a special place in my heart.

I extend my sincerest thanks to Professor de Leon for entrusting me with the opportunity to work in his laboratory. Your guidance and wisdom have opened countless doors of knowledge and growth, propelling me toward new heights in my academic pursuits.

Gratitude also goes to Dr. Han Kim, whose mentorship provided me with an invaluable toolbox of techniques and skills that have been woven into the fabric of this work. Your dedication to your work and willingness to share your knowledge has been transformative.

Finally, to my parents, your unwavering support and unconditional love have been the bedrock of my journey. Your belief in me and your sacrifices have given me the strength and determination to complete this work, and I am forever grateful for the values you instilled in me.

This dissertation stands as a testament to the collective efforts of these exceptional individuals, each of whom played a vital role in shaping both the work and the person I have become.

With heartfelt gratitude,

Will Green

TABLE OF CONTENTS

INTRODUCTION	15
1.1. <i>The Next Era of Spacesuits</i>	15
1.2. <i>EVA Spacesuits</i>	15
1.2.1. General EVA Spacesuit Design Considerations	16
1.3. <i>Spacesuit Torsos</i>	18
1.3.1. Spacesuit Torso Interfaces	19
1.3.2. Spacesuit Entry methods	22
1.3.3. Padding	25
1.4. <i>Microgravity Spacesuit Design Considerations</i>	25
1.4.1. The EMU	26
1.4.2. EMU Sizing	26
1.4.3. Scye Bearing Issues	27
1.4.4. Tasks	28
1.4.5. Work and Reach Envelope	29
1.5. <i>Planetary Spacesuit Design Considerations</i>	30
1.5.1. Historical and Developmental Planetary Spacesuits	30
1.5.2. Apollo	30
1.5.3. Apollo Application Spacesuits	31
1.5.4. Mark III, Z Series & xEMU Spacesuits	31
1.5.5. Contractor Suits	32
1.6. <i>Planetary EVA Activities</i>	32
1.6.1. Work and Reach Envelope and Field of View.....	33
1.6.2. Ambulation	34
1.6.3. Lunar Conditions	34
1.6.4. Martian Conditions	36
1.7. <i>Anthropometry</i>	37
1.7.1. NASA’s Spacesuit Sizing Requirements	38
1.8. <i>Garment Sizing</i>	39
1.9. <i>A Changing Astronaut Population</i>	40
SPACESUIT DESIGN FRAMEWORK DEVELOPMENT	42
2.1. <i>HUT Design Frameworks</i>	42
2.2. <i>Issues of Anthropomorphic Suit Design</i>	42
2.2.1. Target Population Definition.....	42
2.2.2. Data Sources: CAESAR Dataset	44
2.2.3. Principal Component Analysis and Torso Shape Analysis	44
2.3. <i>Selection of Optimal Entry Method</i>	45
2.3.1. Zipper Entry Method.....	46
2.3.2. Diagonal Entry Method	47
2.3.3. Waist Entry Method	47
2.3.4. Hatch Entry Method	47
2.3.5. Dual Planar Entry Method	48
2.3.6. Entry Method Selection Process and Criteria	48
2.4. <i>HUT Interface and Architecture Definition</i>	49
2.4.1. HUT Interface Definitions	50
2.4.2. Scye Bearing Selection	50
2.4.3. Helmet Size Selection.....	51
2.4.4. EVAA Size Selection.....	52
2.4.5. Hatch Geometry Selection	53

2.5.	<i>Design Methods</i>	53
2.5.1.	Reconfigurable HUT Model.....	53
2.5.2.	Torso Shape to HUT Shape Model	55
2.5.3.	Clustering Analysis	55
2.5.4.	HUT Shape Dataset	56
2.5.5.	Historical HUT Fit Rules.....	57
2.5.6.	HUT Space Model	58
2.5.7.	Standard HUT Design Framework	58
2.5.8.	Optimization of a Standard HUT System Size Distribution.....	59
2.5.9.	Method for Generating Standard HUTs.....	60
2.5.10.	Custom HUT Design Framework	60
2.6.	<i>Results</i>	61
2.6.1.	Implementation of the Standard and Custom Design Frameworks.....	61
2.6.2.	Design Framework Limitations	62
DESIGN EVALUATION 1: SUBJECT FIT SURVEY		63
3.1.	<i>Study Goals</i>	63
3.2.	<i>State of the Art: Spacesuit Fit Assessment</i>	63
3.2.1.	Feature Alignment	63
3.2.2.	Discomfort	65
3.2.3.	Indexing	65
3.3.	<i>Assessment Methods</i>	66
3.4.	<i>Results</i>	67
3.5.	<i>Discussion</i>	70
3.6.	<i>Conclusion</i>	72
DESIGN EVALUATION 2: MOBILITY TESTING		73
4.1.	<i>Study Goals</i>	73
4.2.	<i>Methods</i>	73
4.2.1.	Motion Capture System	73
4.2.2.	Protocol 1: Range of Motion.....	75
4.2.3.	Protocol 2: Reach Envelop	76
4.3.	<i>Results</i>	80
4.3.1.	Results 1: Range of Motion Results	80
4.3.2.	Results 2: Reach Envelop Results.....	82
4.4.	<i>Discussion</i>	84
4.4.1.	Ranges of Motion.....	84
4.4.2.	Reach Envelops	84
DESIGN EVALUATION 3: STRESS ANALYSIS BY FINITE ELEMENT MODELING		86
5.1.	<i>Goals of this Study</i>	86
5.2.	<i>State of the Art</i>	86
5.2.1.	Fused Filament Fabrication.....	87
5.2.2.	Multi-Material Printing	87
5.2.3.	Selective Laser Sintering	88
5.2.4.	In-situ materials sourcing.....	89
5.2.5.	Metal 3D Printing	89
5.2.6.	Spacesuit Structures	90
5.2.7.	Design of 3D Printed Bending Elements	91
5.2.8.	Design of a 3D Printed Glove Quick Disconnect.....	92
5.2.9.	Design of a 3D Printed Spacesuit Arm Assembly	93
5.2.10.	Design and construction of the NDX-3 and NDX-4.....	94
5.3.	<i>Methods</i>	96
5.3.1.	HUT Construction.....	96
5.3.2.	Material Selection	98

5.3.3.	Stress Requirements	99
5.3.4.	SolidWorks FEA	100
5.4.	<i>Results</i>	101
5.5.	<i>Discussion</i>	104
5.5.1.	Future Optimization.....	104
5.5.2.	Sizing of 3D Printed Spacesuits	104
5.5.3.	Barriers to 3D printing Spacesuits.....	105
CONCLUSION		106
6.1.	<i>The Next Generation of Spacesuit Torsos</i>	106
6.2.	<i>HUT Design Frameworks</i>	107
6.3.	<i>Subject Fit Survey</i>	107
6.4.	<i>Mobility Testing</i>	107
6.5.	<i>3D Printed Spacesuits</i>	108
6.6.	<i>Next steps in Spacesuit HUT Design</i>	108
6.7.	<i>Next Steps in 3D Printed Spacesuits</i>	108
BIBLIOGRAPHY		110
APPENDIX 1: HARD UPPER TORSO FIT RULES		116
APPENDIX 2: SUBJECTIVE FIT SURVEY BASIS		117
APPENDIX 3: SUBJECTIVE FIT SURVEY USED FOR HUT EVALUATION		119
APPENDIX 4: RANGE OF MOTION RAW DATA		120
APPENDIX 5: RANGE OF MOTION RAW DATA		122
APPENDIX 6: HUT PRESSURIZATION FEA RESULTS		124

TABLE OF FIGURES

Figure 1.2.-1. Spacesuits Type Examples, A: Shuttle Crew Escape Launch and Entry Spacesuit, B: Shuttle EMU EVA Spacesuit, C: Apollo A7-LA Hybrid Spacesuit configured in an EVA Configuration.....	16
Figure 1.2.1.-1. Effects of Gravity on Posture and Anthropometry. A: Effect of gravity on neutral resting posture, B: Effect of lunar gravity on height (Thornton, Hoffler, & Rummel, 1974)18	18
Figure 1.3.-1. Spacesuit Torsos, A: A7L-B Soft Torso Spacesuit, B: NDX-1 Hard Upper Torso Spacesuit, C: Morphing Upper Torso.....	19
Figure 1.3.1.-1. xEMU Hard Upper Torso, with labeled interfaces	20
Figure 1.3.1.-2. Effect of entry method on spacesuit torso shape, A: NDX-2AT, rear entry hatch spacesuit, B: NDX-1, dual planar spacesuit	21
Figure 1.3.1.-3. Additional components attached to spacesuit torsos, A: AX-5 spacesuit with air and water connectors visible, B: Shuttle EMU, PLSS outlined in green, C: Apollo A7-LA Outer layer Cutaway Exhibit	22
Figure 1.3.2.-1. Suitport patent line art showing an EVA access facility with an installed spacesuit. A crewmember dons the suit via the rear entry hatch (United States of America Patent No. US4842224A, 1989).....	24
Figure 1.3.2.-2. Alternative suit entry methods, [Left] Mercury spacesuit, with spiral zipper entry [Middle] SK-1 Soviet training spacesuit, with a neck entry method [Right] Shuttle EMU, with a waist entry method.....	25
Figure 1.4.2.-1. Shuttle EMU Sizing Chart (Harris, 2001).....	27
Figure 1.4.3.-1. [Above] Sonny Carter Neutral Buoyancy Laboratory, [Below] Rashes and bruises caused by a hard contact with the interior of the EMU during NBL training exercises. (Williams & Johnson, 2003).....	28
Figure 1.4.5.-1. EMU Work Envelope Visualization (Griffin, Howard, Rajulu, & Smitherman, 2009).....	30
Figure 1.6.-1. Apollo Geology Tools.....	33
Figure 1.6.1.-1. A: Planetary EVA Suit Work Envelope Visualization	33
Figure 1.6.2.-1. Waist-Brief-Hip Components of the Mark III EVA Spacesuit Prototype	34
Figure 1.6.3.-1. A: Apollo Astronaut in the Lunar Excursion Module with visible dust contamination, B: Lunar Dust Simulant.....	35
Figure 1.7.-1. [Left] Davinci’s Vitruvian Man [Right] Corbusier’s Modular Man.....	38
Figure 1.8.-1. [Left] Glove Sewing Patterns [Right] Assembled Glove.....	39
Figure 2.2.1.-1. Example of stacking effects of anthropometry percentile cutoffs	43
Figure 2.3.-1. Spacesuit Entry Methods, A: Zipper entry method, B: Diagonal entry method, C: Hatch entry method, D: Waist entry method, E: Dual planar entry method.	46
Figure 2.4.-1. Skeletonized HUT Mockup with Additional Hardware Mockups and Bearings Installed.	50
Figure 2.4.2.-1. Scye Bearing	51
Figure 2.4.4.-1. EVAAs A: xEMU EVVA prototype B: Mockup EVVA used for HITL testing of HUT mockups.....	52
Figure 2.4.5.-1. Various rear entry hatch geometries (de Leon & Harris, 2009).....	53
Figure 2.5.1.-1. HUT Geometry Morphing Example. [Left] Base HUT Geometry [Middle] HUT Geometry post morphing [Right] Final HUT Geometry	54

Figure 2.5.1.-2. HUT Interstitial and Interface Geometry Morphing Example. <i>[Left] Skeletonized Interstitial HUT Geometry [Middle] HUT Interface Geometry [Right] Combined Interstitial and Interface Geometry</i>	55
Figure 2.5.3.-1. Torso Shape Principal Component Space. <i>Green: Caesar Database Subjects, Blue: Affinity Cluster Exemplars, Red: Boundary Mannequin Datapoints, Orange: Torsos Used to Generate Standard HUT Sizes</i>	56
Figure 2.5.5.-1. Examples of different opinions of optimal chest/HUT contact A: Minimal contact, B: significant contact	58
Figure 2.5.8.-1. Standard HUT Size Selection Process, K-means vs. geometric segmentation ...	60
Figure 2.6.1.-1. Scan Processing. A: Test subject, B: 3D scan data, C: Ho-model deformed to fit 3D scan data.....	62
Figure 3.2.1.-1. Demonstration of typical scye bearing orientation for rear entry hatch spacesuits.	64
Figure 3.2.1.-2. Location of waist interface on a rear entry suit.....	65
Figure 3.3.-1. A: Illustration of sweeping arm motions for reach envelope estimations, including side-to-side and up-down extremes, B: Right arm reach envelope hand traces, with the red trace representing standard HUT condition and blue trace custom HUT condition. C: Reach envelopes abstracted from the hand motion traces. Red envelope: standard HUT condition. Blue envelope: custom HUT condition.	67
Figure 3.3.-2. Subjective spacesuit fit survey, A: Discomfort survey field, B: Feature alignment survey field, C: Indexing survey field	67
Figure 3.4.-1. Percent of subject responses for scye bearing-shoulder feature alignment, helmet-head feature alignment, and shoulder discomfort.....	70
Figure 3.5.-1. Common HUT sizing issues. A: head contacting with the top of the helmet due to poor vertical helmet-scye distancing. B: chin contacting with the neck ring due to poor vertical helmet-scye distancing. C: chin contacting with the neck ring due to poor horizontal helmet-scye distancing. D: head contact with the top of the helmet due to poor horizontal helmet-scye distancing.	71
Figure 4.2.1.-1. BiPED Laboratory VICON Motion Capture Volume.....	74
Figure 4.2.1.-2. IR Motion Capture Tracker Plates. <i>[Left] suited tracker system [Right] shirt sleeve tracker system.</i>	75
Figure 4.2.3.-1. Single Hand Reach Envelope Visualization	77
Figure 4.2.3.-2. Full Body Reach Envelope Visualization of the EMU, While Using ISS Foot Restraint (Kim, et al., 2019)	78
Figure 4.2.3.-3. Reach Envelope Mapping Technique. [Top] vertical and horizontal sweeping motions used to generate reach envelopes, (Abercromby, Thaxton, Onady, & Rajulu, 2006) [Bottom Left] recorded hand sweeps [Bottom Right] resultant reach envelopes.....	79
Figure 4.2.3.-4. Reach Envelope Measuring Technique. [Top Left] Single hand reach envelope width and height, [Top Right] Single hand reach envelope depth definition, [Bottom Left] Double hand reach envelope width and height definition [Bottom Right] Double hand reach envelope depth definition	80
Figure 5.2.-1. 3D Printed Mockup Process. [Left] CAD geometry of skeletonized HUT mockup [Right] 3D Printers used to fabricate HUT mockups.	87
Figure 5.2.5.-1. 3D Printing in Space Capabilities. <i>[Left] first object 3D printed in space, a small ratchet tool [Right] 3D printed titanium glove disconnect part</i>	90

Figure 5.2.7.-1. 3D Printed Flexible Bellows Assembly Mobility Demonstration, Pressurized to 4.3 PSI 92

Figure 5.2.7.-2. Bellows Assembly [Left] flexible bellows component as [Right] assembled bellows assembly. 92

Figure 5.2.2.-1. 3D Printed Glove Disconnects. [Left] updated glove disconnect [Right] original bayonet type glove disconnect 93

Figure 5.2.4.-1. Spacesuit Arm Assembly Design Evolution. [Left] 1st generation 3D printed spacesuit arm assembly [Right] 2nd generation 3D printed spacesuit arm assembly. 94

Figure 5.2.7.-1. NDX-3 3D Printed Spacesuit Prototype 95

Figure 5.3.1.-1. 3D Printed HUTs. [Left] custom sized NDX-4 HUT, featuring a rear entry hatch [Right] NDX-3 HUT, featuring a dual planar entry method..... 95

Figure 5.3.4.-1. HUT FEA Visualization. [Left] FEA boundary conditions, red arrows show pressure load [Right] blue geometry shows rigid plate geometry integrated into the HUT to replicate the plug loads experienced on HUT interfaces 101

Figure 5.4.-2. 4mm Thick PLA HUT FEA Results. [Left] 4.3 PSI [Middle] 6.2 PSI [Right] 8.2 PSI 103

Figure 5.4.-3. Highest Stress Cases for PEEK and Aluminum HUTs. [Left] PEEK 4mm HUT at 8.23 [Right] Aluminum 4mm HUT at 8.23 PSI 103

Table 5.4.-2. Polymer Material Characteristics (Material Property Database, 2023)..... 103

Figure 6.1.-1. Conceptual Design of a Dual Planar 3D Printed Spacesuit 106

TABLE OF Equations

Equation 5.2.7.-1. _____ 91

Equation 5.4.-1. _____ 102

List of Acronyms

ABF	= Anthropometry and Biomechanics Facility
ABS	= Acrylonitrile Butadiene Styrene
AxEMU	= Axiom Extravehicular Mobility Unit
ANSUR	= Anthropometric Survey of US Army Personnel
BiPED	= University of North Dakota's BiPED Laboratory
CAD	= Computer-Aided Design
CAESAR	= Civilian American and European Surface Anthropometry Resource
DCU:	= Display and Control Unit
EMU	= Extravehicular Mobility Unit
EVA	= Extravehicular Activity
EVAA	= Extravehicular Visor Assembly
FFF	= Fused Deposition Modeling
FEA	= Finite Element Analysis
FFF	= Fused Filament Fabrication
HSFL	= University of North Dakota's Human Spaceflight Laboratory
HUT	= Hard Upper Torso
ICP	= Iterative Closest Point
IMU	= Inertial Measurement Unit
ISRU	= In-Situ Resource Utilization
ISS	= International Space Station
IR	= Infra-Red
JSC	= Johnson Space Center
LCVG	= Liquid Cooling and Ventilation Garment
LTA	= Lower Torso Assembly
MPII	= Max
NASA	= National Aeronautics and Space Administration
NBL	= Neutral Buoyancy Laboratory
NDX	= North Dakota experimental
OES	= Orbital Extravehicular Spacesuit
PC	= Principal Component
PCA	= Principal Component Analysis
PE	= Polyethylene
PEEK	= Poly Ether Ether Ketone
PGA	= Pressure Garment Assembly
PLA	= Polylactic Acid
PLSS	= Portable Life Support System
PP	= Polypropylene
PSI	= Pounds per Square Inch
RBF	= Radial Basis Algorithm
RE	= Reach Envelope
ROM	= Range of Motion
SSA	= Spacesuit Assembly
SSAA	= Spacesuit Arm Assembly
SLS	= Selective Laser Sintering
TPU	= Thermoplastic Polyurethane
UHMWPE	= Ultra High Molecular Weight Polyethylene
UV	= Ultraviolet
xEMU	= Exploration Extravehicular Mobility unit

Introduction

“Of course, Apollo was the god who carried the fiery sun across the sky in a chariot. But beyond that, how would you carry fire? Carefully, that's how with lots of planning and at considerable risk. It is a delicate cargo, as valuable as moon rocks, and the carrier must always be on his toes lest it spill. I carried the fire for six years, and now I would like to tell you about it, simply and directly as a test pilot must, for the trip deserves the telling.”

– *Michael Collins.*

1.1. The Next Era of Spacesuits

The next era of space exploration will see humans return to the Moon for extended durations. These missions will pave the way for future Martian missions. Extended planetary exploration missions need advanced surface exploration equipment, including spacesuits. These spacesuits will see frequent use, performing complex planetary EVAs by an increasingly diverse astronaut population. These spacesuits will benefit from advanced sizing systems, including custom sizing. One of the critical areas for spacesuit sizing is the torso. The torso of the spacesuit connects to many different components. The location and orientation of these components are critical for spacesuit fit, comfort, and mobility.

1.2. EVA Spacesuits

Astronauts wear spacesuits during the most dangerous phases of a space mission. Different phases present different dangers and operating environments to the astronaut. Intra-vehicular activity (IVA) or launch and entry spacesuits mitigate the increased risk seen during launch and re-entry of the spacecraft to help insulate the astronaut from the increased temperature of the spacecraft interior caused by atmospheric re-entry, provide some padding from the vibration and shock of landing, and provide a breath-able atmosphere should the spacecraft depressurize. Designers create these suits with minimal mobility, as the astronauts will only need to be able to reach and manipulate their controls while using this type of spacesuit. Due to the minimal mobility requirements, these launch and re-entry suits are comparatively form-fitting and lightweight (Figure 1.2.-1. A). Life support functions such as atmospheric conditioning and heat rejection systems are typically integrated into the spacecraft systems and interfaced with the suit through an umbilical system (Thomas & McMann, 2012).

When an astronaut leaves the protected environment inside the spacecraft, station, lander, or rover to work outside, this is called an Extra-Vehicular Activity. EVAs require the astronaut to operate in extreme space conditions to perform complex tasks such as deploying and repairing equipment. EVA spacesuits require increased mobility as the astronaut must translate to work

areas and operate complex tools and equipment. This mobility has historically been accomplished through rotary bearings and complex mobility joints, adding bulk and mass to the spacesuit (Ayrey, 2020), (Harris, 2001) (Figure 1.2.-1. B). During early EVAs, spacecraft-integrated systems drove life support functions. As later EVAs became increasingly complex, this life support functionality was built into the spacesuit system through a Portable Life Support System (PLSS), allowing for the autonomous operation of the suit separate from the spacecraft. While on an EVA, the astronaut will experience the thermal extremes of space. The suit's outer layer must be insulated to prevent overheating or cooling. In some cases, specific regions of the suit, such as the inside of gloves, are actively heated for comfort. The increased mobility, PLSS, and thermal insulation of EVA suits result in bulkier, more massive suit systems than launch and re-entry spacesuits (Harris, 2001).

Astronauts can use hybrid spacesuits for launch, re-entry, and EVA mission segments. These spacesuits have the benefit of removing the need for two spacesuit systems but often result in a compromise between the two sets of requirements (Figure 1.2.-1. C).

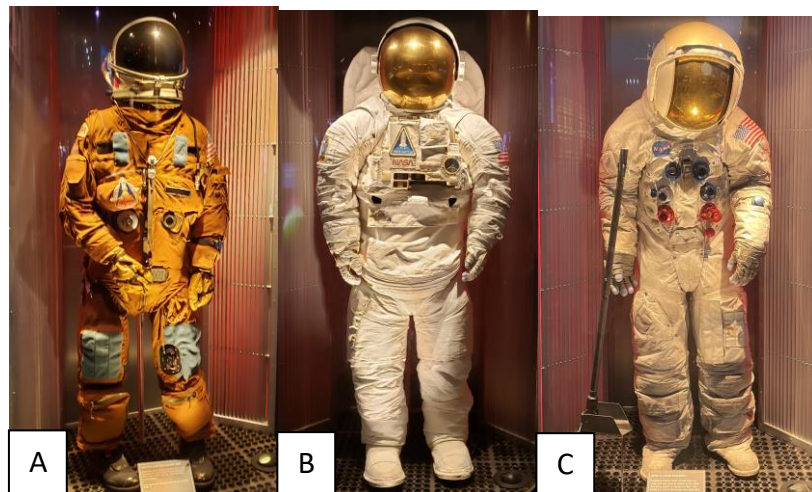


Figure 1.2.-1. Spacesuits Type Examples, A: Shuttle Crew Escape Launch and Entry Spacesuit, B: Shuttle EMU EVA Spacesuit, C: Apollo A7-LA Hybrid Spacesuit configured in an EVA Configuration

1.2.1. General EVA Spacesuit Design Considerations

For a spacesuit to be functional, the wearer must be able to move enough to complete their tasks. In addition, EVAs can last anywhere from 6-8 hours (Gast & Moore, 2011). As such, suits should provide maximum mobility to allow astronauts to work for that duration as efficiently as possible.

The operating environment is also a factor in spacesuit design. For example, for planetary missions, it may be beneficial to include a suit port into the suit's design to mitigate regolith issues on the interior habitable volume of the habitat (United States of America Patent No. US4842224A, 1989). In addition, dust contamination is a significant consideration in an

atmosphere-less environment such as the moon (Ayrey, 2020). Finally, the planetary body's gravity also drives spacesuit design (Harris, 2001). All of these factors must shape the design of the spacesuit's torso.

The spacesuit torso must be robust enough to handle any reasonable loads that could occur. The pressure loads resulting from the pressure differential when the suit is used are of primary concern. Also included are any impact loads the suit may encounter. Microgravity EVAs can include human-induced loads and impacts on other rigid structures. For planetary EVAs, this includes trips and falls.

In spaceflight, the microgravity environment causes different effects on posture compared to Earth due to the absence of gravity. As a result, astronauts experience reduced forces acting upon their bodies, which can significantly affect their posture. For instance, the natural curves of the spine that help distribute forces evenly throughout the body are no longer necessary in microgravity, resulting in a change in spinal curvature. As a result, microgravity can cause discomfort and changes in posture, with the spine possibly straightening or developing a backward curve. The decompression of the spine also compounds this postural change. On Earth, gravity compresses the spine, but in space, the lack of gravity unloads it, allowing it to extend. As a result, astronauts gain a slight but noticeable amount of height. On Earth, gravity induces a blood pressure gradient in the body, with the highest pressure in the feet and the lowest in the head. In microgravity, this gradient is absent, resulting in an upward fluid shift in the body, which can cause facial puffiness and reduced calf diameters during missions. In addition, re-introducing a gravity field causes the body to re-adjust to have a blood pressure gradient, leading to orthostatic intolerance that compromises the astronaut's ability to function immediately after landing. To counteract microgravity's effects on posture and anthropometry and replicate the pressure gradient seen on Earth, astronauts use specialized exercise equipment and perform daily exercise routines to maintain strength and flexibility. Other devices, such as lower body negative pressure and elastic garments, have also been used experimentally. However, even with mitigation efforts, there is a persistent change in the body's neutral resting posture, anthropometry, and blood pressure gradient in a microgravity environment. (Thornton, Hoffler, & Rummel, 1974).

The effect of lunar gravity on posture would be different than on Earth but similar to the effect of microgravity experienced by astronauts in spaceflight. Lunar gravity is about one-sixth of Earth's gravity. Therefore, objects on the surface of the Moon experience much less gravitational force when compared to Earth. However, there is a lack of data on how the human body will adapt to the lunar gravity environment over a long period. Therefore, lunar gravity may offset some of the effects of micro-gravity but to a lesser extent than the earth's gravity (Thornton, Hoffler, & Rummel, 1974) (Figure 1.2.1.-1.).

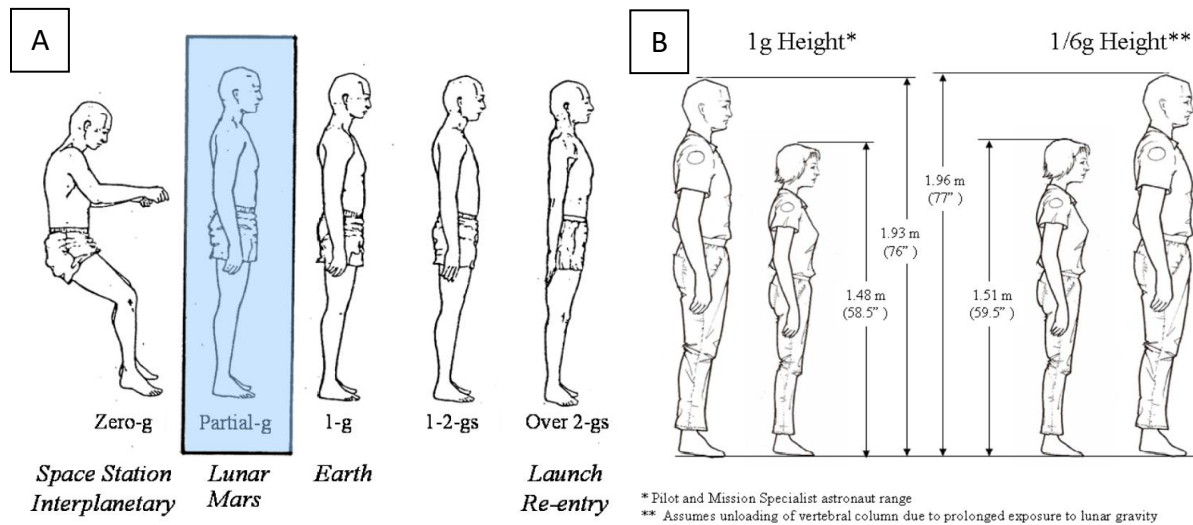


Figure 1.2.1.-1. Effects of Gravity on Posture and Anthropometry. A: Effect of gravity on neutral resting posture, B: Effect of lunar gravity on height (Thornton, Hoffer, & Rummel, 1974)

1.3. Spacesuit Torsos

The original EVA spacesuits were a direct evolution of the launch and entry suits of the early space programs. Because of this, the suits were typically entirely comprised of fabric materials, save for restraint hardware, disconnects, and the helmet (Figure 1.3.-1. A). These fabric torsos allowed for mobility, comfort for Intra-Vehicular Activities, and low storage volumes. Additionally, the suit's design used a zipper entry to don and doff the spacesuit due to the fabric construction of the suit. A zipper entry method was the standard construction of the EVA spacesuit through the Apollo and Skylab programs and was only changed with the Shuttle EMU design (Thomas & McMann, 2012). The zipper entry method is being employed again for SpaceX's EVA adaptation of their launch and entry suit (Polaris Program, 2023).

A hybrid upper torso is a torso section comprised of hard and soft components (Figure 1.3.-1. B). The benefits are that the design maintains the rigid structural features to mount hardware but also has flexible elements that could improve fit or ease of donning and doffing. An example of a hybrid upper torso would be the original design of the Shuttle EMU's HUT. This torso section is a rigid structure with a pivoting shoulder mechanism. This pivoting allowed astronauts to don and doff the suit easier. In addition, this mechanism included a soft component that would maintain the pressure in the gap between the rigid components (Reid, et al., 2014). Previous work on hybrid torsos has included built-in sizing and shaping features (Muller & Graziosi, 2015).

Modern spacesuits typically utilize a solid one-piece rigid structure to enclose the torso, called the Hard Upper Torso (HUT) (Figure 1.3.-1. C). Using a HUT allows for the rigid mounting of ancillary hardware, including bearings, softgood joints, helmets, DCUs, and entry hatches.

However, this structural advantage comes at the cost of having a rigid, static structure inside which the wearer must move.

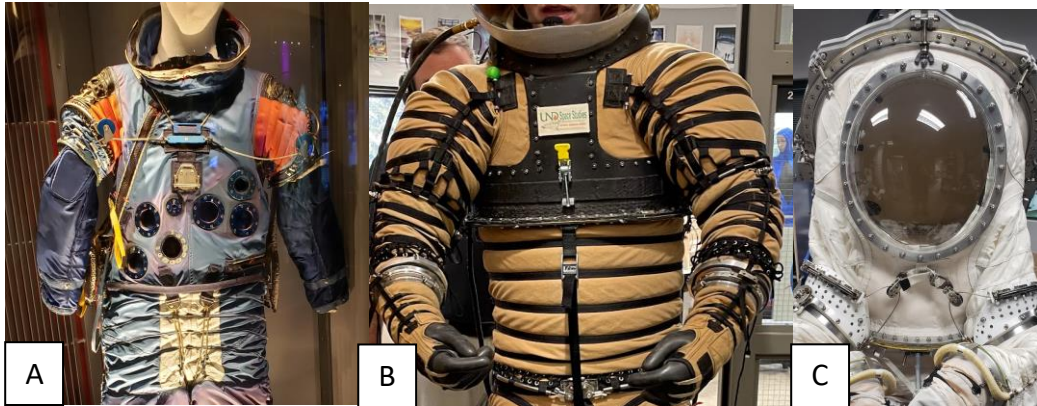


Figure 1.3.-1. Spacesuit Torsos, A: A7L-B Soft Torso Spacesuit, B: NDX-1 Hard Upper Torso Spacesuit, C: Morphing Upper Torso

Regardless of the suit torso construction method, the shape of the suit's torso is critical to avoid painful suit-body contact, ensure suit and body-joint centers coincide, and ensure the head is positioned correctly in the helmet for the adequate field of view (Jarvis, Norcross, & Abercromby, 2017).

1.3.1. Spacesuit Torso Interfaces

The torso of the spacesuit is a central component of the suit. Connected to it are the Lower Torso Assembly (LTA), which encompasses the entire lower body portion of the spacesuit, the helmet, the Display and Control Unit (DCU), the shoulder joints and associated bearings, if present, the suit donning/doffing method, and other smaller components such as gas and water ports, pressure relief valves, and protective outer layer attachment points (Figure 1.3.1.-1.).

The Scye bearing is a bearing that allows for the free rotation of the shoulder joint relative to the torso. Good placement of the scye bearing contributes to the suit's range of motion for shoulder flexion, extension, and abduction. The bearing housing is located in the interior of the HUT, held in place by attachment features, and, when pressurized, pressed into the integrated housing that is part of the HUT. The bearing's size, location, and orientation are critical for comfort, reach envelope, and range of motion (Anderson, 2014), (ILC Dover, 1975).

The xEMU features a rigid connection to the Waist-Brief-Hip component of the suit. This connection is below the waist disconnect rings. For modular suit systems, one way of adjusting torso length is through waist-sizing rings (USA Patent No. 4593415, 1986). Other suits, such as the EMU, only have a soft good- hard goods transition under the HUT (Harris, 2001). Therefore,

this interface's location, shape, and orientation will change depending on the LTA architecture and suit type.

Helmets of rear entry suits are typically hemispherical or elliptical bubbles. This bubble helmet is mounted onto the HUT through a quick disconnect system allowing for quick removal and attachment. The location and orientation of the helmet are critical for the field of view of the suit.

Life support, communications, and other suit functions are monitored and controlled through the Display and Control Unit (DCU). Historically, this hardware mounts onto the front of the HUT under the helmet. Ideally, the astronaut can look down and directly read the DCU display. The EMU DCU required a wrist-mounted mirror to read dial labels on the front of the unit. For planetary spacesuits, the thickness of the DCU is vital to be as thin as possible to allow the astronaut to look over the DCU when needing to look down at their feet.

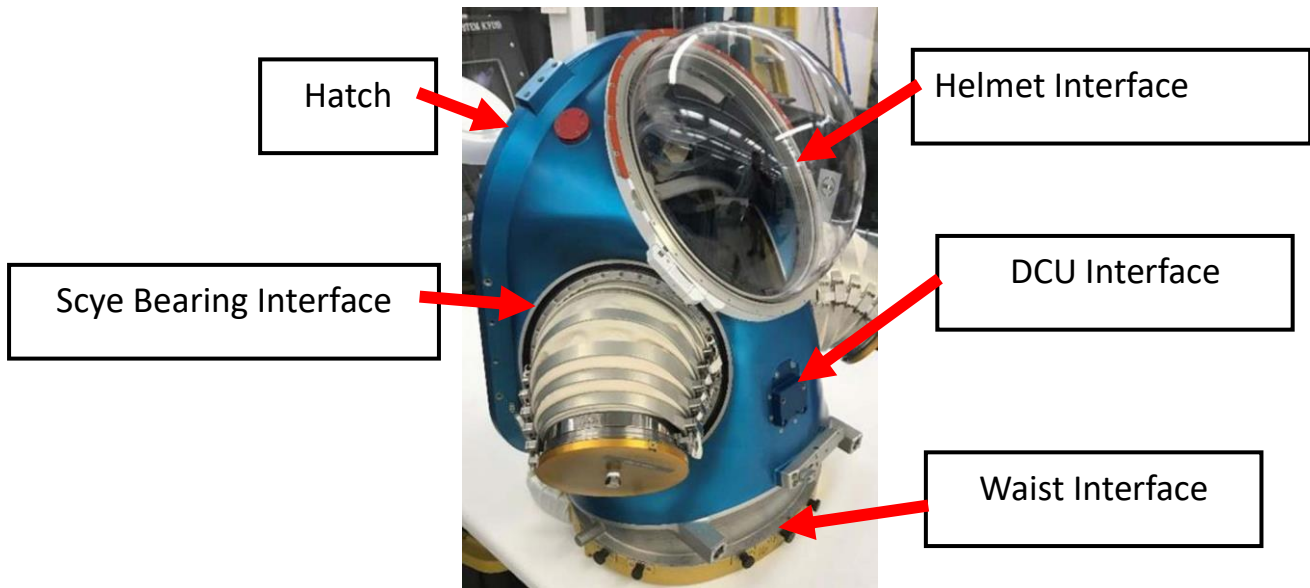


Figure 1.3.1.-1. xEMU Hard Upper Torso, with labeled interfaces

The entry mechanisms for dual planar and hatch entry suits are integrated into the HUT, defining much of the HUT's shape. Depending on the entry method, different scye-bearing positions are possible. Also, the entry method may affect the padding thickness and placement. The hatch entry method allows for the use of a suit-port system. A suit-port allows the suit to dock on the exterior of a spacecraft, habitat, rover, or the interior of an EVA access facility. The additional hardware would consist of an Interface Plate mounted between the PGS and the PLSS/hatch (United States of America Patent No. US4842224A, 1989).



Figure 1.3.1.-2. Effect of entry method on spacesuit torso shape, A: NDX-2AT, rear entry hatch spacesuit, B: NDX-1, dual planar spacesuit

On the HUT, several connectors often allow air and water inlets, outlets, power, and communication equipment to be attached. These usually do not affect the overall shape of the HUT and are typically placed in empty regions on the surface of the torso (Ayrey, 2020).

The outer layer of the spacesuit also covers the HUT. The outer layer protects from environmental temperature extremes, Micro meteoroids, Orbital Debris impacts, Abrasions, and piercing threats (Dombrowski, et al., 2022). On a planetary suit, this outer layer must be dust-tight to prevent dust intrusion into the interior layers of the spacesuit. The attachment mechanisms of the outer layer, while not a primary design concern, should be considered as early as possible in the design process to ensure smooth integration of the HUT with the protective outer layer.

The PLSS is the component of the suit that supplies the suit with breathing air, air conditioning, CO₂ and humidity removal, cooling water, and communications. This "backpack" can be seen on the exterior of Apollo, EMU, and xEMU spacesuits. With a HUT, there is usually a rigid connection with the PLSS.

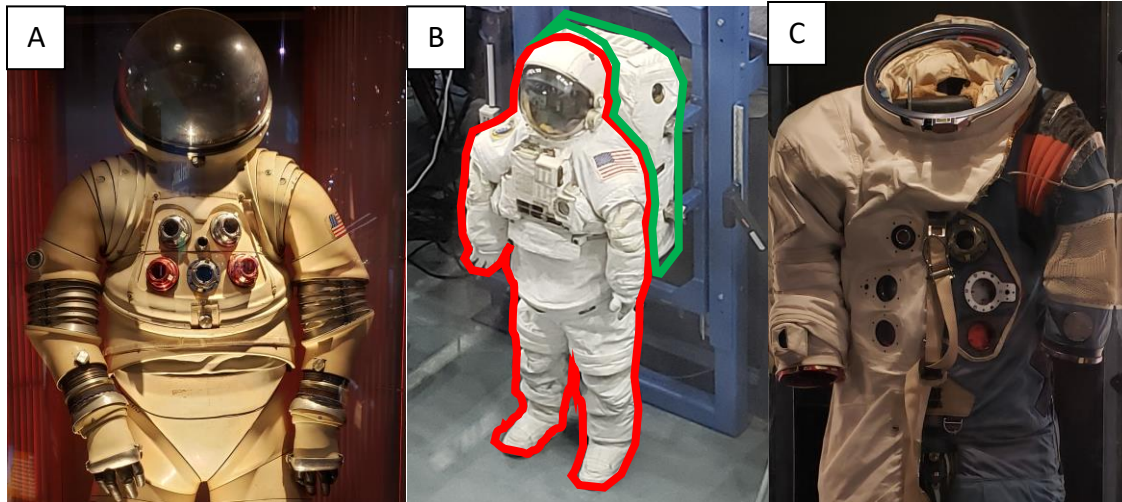


Figure 1.3.1.-3. Additional components attached to spacesuit torsos, A: AX-5 spacesuit with air and water connectors visible, B: Shuttle EMU, PLSS outlined in green, C: Apollo A7-LA Outer layer Cutaway Exhibit

The Portable Life Support System has a water-cooling system that keeps the astronaut cool in the spacesuit. This water flows through a Liquid Cooling/heating and Ventilation Garment. This connection is usually through the DCU, where the wearer has direct control over the flow rate (therefore cooling rate) of the LCVG (Harris, 2001). This connection penetrates the HUT.

The xEMU PLSS water system used suit pressure to pressurize the cooling loop. Because of this, the hatch's interior has a volume of water. This volume provides a somewhat conformal shape helping with the indexing of the wearer in the HUT (Miller & Hargrove, 2022). Any padding would be on top of this filled volume.

1.3.2. Spacesuit Entry methods

Due to the body's shape, the torso is the logical location for a spacesuit's donning and doffing method. Early USA spacesuits utilized a zipper on the torso to get in and out of the spacesuit. Historical spacesuit designs have featured several zipper location configurations. In the early apollo spacesuit design (A7L-A), the zipper ran vertically along the torso of the spacesuit. For the updated design of later missions (A7L-B), the zipper orientation changed to where the zipper ran under and in front of the shoulder. In the mercury suits, the zipper was in a spiral around the torso of the suit (Ayrey, 2020). Recently the SpaceX launch and entry suit featured a zipper running up and down both legs, allowing the wearer to enter the one-piece suit from the bottom of the torso (Dodd, 2019).

Historically the zipper has worked well for launch and entry suits but had several issues for EVA suits and planetary missions. First, the zipper had to form an airtight seal to allow the suit to hold pressure. As a result, the zippers had to be extraordinarily heavy-duty and complex. The chosen zippers had a moderate cycle life; the degradation of the zipper over time was a source

of leakage. Dust intrusion into the zipper also caused the zipper to jam and the seal to degrade (Christoffersen, et al., 2008). Because of this, there is resistance in the EVA community to using a zipper donning and doffing method on EVA suits.

An alternative entry method is a waist entry. Over the years, the waist entry design concept has been used in the EMU and several development suits (Harris, 2001). This system breaks the spacesuit into two parts the Lower Torso Assembly (LTA) and everything else. First, the wearer dons the LTA like pants. Next, the wearer dons the HUT and arms like a sweater. Finally, the wearer completes the suit with the gloves and helmet assembly.

This system uses two rigid surfaces to press against a seal. This is a benefit because the closure mechanism is simpler and easier to actuate. An additional benefit is that this type of entry does not have the additional weight of a hatch mechanism. However, a downside is that the new seal will have to be sufficiently rigid, limiting the suit's mobility.

The Soviet Union successfully adopted a hatch closure for their spacesuits after early Salut missions. A rear entry hatch has been used on almost all NASA developmental suits in recent years, including the xEMU (Harris, 2001). It has many benefits of the waist and dual planar entry methods, including the simplicity of creating a sealing surface between two rigid surfaces. Like the dual planar method, the rear entry hatch allows the wearer to place their arms more naturally into the suit. These benefits and suit port compatibility make the rear entry hatch attractive for future suit architecture. The downside is mass. The hatch size must accommodate the widest and tallest individual in the EVA astronaut pool. This standard hatch size means smaller HUTs will carry extra mass compared to other systems. Using lightweight materials limits the excess weight of an oversized hatch, but the bulk of the suit will still be present, and the mass will still be higher than an equivalent dual planar or waist entry suit.

In the 1980s, NASA developed the suitport. The suitport is an advanced suit entry system that worked to address many of the issues experienced with lunar dust on Apollo missions. The suit port builds off of the idea of entering a suit through the back but additionally has the spacesuit docked to the exterior of the habitat, rover, or spacecraft and enter the spacesuit through a rear entry hatch (United States of America Patent No. US4842224A, 1989).

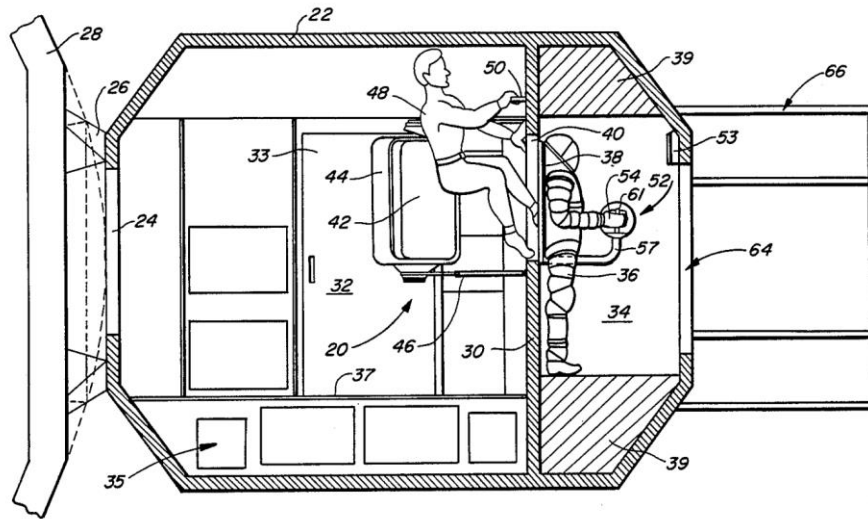


Figure 1.3.2.-1. Suitport patent line art showing an EVA access facility with an installed spacesuit. A crewmember dons the suit via the rear entry hatch (United States of America Patent No. US4842224A, 1989).

The suitport design has several benefits over the conventional hatch design. First, if the suit is operating in a dusty or contaminated environment, using a suit port can prevent the backward contamination of the interior living space of the architecture. Second, the suit port removes the need for an airlock. Airlocks take time and energy to operate, typically venting the gas in the airlock into space. Since the suit port does not require the pressurization and depressurization of an airlock, it has the potential to conserve resources, which would be critical for an exploration class space mission (United States of America Patent No. US4842224A, 1989).

Other alternative methods for donning and doffing spacesuits exist. For example, early Soviet Union suits utilized a neck entry method. The contemporary Russian launch and entry suit uses a system called the appendix. The appendix comprises a large flange on the opening of the soft torso of the suit. This flange is bunched up and tied with a rubber band resulting in an airtight seal (Abramov & Skoog, 2003).

The entry methods above comprise all flown EVA suit entry methods. However, development suits such as those designed for extended Apollo missions and future Mars missions have demonstrated other possible donning and doffing methods. One such example is the dual planar entry method. This method splits the suit again into two parts, but the split happens across a dual planar surface. The resulting parts fit together linearly, making securing the closure easy with a single latch. The dual planar entry method uses a similar sealing method to the waist entry system with rigid surfaces and a rubber seal. Additional benefits are easier donning and doffing due to the opening in the back of the upper portion of the HUT.

The first vacuum suits featured diagonal hatches. The Mark I vacuum suit designed for vacuum tube research can be considered the forefather of all spacesuits. Some extended Apollo development suits also featured a diagonal entry hatch (Young & Avino, 2009).

Future mechanical counter pressure suits may be skintight, donned, and doffed through the actuation of shape memory materials and may require new innovative entry methods not mentioned here (Newman, 2002).



Figure 1.3.2.-2. Alternative suit entry methods, [Left] Mercury spacesuit, with spiral zipper entry [Middle] SK-1 Soviet training spacesuit, with a neck entry method [Right] Shuttle EMU, with a waist entry method.

1.3.3. Padding

Additionally, the wearer can add padding inside the HUT to provide a tighter fit. The foam padding takes up space in the suit. A tighter-fitting suit can improve wearer mobility and comfort. This padding increases the suit's comfort and improves the fit. It also allows the wearer to customize the fit of the spacesuit to their preference.

The current xEMU padding system is a uniform closed-cell foam sheet cut to fit inside the hatch. However, NASA's Anthropometry and Biomechanics Facility has developed an advanced padding system using a multi-material padding system. This system provides more rigid padding on hard locations of the body and softer padding on locations of the body where more movement is needed (Bernal, Gordon, Gupta, Kim, & Sudhakar, 2021).

1.4. Microgravity Spacesuit Design Considerations

The majority of EVA experiences have taken place in microgravity. Objects orbiting celestial objects or existing in open space are said to experience microgravity. It is characterized by the

lack of sensible gravity, resulting in a weightless environment—this lack of gravity results in many challenges for the spacewalker.

On Earth, one can tighten a bolt with a wrench without any issues because the person can push against the ground with their feet to counteract the torque, they are inducing to twist the bolt. In microgravity, this is not as easy. For example, if an astronaut floating in free space attempts to tighten a bolt, they would be able to tighten the bolt, but they would also create an equal and opposite torque that would begin moving the astronaut. Similarly, if an unrestrained astronaut pushes against or throws an object, they create a force that pushes them back in the opposite direction of their push. Historically foot restraints and handrails have provided the needed counterforce to prevent this. Handling reaction forces is of continual concern for spacewalking astronauts and EVA planners.

Second, it is impossible to walk in microgravity. As a result, astronauts translate to and from different locations using their hands and arms. As a result, microgravity spacesuits have highly developed upper body mobility while ignoring lower body mobility.

1.4.1. The EMU

The space shuttle Extravehicular Mobility Unit (EMU) is a spacesuit system that NASA developed in the late 1970s to support spacewalking missions from the Space Shuttle. The first EMU was flown on the Space Shuttle in 1983, on the sixth Space Shuttle mission, STS-6. Astronauts Robert Crippen and Story Musgrave were the first to use the EMU during a spacewalk to test the suit's performance in space. Since then, the EMU has been further refined with upgrades to the suit's thermal control system, communications equipment, and other subsystems (Harris, 2001). Throughout the Space Shuttle program, the EMU was used in over 250 spacewalks, totaling over 1,300 hours of spacewalking time. In addition, the EMU enabled several satellite retrieval and repair missions and the construction of the ISS (Ta & Treviño, 2016).

The EMU is still in use today on the ISS, which supports the deployment of experiments and equipment and general maintenance of the station.

1.4.2. EMU Sizing

The shuttle era required a new suit with new requirements. Suit designers created the shuttle EMU to address these challenges. Modular suits fit the wearer by being assembled from a selection of standard-sized components with some level of adjustability. The original suit system featured a full array of 37 components (excluding gloves). Over time the number of sizes of certain parts was reduced. This results in a system where astronauts must first prove that they fit in and can operate the EMU before they are selected for EVA training. The fit constraints limit the pool of EVA-capable astronauts.

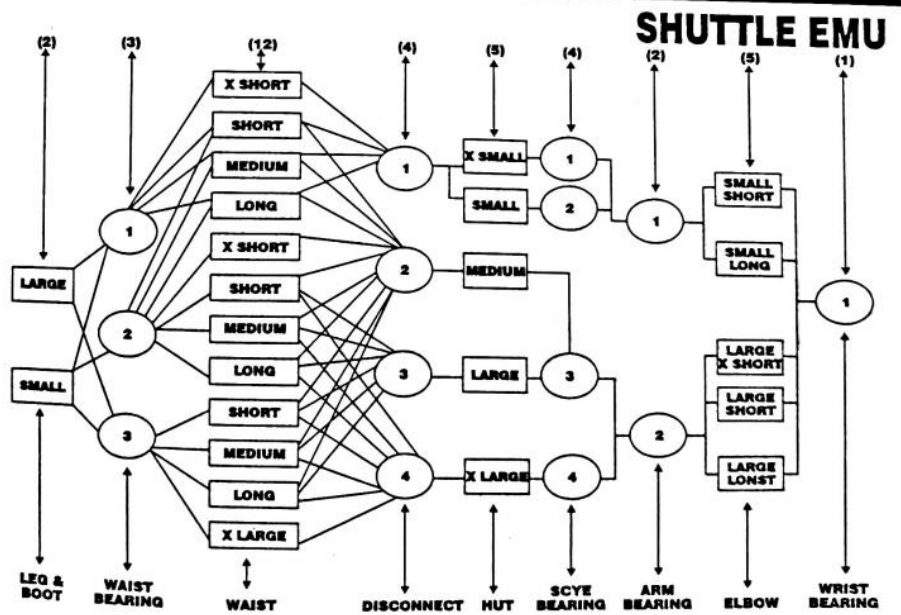


Figure 1.4.2.-1. Shuttle EMU Sizing Chart (Harris, 2001)

The microgravity environment also shapes the sizing system. For example, in microgravity, astronauts primarily move with their arms. As a result, the hands, arms, and torso for the shuttle EMU have more components and size options than the leg assemblies. The LTA, conversely, is assembled from fewer parts and offered in fewer standard sizes.

1.4.3. Scye Bearing Issues

Even with such a successful track record, the EMU has had significant issues with sizing and fit. One issue has been training injuries from EVA training in the National Aeronautics and Space Administration's (NASA's) Neutral Buoyancy Laboratory (NBL). The neutral buoyancy of a weighted spacesuit submerged in water simulates the feelings and effects of microgravity. However, gravity still acts on the wearer's body in the suit, pressing the wearer against the inside. The effect of gravity is especially problematic when training requires inverted body positions where the shoulder is driven into the scye bearing of the suit, creating hard contact (Williams & Johnson, 2003).



Figure 1.4.3.-1. [Above] Sonny Carter Neutral Buoyancy Laboratory, [Below] Rashes and bruises caused by a hard contact with the interior of the EMU during NBL training exercises. (Williams & Johnson, 2003)

A tiger team worked to address the NBL training injury issue. Their findings found that a significant portion of the astronauts training in the NBL suffered from discomfort or injuries. Some of the discomforts were not severe enough to affect performance. However, a significant percentage of the crewmembers required surgery directly due to training in the NBL. As a result, mitigation measures were adopted, including using the shoulder pivot HUT during training, which featured additional shoulder mobility allowing for easier donning, doffing, and more natural shoulder movement. Time spent inverted in the suit was also limited. Despite these mitigation efforts, shoulder injuries are frequently seen during NBL training activities (Williams & Johnson, 2003).

1.4.4. Tasks

Except for the first several EVAs performed to determine if humans were even capable of working in open space, microgravity EVAs have fallen into several categories.

While building the ISS, construction EVAs were very common. For those EVAs, astronauts with robotic arms moved around station components and connected them to existing hardware and modules. Even now, additional hardware and experiments are occasionally added to the exterior of the ISS, requiring EVAs.

Repair EVAs are when astronauts go on an EVA to repair some external hardware. The type of repair can range from fixing solar panels and deploying heat shields to fixing the Hubble telescope.

Both construction and repair EVAs are highly choreographed activities. On average, an astronaut will spend 6-7 hours of training for every hour they spend on EVA (Gast & Moore, 2011). The training is so that they can familiarize themselves with the tools they will be using, the work site, how best to get there, and how to secure themselves by handrail or foot restraint so that they can reach the work area comfortably and have a way to mitigate counter forces.

Contingency EVAs are unplanned activities where astronauts must act quickly to repair critical systems. Astronauts are trained on 13 generic contingency EVA operations and general skills to improvise while performing EVAs (Gast & Moore, 2011).

1.4.5. Work and Reach Envelope

A work envelope is a three-dimensional space that defines the boundaries of where a robot or a human can perform work within a given environment. The crew member's total mobility, the spacesuit's mobility, and the specific operating environment shape the work envelope (Abercromby, Thaxton, Onady, & Rajulu, 2006).

On the other hand, the reach envelope is a subset of the work envelope that defines the maximum distance an astronaut can reach. The reach envelope considers the length of the arms and any constraints that may limit the range of motion (Griffin, Howard, Rajulu, & Smitherman, 2009).

In other words, the work envelope provides an overall view of the space where the astronaut can work, while the reach envelope defines the specific areas they can reach within that space. Therefore, the reach envelope is an essential factor in determining the placement and orientation of the spacewalker for specific tasks, as it can affect the efficiency, safety, and overall EVA effectiveness of the astronaut.

One must overcome the mechanics of a spacesuit to move. Designers create spacesuits to accommodate many of the body's joint's degrees of freedom. The astronaut must still work against the pressure of the spacesuit and the limited mobility of the suit. Spacesuit designers must consider the type of work and gravity environment when designing a spacesuit. The work area, reach envelope and field of view of the suit-human system must overlap to allow the astronaut to do their work. (Griffin, Howard, Rajulu, & Smitherman, 2009)

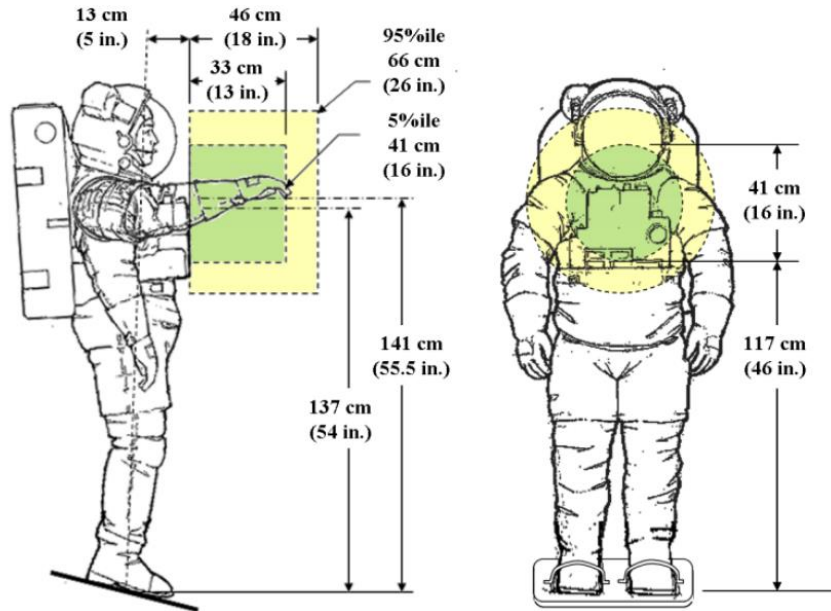


Figure 1.4.5.-1. EMU Work Envelope Visualization (Griffin, Howard, Rajulu, & Smitherman, 2009)

1.5. Planetary Spacesuit Design Considerations

Planetary EVAs are fundamentally different from microgravity EVAs. The effect of gravity, local geological conditions, lighting, and local temperature environment all drive spacesuit design. Many groups have done work over many decades to develop planetary spacesuits, but upcoming Artemis missions and future long-duration lunar and Martian missions will require significant innovation for mission success.

1.5.1. Historical and Developmental Planetary Spacesuits

As of 2022, there have been well over 400 microgravity EVAs, resulting in a well-developed understanding of microgravity spacesuits and operational concepts. In stark contrast, there have only been 13 planetary EVAs performed by 12 men over three years during the Apollo program (Ayrey, 2020).

Because of this, the only EVA spacesuits used in a planetary mission have been the Apollo A7-1 Spacesuits. However, numerous suit development programs have occurred since then, showing how future suit systems could look. In addition, developmental suits showcase novel technologies and suit architectures (Harris, 2001).

1.5.2. Apollo

These EVAs used one of two versions of the A7L spacesuit developed by ILC Dover. Flexible materials comprised almost all of the pressure garments of the suit. The torso of the suit was of

fabric construction and used a zipper entry method. The zipper was oriented vertically for the A7L-A spacesuits. The zipper orientation was changed for the A7L-B spacesuit to accommodate the waist mobility needed for sitting in the unpressurized lunar rover. Despite the soft construction, lots of hardware was on the Apollo suit's torso. This hardware included two sets of air and cooling water connectors, a display and control unit, a helmet ring, and a helmet ring tiedown assembly. The torso to shoulder transition was entirely flexible, lacking a scye bearing (Ayrey, 2020).

Several standard-sized sewing patterns comprised the patterns used to make the base Apollo spacesuits. Designers then modified the patterns to fit the individual astronauts through a series of fit checks. As a result, each astronaut had several suits explicitly made for them for different uses: one for flight, one for training, and one as a backup. This level of care and effort was possible due to the large budget of the Apollo program, the small number of astronauts, and the short service life of the suits (Ayrey, 2020).

The A7L series of spacesuits also saw use for microgravity EVAs. During the later Apollo missions, the Command Module Pilot performed microgravity EVAs to retrieve a film canister from the exterior of the service module. As part of the Skylab program, astronauts wore A7L suits to repair the space station and as the sole EVA-capable suit (Ayrey, 2020).

1.5.3. Apollo Application Spacesuits

Initially, government decision-makers planned the Apollo program to extend well beyond Apollo 17. Later lunar missions would have been much longer and required new and improved spacesuits. As a result, NASA and government contractors developed several suits to address the shortcomings of the A7L series spacesuits. These shortcomings included the low operating pressure, the low cycle life of the zipper closure, the low dust tolerance of the soft goods components of the suit, and poor mobility. This effort resulted in an explosion of creative spacesuit designs, none of which would ever make it to space (Young & Avino, 2009).

1.5.4. Mark III, Z Series & xEMU Spacesuits

Over the past several decades, there have been attempts to return to the Moon or begin planning missions to Mars. Parts of these efforts have been the development of new planetary suits, primarily based on the technology used in the EMU. For example, the Mark III Planetary suit was initially constructed in the mid-2000s for NASA by ILC Dover. This suit is a zero-pre-breath planetary suit. The benchmark for planetary suit development programs has been the Mark III. The Mark III laid the groundwork for the Z-series spacesuits and the xEMU. Rovers, suit ports, and EVA tools have been developed for use with the Mark III and will contribute to the designs of future flight-ready hardware. The Mark III has a rigid aluminum HUT with integrated scye bearings (Mitchel, 2012).

The Z series of spacesuits built upon the work started with the Mark III. Further advancements include the integration of a functional suitport. The Z-1 utilized a soft upper torso with integrated bearings. The Z-2 had a rigid HUT returning to an architecture more similar to the Mark III (Graziosi, et al., 2016).

Following the Z series of spacesuits, NASA began the development of the xEMU. The xEMU project began as a new Portable Life Support System (PLSS) program. Advanced technology was to be added to the PLSS to allow more extended missions with reduced consumables. Over time the PLSS-only project expanded to include a new upper torso assembly. The xEMU project finally expanded into the final project scope of a complete integrated suit system when NASA began its work to return to the Moon by 2024. With such a short deadline, the xEMU project was the only feasible suit development program that could rise to that challenge. As such, the xEMU project shifted into a complete suit system development program with a full range of components manufactured (Rhoades, MacFarland, & Campbell, 2022). The baseline xEMU has an aluminum HUT to reduce schedule risk, but parallel development of a composite version of the xEMU HUT has been advancing. The xEMU HUT comes in 2 sizes with the additional accommodation of moving the scye bearings in 1" on both sides. With this method, getting four different HUT sizes from a 2-size system is possible. The xEMU features an elliptical helmet, scye bearings, a DCU, a rear entry hatch, and a waist disconnect (Meginnis, Rhodes, & Kim, 2022).

1.5.5. Contractor Suits

In 2021 it was decided that NASA would pursue commercial options for replacement microgravity and lunar spacesuits. As a result, in June 2022, Collins Aerospace and Axiom were awarded contracts to develop microgravity and planetary spacesuits. NASA will then choose which suit to source on a competitive case-by-case basis. Axiom and Collins were selected as prime contractors for the xEVAS contract (Exploration Extravehicular Activity Services (xEVAS), 2022).

1.6. Planetary EVA Activities

For the Apollo missions, the primary objective of the EVAs was to collect geological samples and set up geological experiments. Geological tools were very similar to those used on Earth, including various types of scoops, rakes, and hammers. Apollo astronauts collected samples so researchers back on Earth could better understand the moon's geological evolution and the solar system's formation. In addition, astronauts deployed experiments on the lunar surface. These included seismic, radiation, and photometric recording devices, giving researchers insight into the lunar environment.

Planetary spacesuits are more versatile than microgravity spacesuits. Astronauts will primarily perform or set up geological experiments beyond construction, repair, and contingency EVAs.

One of the primary motivations for planetary space missions is to gain a deeper understanding of the various planetary bodies in our solar system.



Figure 1.6.-1. Apollo Geology Tools

As a result of the new focus on geologic research, the tools the astronaut will be using will be different. For example, in Figure 1.6.-1., the Apollo geological tools can be seen.

1.6.1. Work and Reach Envelope and Field of View

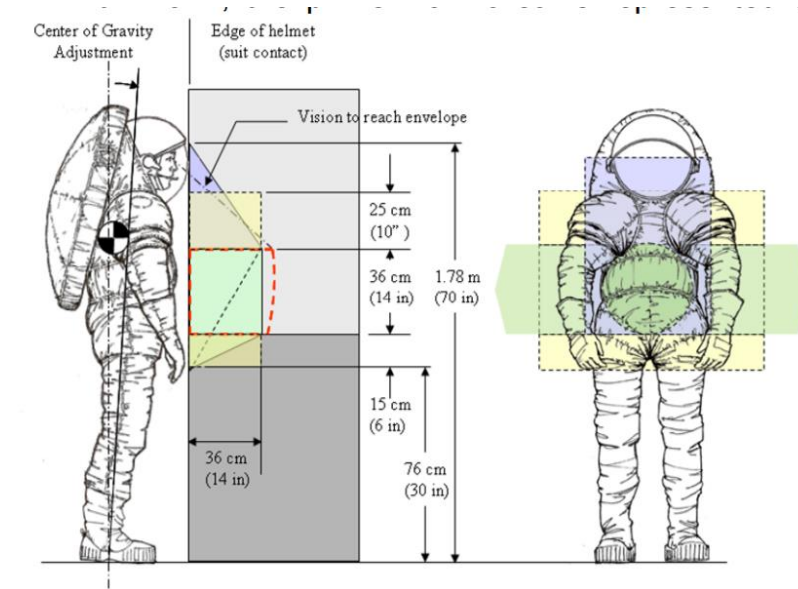


Figure 1.6.1.-1. A: Planetary EVA Suit Work Envelope Visualization

Due to the increased focus on geological tasks and needing to walk on the planetary surface, the work envelope and reach envelope must include access to the ground with and without tools. Therefore, less work will be done directly in front of the astronaut's face except for inspecting samples or reading checklists.

1.6.2. Ambulation

On planetary surfaces, the primary mode of transportation while on EVA will be walking. Because of this, the lower body and waist of the spacesuit must be more mobile than a microgravity spacesuit.

The A7L series of spacesuits lacked bearings in the lower torso. As a result, the astronauts adopted a distinct lopping gait, using the “springiness” of the suit to propel them along. The bunny hopping gait worked well, but the limited range of motion was problematic when recovering from falls and bending down to pick up samples (Ayrey, 2020). As a result, subsequent suit designs often incorporated more complex mobility elements into the Lower Torso Assembly of the spacesuit (Harris, 2001).

The Mark III and xEMU feature a complex Waist-Brief-Hip section with a rigid connection to the HUT. Integrated into the HUT is a sizable planar bearing allowing for rotation about the waist. Integrated into the Waist-Brief-Hip section of the suit are at least two thigh bearings allowing for free movement of the legs. Additional bearings are located throughout the legs allowing for free movement and rotation of the leg and foot (Rhoades, MacFarland, & Campbell, 2022).



Figure 1.6.2.-1. Waist-Brief-Hip Components of the Mark III EVA Spacesuit Prototype

1.6.3. Lunar Conditions

The moon's surface has a long geological history, as evidenced by the many impact craters. These impacts have covered the moon's surface in a fine rocky powder called regolith. The regolith's exact morphology and chemical makeup vary across the moon, but there are some consistent challenges that lunar regolith poses to surface operations. First, since there is no wind on the moon, there is no alluvial smoothing of the regolith particles. An analogy for this is comparing a rock found in a desert to a rock found in a riverbed. The river stone will have been

worn smooth from constant tumbling, whereas the desert stone will have sharp jagged edges. Due to the lack of smoothing, lunar regolith has an additional abrasive glass shard component resulting from high-energy meteoroid impacts. Finally, radiation from the sun and galactic sources, along with the lack of atmosphere, causes the particles to develop an electrostatic charge. This charge makes the regolith clingy, quickly coating anything on the moon's surface (Manyapu, 2017).

This contamination was problematic for the Apollo missions. When the astronauts returned to the lander and later the command module, they returned significant amounts of dust (see Figure 1.6.3.-1.). This dust fouled up the hook and loop closures, induced hay-fever-type symptoms in the crew members, affected the air filtration systems, and led to enduring discomfort (Christoffersen, et al., 2008).

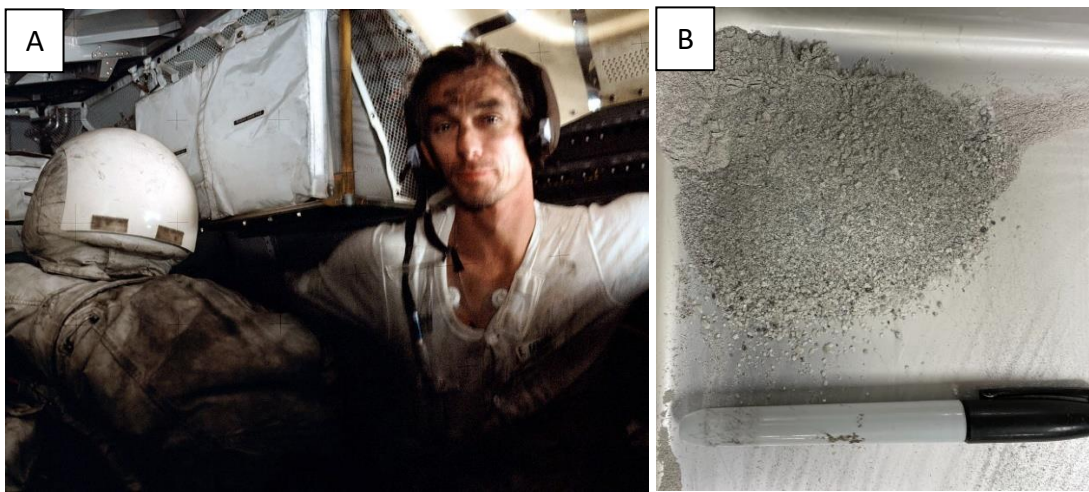


Figure 1.6.3.-1. A: Apollo Astronaut in the Lunar Excursion Module with visible dust contamination, B: Lunar Dust Simulant

The regolith's abrasive nature and electrostatic charging will be an ever-present challenge to lunar EVAs. Industry and academia have pursued technologies that will mitigate this issue. Possible solutions include flexible electrodynamic dust shields, new, more abrasion-resistant textiles, and novel suit architecture concepts like the suit port (Manyapu, 2017), (United States of America Patent No. US4842224A, 1989).

An additional challenge for lunar EVAs is the lighting conditions on the lunar surface. In the moon's polar regions, the sun never rises high in the sky, resulting in a shallow lighting angle. The incident angle of the sun means that the bottoms of some craters in these regions never receive direct sunlight, creating what is known as Permanently Shadowed Regions. It is theorized, with some evidence, that there may be water ice deposits in these craters. Future lunar settlements could leverage these water ice deposits to make rocket fuel and supply water for drinking and industrial uses (Brown, et al., 2022).

The operating conditions near and inside these craters will be very extreme. Since there is never any light, these regions are some of the coldest locations in the solar system, with temperatures reaching as low as 25 Kelvin. The lighting situation will also be challenging. The light will always be coming in near horizontally and never overhead. As such, the helmet angle and visor assembly must account for this (Casting Light on Permanently Shadowed Regions, 2018).

The moon is much smaller than the Earth and has a weaker gravity field. Lunar gravity is approximately $1/6^{\text{th}}$ of the Earth. Therefore, the gravity of the operating environment will impact any design trades that consider mass, the design of the lower body mobility, and the mass requirements of the total system.

NASA's Artemis program has been directed to land near PSRs so astronauts can descend into the craters to perform geological surveys and look for water ice. The next-generation suits will have to handle the most challenging areas to explore on the moon's surface (Coan, 2020).

1.6.4. Martian Conditions

Many of the challenges associated with lunar exploration are not present on Mars, partly due to the Martian atmosphere. This atmosphere is sparse and composed almost entirely of CO₂. However, wind on the Martian surface causes alluvial smoothing of the regolith, referring to the smoothing effect of regolith particles tumbling in the wind. Tumbling initiated by wind knock off sharp features, creating smoother regolith particles.

In addition, the Martian atmosphere allows electrostatic charges to dissipate, preventing the buildup of static electricity seen on the lunar surface. The absence of electrostatic charge means the particles do not cling to surfaces in the same way as lunar regolith, making cleaning surfaces easier.

The Martian surface temperatures, ranging from -143 to 35 degrees C, will also be less of a concern. However, different insulating methods will need to be used, as heat transfer through the Martian atmosphere circumvents the current insulative strategy primarily based on reflective mylar layers.

Mars's commonly proposed landing areas are near-equatorial regions, often inside dried-up lake beds. Therefore, the lighting scenario and surface topography will be less extreme than the proposed lunar landing sites on the moon's south polar region.

Like the moon, Mars is smaller than Earth and has a weaker gravity field, with Martian gravity approximately $1/3^{\text{rd}}$ that of Earth. As a result, the mass will be a more important consideration in any Martian spacesuit design.

1.7. Anthropometry

Anthropometry is the study of human body measurements and proportions. It involves the measurement of various physical characteristics of the body, such as height, weight, limb length, and circumference of body parts, to establish standards and averages for different populations.

Anthropometry has contributed to many fields, including medicine, ergonomics, product design, and clothing and equipment design. For example, in medicine, anthropometry can be used to assess a person's health status and to identify health risks associated with body size and shape. In ergonomics, anthropometry helps design workspaces, tools, and equipment that fit the human body and minimize the risk of injury or strain.

Anthropometry is also essential in the design of spacesuits for astronauts. The spacesuits must fit the individual astronaut precisely, as a poor fit can lead to discomfort, injury, or even death in the extreme space environment. Therefore, the design and sizing ranges of spacesuits are tightly related to the anthropometry of the EVA-capable crew population.

Overall, anthropometry is an important field that helps us to understand the human body and to design products and environments that are safe, comfortable, and functional for people of different sizes and shapes.

The field of anthropometry has evolved and has reflected the available technologies and knowledge of the times. Early anthropometrists were artists focused on defining the ideal human as a set of proportions. Da Vinci's Vitruvian Man aimed to define the archetypical male human form (The "Vitruvian Man" Da Vinci – Why Was the "Vitruvian Man" Created?, 2022). Nevertheless, of course, this idealized man can never be truly realized, let alone represent an entire population.

Over time the need to measure and understand the human form spread from art into general society. As the field moved towards applied science, a shift occurred. While still interested in defining an ideal form (Buzzi, 2017). The theoretical ideal form informed the design of objects and architecture. Anthropometry also worked to describe the measurements of individuals and populations.

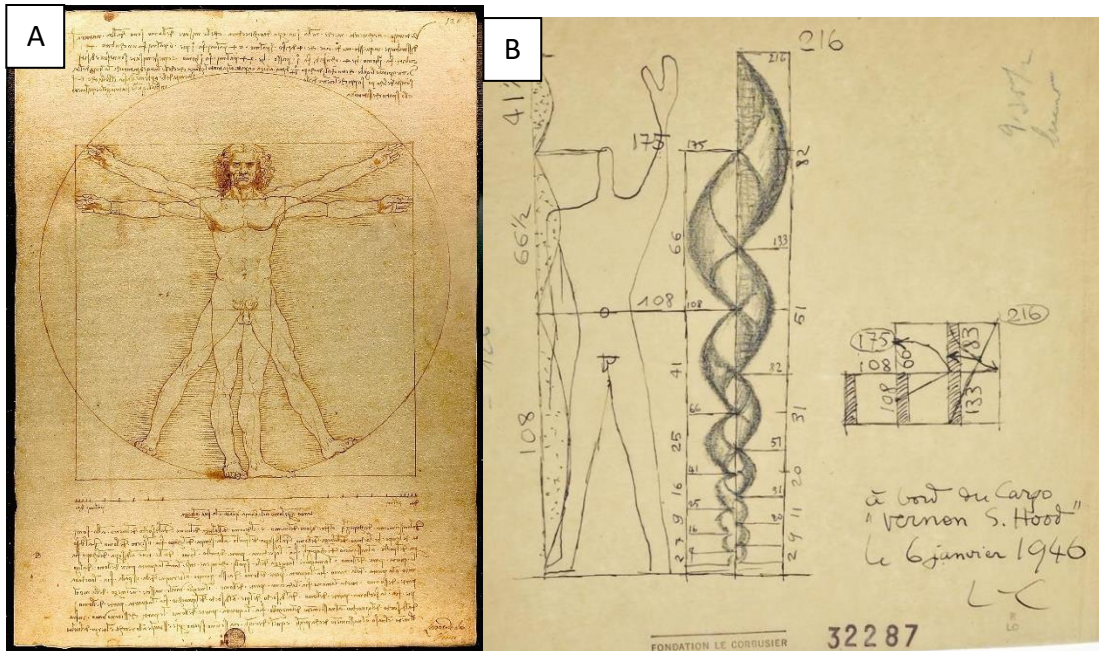


Figure 1.7.-1. [Left] Davinci's Vitruvian Man [Right] Corbusier's Modular Man

One of the landmark anthropometric surveys was the U.S. Army's ANSUR I survey. This survey was run in 1988 and aimed to understand how the body shape of the U.S. military population was distributed and varied. Measurements included lengths and circumferences of specific body parts and distance between landmarks on the body (GORDON, et al., 1989).

ANSUR I preceded the ANSUR II survey, which reproduced many exact measurements, but on the 2012 U.S. military population. In addition, 3D scans, including head, foot, and body scans, were also taken. The ANSUR surveys and similar studies represent an effort to include new ways of describing and measuring the human form (Gordon, et al., 2014).

The Society of Automotive Engineers (SAE) International executed the Civilian American and European Anthropometry Resource (CAESAR) project to create a database of human physical dimensions for men and women of various weights and ages. The Max Planck Institut Informatik processed and aligned the raw scan data. The database contains the body scans of 4300 North American and European civilians (CAESAR 3-D Anthropometric Database , 2012).

1.7.1. NASA's Spacesuit Sizing Requirements

In the early days of spaceflight, each crew member had a bespoke spacesuit explicitly made for them. Since the astronaut population was small, customizing the suits to accommodate unusual anthropometry was not a problem. For instance, when an astronaut with an abnormally large head was selected, a larger helmet bubble was used to accommodate this requirement (Ayrey, 2020).

However, a standardized sizing system for spacesuits became necessary as space exploration progressed. The Shuttle suit requirements were based on the 95th percentile male and 5th percentile female measurements, calculated from the ANSUR survey data. Unfortunately, many of these measurements were not well-correlated, meaning that if only one measurement with a 95th to 5th percentile were considered, 10 percent of the total population would be excluded. Furthermore, people would be excluded if a second uncorrelated measurement was added with similar but not overlapping cutoffs. This stacking effect resulted in systems that could only accommodate a small sub-population of the target user population.

The current sizing requirements derived from the ANSUR II survey address the problem of compounding anthropometry range limits by considering the 99th percentile male to the 1st percentile female measurements. Increasing the range limits was done to limit the stacking effect and ensure that the spacesuit sizing system accommodates a larger portion of the crew member population (Rhoades, MacFarland, & Campbell, 2022).

1.8. Garment Sizing

Textiles are applied in garments because of their soft and flexible nature, making them ideal for clothing. These fabrics are typically made from woven or knit yarns. The manufacturing process involves creating rolls or "bolts" of fabric from these yarns and then using them to create the final product.

When creating a garment, the fabric is cut based on 2-dimensional patterns and sewn together to form a 3-dimensional garment. Translating the 2D patterns into the final 3D product is a highly skilled process that requires much expertise. Although there have been attempts to automate this process, the most complex patternmaking requires highly skilled pattern drafters.



Figure 1.8.-1. [Left] Glove Sewing Patterns [Right] Assembled Glove.

The history of garment sizing is constantly evolving and complex; changes have influenced human bodies and fashion trends. For much of human history, garments were typically bespoke and made to fit the individual wearer. The personalized clothing nature was because it was expensive and time-consuming to produce, so people invested in garments that fit them well and lasted a long time. Additionally, societal standards reserved specific dress codes or garments for certain social classes or occasions. The advent of mass production in the 19th century led to clothing production in larger quantities and sold in stores. However, there were no standardized sizes, so customers had to try on multiple garments to find one that fits. In the early 1900s, the National Bureau of Standards in the United States began to study body measurements and develop standard sizing charts. These charts were based on measurements of large groups of people and provided a starting point for garment manufacturers to create more consistent sizing. However, these charts mainly focused on men's clothing and did not consider body shape or proportions variations. In the 1940s and 1950s, the fashion industry developed more standardized sizing systems for women's clothing. The growing popularity of ready-to-wear clothing and the desire to make clothes shopping more convenient for women drove the rise of standardized clothing sizes. However, these sizing systems were still limited in their range of sizes and did not necessarily reflect the diversity of body shapes and sizes. In recent decades, there has been a growing awareness of the limitations of traditional sizing systems and a push towards more inclusive and diverse sizing. Retailers and designers now offer a more comprehensive range of plus and petite. Some are also experimenting with more flexible or customizable sizing options. Now, tools and technologies are available to help individuals take more accurate body measurements and find clothing that fits well (Ashdown, 2007).

1.9. A Changing Astronaut Population

The type of people who become astronauts has changed significantly over time. In the early years of space exploration, the focus was on selecting military test pilots with extensive aviation experience. The first American astronauts, known as the "Mercury Seven," were all male military pilots with backgrounds in engineering and science.

As the space program evolved and became more diverse, so did the astronaut selection criteria. In the 1970s, NASA opened the astronaut program to women and minorities, leading to the selection of the first female and African American astronauts in 1978.

Today, the astronaut corps is more diverse than ever, with members from various backgrounds and disciplines. While many astronauts still have aviation or military experience, there are also astronauts with medical, engineering, and science backgrounds (Historical Evolution of Astronaut Selection, 2016).

NASA and other space agencies are now looking for individuals who are not only highly skilled in their areas of expertise but also can work effectively in a team and cope with the unique

challenges of spaceflight. The skills needed for spaceflight include adapting to changing situations, communicating effectively, and maintaining mental and physical health in a confined and isolated environment.

In addition, there is now more emphasis on international cooperation in space exploration, with astronauts from different countries working together on missions. International cooperation has led to the selection of astronauts from a growing number of countries, further increasing the diversity of the astronaut corps.

Overall, the type of people who become astronauts has changed from a narrow group of military test pilots to a diverse group of highly skilled professionals with various backgrounds and experiences. This trend will likely continue as space exploration becomes more international and focused on long-duration missions to the moon and Mars (Byrne, 2023).

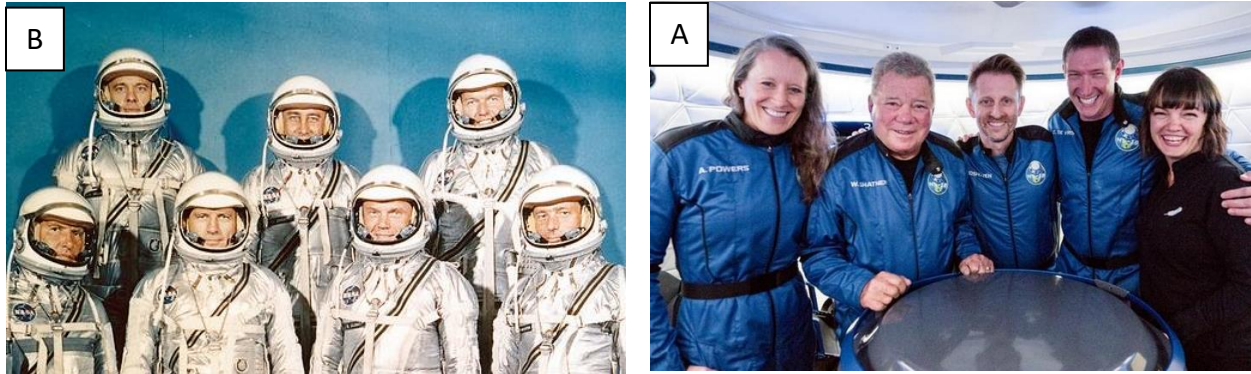


Figure 1.9.-1. A: Mercury 7 Astronaut Class (Image courtesy of NASA), B: Blue Origin Commercial Crew (Image courtesy of Blue Origin)

Spacesuit Design Framework Development

“A classic case of poor cockpit design is the ejection procedure which used to be in one Air Force trainer. It was a placard listing half a dozen important steps, printed boldly on the canopy rail where the pilot could not miss seeing it. The only flaw was that step 1 was “jettison the canopy.”

– *Michael Collins*

2.1. HUT Design Frameworks

In order to evaluate the effect of HUT customization on fit, comfort, and mobility of spacesuits, a custom and standardized design framework was created. These frameworks were built upon analysis of the torsos shape seen in the general population and a HUT shape prediction model. The novel frameworks are largely automated, such that a processed 3D scan can be uploaded, and a standard HUT can be suggested, or a custom HUT predicted.

Through large 3D scan databases, predictive modeling, 3D scanning, and the creation of the HUT shape prediction model, it is possible to create novel, custom, and standardized HUT design frameworks.

Using these design frameworks, both custom and standard sized HUT mockups were printed and used in HITL testing. The suit architecture for was defined as a lunar EVA spacesuit, this choice drove the entry method definition.

2.2. Issues of Anthropomorphic Suit Design

For both standardized and custom HUT design frameworks, it is essential to understand how the shape of the torso varies across the target user population.

2.2.1. Target Population Definition

Barriers to spaceflight are being lowered and eliminated. In the future, spaceflight may become possible for much of humanity. As such, future spacesuit systems should accommodate as much of the general population as possible. Previously, NASA has defined its spacesuit target user population as individuals who fit within the 95th and 5th percentile of several anthropometric measurements. Percentile measurements from military anthropometry databases became the specific anthropomorphic size limit requirements for the shuttle EMU.

The issue with using percentile ranges for anthropometry limits is that the various measurements are often not tightly correlated, meaning that the portion of the population excluded through one cut-off may differ from those excluded through a separate measurement. A theoretical example of this would be height and BMI. If a suit system were only designed to fit those within the 5th and 95th percentiles of height and BMI, the actual size of the

accommodated population would be much less than the 90% seen if only one measurement was considered, see Figure 2.2.1.-1. Similarly, due to the stacking effects of various 95th to 5th percentile cutoffs, the current EMU spacesuit can only fit a fraction of the total NASA astronaut population. Designers can work against this issue by increasing the accommodation ranges, say to 1st and 99th percentile cutoffs. However, this causes additional issues as a broader range of body shapes and sizes must be accommodated with minimal additional hardware sizes.

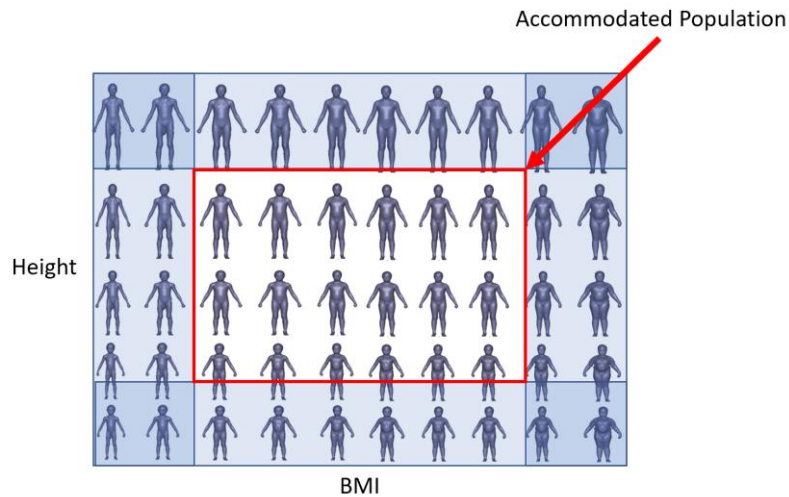


Figure 2.2.1.-1. Example of stacking effects of anthropometry percentile cutoffs

Compared to the general population, the military population is meaningfully different. The military population overly represents males, as 72.6% of the U.S. Army is male, whereas the general U.S. population is approximately 50% male. The military also requires service members to maintain fitness standards. When comparing the young adult population of the U.S. to the military standards, 1 in 3 are too heavy for service. In the 2/3rds that are light enough, 1/4th is not active enough to adequately prepare for service (Centers for Disease Control and Prevention, 2023). While this was only looking at young adults aged 17-24, the discrepancy between the military and the general population would likely increase as the target population's age increases.

Spacesuit designers should develop suit systems that fit as many people as possible. As such, anthropometry size accommodation limits should reflect the survey covering the most diverse population. Such a survey would include people of a more extensive range of ages and physical fitness levels. To this end, the CAESAR 3D body scan database was used to represent the target user population of the customizable HUT system (CAESAR 3-D Anthropometric Database , 2012).

2.2.2. Data Sources: CAESAR Dataset

The CAESAR 3D body scan data underwent preprocessing by the Max-Planck-Institut für Informatik (MPII) to correct the subjects' posture, align the scans to a standard coordinate system, and convert the raw data into a ho-model vertex layout (Pishchulin, Wuhrer, Helten, Theobaltd, & Schiele, 2017). The original data, as provided, was formatted to work with a Matlab program and stored as Matlab Data .mat files. The .mat files were converted into a format compatible with Python (Van Rossum & Drake, 2009). A 3D surface modeling program was used to visualize the data (Blender Foundation, 2018).

The conversion process involved loading the vertex locations from the .mat files and updating a template model in the 3D visualization environment. Next, a non-rigid iterative closest point algorithm was applied to deform a base ho-model in the 3D environment to fit the CAESAR template model. Finally, the non-rigid ICP algorithm converted all 4300 scans in the CAESAR database into the ho-model vertex layout and added the vertex locations for each processed scan to a scan database that could be used for further analysis (Amberg, Romdhani, & Vetter, 2007).

2.2.3. Principal Component Analysis and Torso Shape Analysis

Principal Component Analysis (PCA) is a technique for reducing the dimensionality of data while retaining as much of its original variability as possible. PCA aims to identify the directions in which the data varies the most and to project the data onto a new coordinate system defined by these directions (the principal components). To do this, PCA finds the eigenvectors and eigenvalues of the covariance matrix of the data, which represent the directions and magnitudes of the most significant variability, respectively. The eigenvectors form the new coordinate system, while the eigenvalues indicate the amount of the original variability retained in each principal component. By choosing a subset of the principal components that explain most of the variability in the data, PCA can effectively reduce the dimensionality of the data while preserving as much of its original structure as possible.

This analysis employed a ho-model to position the vertices in the exact relative locations on each scan. The vertices comprising the torso were grouped to isolate the surface of the torso. A database was made containing all the torsos in the dataset. Principal component analysis was used to determine how the shape of the torso varies across the population. The results showed that four principal components were sufficient to describe over 94% of the variance in torso shape.

Table 2.2.3.-1. Torso shape analysis explained variance.

	PC1	PC2	PC3	PC4
Explained Variance	0.55	0.21	0.13	0.05
Cumulative Sum of Explained Variance	0.55	0.76	0.89	0.94
99.5 th percentile PC Mannequin Torso				
Principal Component Description	Size	Fat Adipose Tissue	Male Gender Characteristics	Female Gender Characteristics

PCA can be used to create a transformation where a torso scan can be analyzed and determine a set of PC values that describe where that torso is in the CAESAR 3D scan database’s torso PC space (PC space). This PCA also allows for generating a synthetic torso shape given any combination of PC values. The PC space description will help describe the torso shapes of individuals and form a framework for choosing optimal standard-sized HUTs and applied in a customizable HUT design framework.

2.3. Selection of Optimal Entry Method

The entry method is a significant factor in the overall shape and function of the spacesuit torso. Various entry methods have flown and found use in developmental suits; see Figure 2.3.-1. Below is a summary of the most common entry methods and a trade study for selecting a suit entry method for micro-gravity, lunar, and Martian missions.

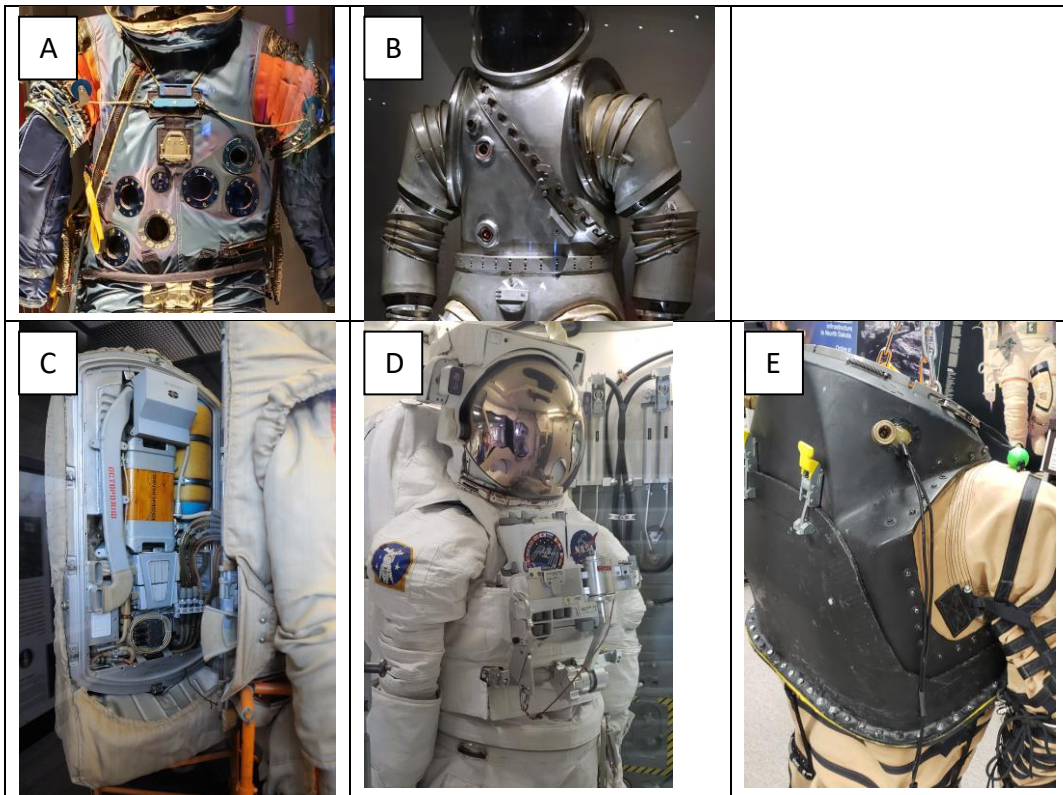


Figure 2.3.-1. Spacesuit Entry Methods, A: Zipper entry method, B: Diagonal entry method, C: Hatch entry method, D: Waist entry method, E: Dual planar entry method.

2.3.1. Zipper Entry Method

Early spacesuits almost exclusively used a zipper entry method. This design creates a low-bulk suit entry while integrating well into all soft suits of the time. The zippers used were heavy-duty zippers usually used in parallel, with one zipper integrated into the gas-tight bladder of the suit and one in the restraint layer of the suit. Maintenance of the zippers was essential, requiring lubrication and limiting the cycle life of the closure. During the Apollo missions, dust contamination of the zippers became a serious concern, with zippers getting jammed with dust and exhibiting high leak rates. Suits with zippers also required the zippers to be mounted either spiraled around the suit torso or vertically on the back of the suit. The zipper location made donning the suit require some body contortions and the help of an additional ground support or crew member (Ayrey, 2020).

Nevertheless, the zipper entry is still used for many launch and entry suits due to its soft, flexible nature and low mass. For example, SpaceX's suits use a zipper entry, but the zipper is mounted on the interior of both legs and across the crotch (Dodd, 2019). The leg-zipper entry is an adequate solution for suits that do not need much lower-leg mobility.

2.3.2. Diagonal Entry Method

The Litton Mark I was one of the earliest vacuum suits designed to operate in a vacuum chamber for research on vacuum tubes (Young & Avino, 2009). It featured a planar opening that ran from above one shoulder to below the armpit of the other arm as the entry method. These two halves of the suit connect through a bolted interface, compressing a seal to create an airtight suit. This entry method has since found use in several developmental suits, such as the Litton RX-2. While it was effective, this method had some limitations, including restricting the placement and orientation of the shoulder joint, failing to reduce the suit mass, and not allowing for unaided donning and doffing of the suit.

2.3.3. Waist Entry Method

The EMU features a waist entry method where the wearer dons the upper portion of the suit like a shirt and the lower torso assembly like a pair of pants. The two halves of the suit connect using a waist disconnect, which has several advantages. The simple planar closure makes manufacturing the sealing surface straightforward, the closure operation simple, and the additional mass of the closure is low compared to alternative entry methods. This entry method has been used throughout the entire Shuttle and ISS programs.

However, there are some drawbacks to this entry method, primarily when used with a HUT. The issue is that for the wearer to don the suit, the arms must be raised above the head and fed through the scye bearings. For proper donning shoulder posture to be achieved, the angle and location of the scye bearings must be oriented unnaturally, contributing to the injury issues seen with the EMU. Using an additional shoulder mobility element to rotate the scye bearing can allow more natural shoulder postures. Nevertheless, such joints can become an additional failure mode and maintenance item.

2.3.4. Hatch Entry Method

The hatch entry method is when the wearer dons the suit through a hatch mounted on the back of the spacesuit. This entry method was first found use in the Russian EVA suit development program. The micro-gravity suit, the Orlan, was developed in parallel with the lunar suit prototype, the Krechet (Abramov & Skoog, 2003). With these suits, the interior volume of the hatch houses the PLSS. There are many benefits of this system. The rear entry of the suit prevents the compromised shoulder position caused by the donning requirements of a waist entry suit. The hatch entry method similarly benefits from a planar closure. Perhaps the most attractive feature of the hatch entry method is the possibility of use with a suit port system. A suit port system would help significantly prevent backward lunar dust contamination for a lunar surface exploration mission. However, there are drawbacks to the hatch entry method. Since the hatch is likely a standard size, there will be an upper size limit to who can fit through the hatch, limiting the population the suit system can accommodate. In addition, since the hatch

must be large enough to accommodate the entirety of the target user population, it will be oversized for a large segment of the population. An oversized hatch adds mass and bulk to the system, particularly for smaller individuals.

2.3.5. Dual Planar Entry Method

The dual planar entry method found use as part of the development process for the Apollo application program suits. Dual planar refers to the double-planar nature of the closure. The first half of the closure is similar to the front of a waist closure in that it is mounted to the front of the HUT and wraps around the torso of the suit. The second half of the closure sweeps up the back of the spacesuit and forms an arch that moves up the torso of the suit toward the helmet. There are many benefits of this type of closure. Similar to the hatch entry method, this type of closure prevents the compromised shoulder position needed to don a waist entry suit. Due to the lack of a standard entry hatch, there is a weight/mass benefit with the dual planar entry method over the hatch entry method. Several drawbacks may have been responsible for this suit architecture never being flown. The extreme shape of the sealing surfaces is difficult to manufacture. If dust is a crucial consideration, a hatch system may be more appropriate since the lack of a hatch in this design makes it impossible to integrate into a suit port system.

2.3.6. Entry Method Selection Process and Criteria

In order to create a HUT design framework, first, the general torso architecture of the suit must be defined. The general suit torso architecture is largely driven by the entry method of the spacesuit, as demonstrated above. The optimal suit entry method is, in turn, driven by the mission requirements. Factors such as the mission duration, crew size, and location influence mission requirements and, therefore, suit design. For this study, the HUTs were designed to be integrated into a long-duration (> 30 days) lunar surface exploration mission.

For upcoming lunar exploration missions, the dust tolerance of spacesuits and the impact of dust brought back into the mission architecture's interior will be a significant driving factor. Since these missions will be comprised of U.S. Astronauts and those of allied space powers, the crew selection process will likely be similar to current crew selection regimes. In addition, since planetary exploration missions introduce a reduced gravity environment, the suit's mass will become more of a factor compared to operations in a microgravity environment. Lastly, a planetary mission aims to better understand the geological features of a new celestial planet. Therefore, EVAs will be a much more prominent mission feature than running a space station. As a result, planetary spacesuits will need to have a much longer lifespan/ in addition to the ability to hold up to any effects of the local dust or regolith.

Table 2.3.6-1. Entry Method Trade Space

	Ease of Donning	Durability	Size Range	Dust Mitigation	Weight	Complexity	Total (Micro-Gravity)	Total (Lunar)	Total (Martian)
Hatch	3	3	4	5	2	3	10	27	23
Waist	3	3	5	2	3	3	10.75	19	22
Dual Planar	5	3	5	2	3	2	11.75	20	23
Diagonal	2	3	2	2	3	3	8.25	16.5	18
Zipper	3	1	5	1	5	2	9.25	14	18
Weights (Micro-Gravity)	1	0.5	0.5	0	0.25	1			
Weights (Lunar)	1	1	0.5	3	0.5	1			
Weights (Martian)	1	2	1	1	1	1			

The trade study results indicate that the dual-planar suit entry is optimal for a microgravity suit system. The ease of donning combined with the ability to accommodate a wide range of individuals make this design an improvement over the current waist entry method. For a lunar spacesuit suit architecture, dust becomes much more of a driving force for suit design. Therefore, the hatch entry, with suit-port compatibility, makes this design the choice for upcoming lunar missions. If alternative technologies, such as electrodynamic dust shields, can help solve the issue of dust contamination, other suit designs can and should be pursued as those technologies mature. For a Martian mission, the dual planar and hatch entry methods are on equal footing. The hatch system, once again, offers superior dust mitigation. In contrast, the dual planar entry method can be adapted to fit a more significant population while reducing the suit's weight. Lowering suit weight will be a considerable challenge as Mars will have twice the gravity of the Moon, so suit systems will weigh twice as much.

2.4. HUT Interface and Architecture Definition

For human-in-the-loop testing of a rear-entry hatch lunar spacesuit system, we created several 3D-printed mockup HUTs designed to simulate the system. During testing, the HUTs were

mounted on a HUT stand and included a mockup helmet and EVAA. In addition, they were designed with functional scye bearings, which were installed for all testing purposes.



Figure 2.4.-1. Skeletonized HUT Mockup with Additional Hardware Mockups and Bearings Installed.

The HUT mockups were skeletonized to allow optical tracking of the test subject's torso during testing, assuming that the interfaces such as the helmet ring, scye bearings, and waist interface were the main contributors to limiting the range of motion and potential problematic contact with the spacesuit. Additionally, during some of the testing, the mockups were mounted on a rigid stand to replicate their proper location on a wearer.

2.4.1. HUT Interface Definitions

The HUT is a central component of the spacesuit. It interfaces with several components, including the scye bearings, helmet ring, entry method, and Waist connection. The location and orientation of these interfaces are critical for suit comfort, safety, and functionality.

2.4.2. Scye Bearing Selection

The scye bearing connects the shoulder assembly of the suit to the HUT. A sealed thin-section bearing is ideal for the scye bearing. Sealed bearings provide the required rotational motion while maintaining an airtight seal, and thin-section bearings help reduce the bulk of the suit in critical movement areas such as under the arm and inner chest. To simplify resupply and assembly logistics and reduce the stock of replacement components, a standard bearing size was chosen to accommodate available hardware so that a single bearing size could be used for each test subject.



Figure 2.4.2.-1. Scye Bearing

During human-in-the-loop testing, a functional bearing was installed into the selected HUT. The bearing aided in the rigidity of the HUT while also simulating the additional bulk of the bearing that would affect the range of motion of the human inside the HUT.

2.4.3. Helmet Size Selection

Hatch entry spacesuits are particular, as the back of the helmet must be integrated into the hatch to allow donning and doffing of the suit. As such, the actual “helmet” of the suit is a visor assembly mounted onto the upper front section of the HUT. Typically, the helmet-HUT interface is a planar closure. Because of this, the helmet is a hemispherical shape. The helmet mockup replicated the bubble helmet of the NDX-2. Elliptical hemispherical helmets are beneficial as they allow for more significant head movement on the sagittal plane without taking up too much side-to-side real estate on the HUT, which could require more space between the scye bearings to accommodate a wider helmet.

Once again, similar to the scye bearing, a single size of the helmet was chosen to reduce the number of components needed to be manufactured for this study while also demonstrating the applicability and benefit of such a system in a realized custom suit system, utilizing standard-sized components.

For human-in-the-loop testing, a helmet mockup was used. This mockup consisted of a 3D-printed helmet ring that would attach to the HUT through a series of pegs. On this ring was an

acrylic frame that would replicate the helmet's geometry and limit the head's range of motion while allowing the test subject unobstructed breathing and hearing.

2.4.4. EVAA Size Selection

The EVAA is the visor assembly mounted onto the pressurize-able helmet bubble. Part of the functionality of the EVAA is to house additional shield visors to block harmful light from reaching the eyes of the suit wearer. The complete visor assembly usually includes a reflective transparent visor, which functions similarly to sunglasses, where the outer coating reflects some light and UV rays. In addition, separate opaque shields or blinds are also commonly integrated. These visors block all light over the portions of the visor when deployed.

The EVAA, even without deploying any of the visors, obscures the view from a portion of the helmet. As such, for human-in-the-loop testing, it is essential to replicate this reduction in the field of view. Therefore, for this testing, a 3D-printed EVAA mockup was designed to replicate an EVAA with no deployed visors, intending to limit the field of view of the test subject.

A hemispherical helmet consists of a see-through helmet bubble covering 180 degrees of the helmet's circumference. In rear-entry suits, one strategy is to divide the helmet into thirds. The EVAA covers one-third, while the bottom two-thirds remain open unless the visor is deployed. The reflective visor comprises two nested 60-degree visors extending down to cover the entire view area of the helmet, and a similar visor array is used for the opaque visor.

For the EVAA mockup, the hemispherical helmet size was the primary driver for the mockup EVAA size. The EVAA covers the upper third of the helmet's viewing area to simulate using an EVAA similar to the xEMU visor array.



Figure 2.4.4.-1. EVAAs A: xEMU EVVA prototype B: Mockup EVVA used for HITL testing of HUT mockups.

2.4.5. Hatch Geometry Selection

The standard hatch geometry replicated the Mark III hatch geometry, a baseline design for NASA's surface exploration program, which means that this geometry will likely reflect future surface exploration systems. In addition, this project focuses on the design of a lunar spacesuit HUT. Therefore, the entry hatch should be compatible with a suit port. To ensure compatibility, the hatch geometry had to be standardized across the size range, allowing any suit to fit into any port.

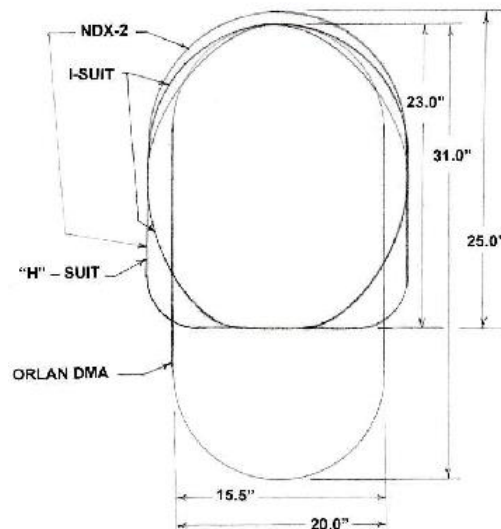


Figure 2.4.5.-1. Various rear entry hatch geometries (de Leon & Harris, 2009)

2.5. Design Methods

Two design frameworks were developed for this study. The first design framework is a standardized discreet sizing system, where a 4 HUT size selection was created to accommodate as much of the population as possible. The second design framework is a custom HUT framework, where the optimal HUT for a given individual is predicted.

Both of these models are built upon a morphing HUT model, a statistical model of the torso shapes of a large general population 3D scan database, and a torso shape-to-HUT shape prediction model. Each design framework can select or design an optimal HUT for a given individual.

2.5.1. Reconfigurable HUT Model

A reconfigurable HUT model is at the foundation of the HUT mockup and the associated custom and standard design frameworks. This model is of the surfaces between all of the interfaces of the HUT. These surfaces comprise complex curves that would be impossible to recreate using

standard solid modeling tools. Due to this limitation, the HUT was designed as a surface model, which was then converted to a solid model through a geometric thickening process.

The HUT model works by morphing a base HUT model into a user-defined configuration. The base HUT model was modeled to represent the rough shape of a rear entry HUT, with the location, size, and orientation of the interfaces roughly in a realistic configuration. This morphing was done to create HUT models of many configurations rapidly. Specifically, the inputs of the HUT morphing tool would specify the target configuration of the HUT's interfaces (helmet, scye bearings, waist, and hatch). Given the interface locations, sizes, and orientations, the morphing tool would deform the base mesh to fit exactly with the specified interfaces. The geometry between the interfaces would be calculated with a Radial Basis Algorithm (RBF). The algorithm calculates the deformed HUT that intersects precisely with the moved interface locations while considering the structure of the original shape when predicting the connecting geometry.

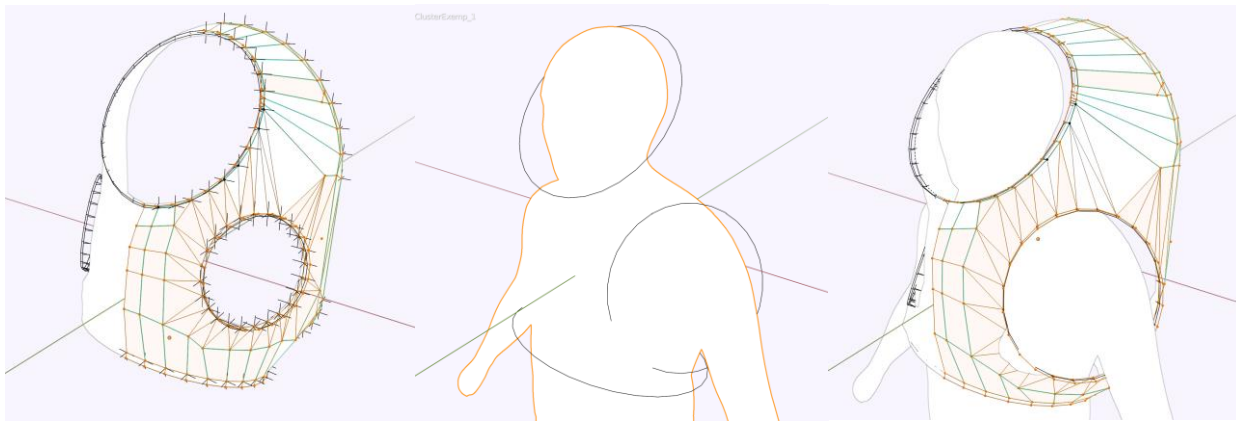


Figure 2.5.1.-1. HUT Geometry Morphing Example. [Left] Base HUT Geometry [Middle] HUT Geometry post morphing [Right] Final HUT Geometry

A generic HUT model was used as the basis for the morphing HUT model. The generic HUT model includes the boundary geometry for the helmet ring, entry hatch, waist connection, and scye bearings. The boundary geometry is marked with several landmarks. A second set of landmarks is generated, indicating where the boundary geometry will be after the morphing process. This second set of landmarks is controlled through several values. For example, the helmet of the generic model was circular and had a specific orientation. The morphed HUT's helmet profile could be stretched into an elliptical shape, resized, and oriented arbitrarily.

Similarly, the scye bearings and waist interface could be reshaped and oriented arbitrarily as needed. The scye bearing was always kept circular to accommodate the rotary bearings. The reshaped HUT's geometry would be solved using the two sets of landmark locations, creating a HUT model that intersects with the final landmark coordinates.

All these manipulations were done on a surface model that ignores material thickness. For the HUT to be manufacturable, the surface model must have a specified thickness. This was

accomplished using a geometry modifier tool that adds thickness to surface models by offsetting surfaces with respect to surface normal.

The surface modeling program generates surfaces but is unsuitable for creating 3D mechanical parts with tight tolerances or exact shapes. Therefore, interface geometry was designed in a parametric solid modeling environment (Dassault Systemes, 2022). The interface geometry was then combined with the thickened HUT surface geometry to form a complete HUT model.

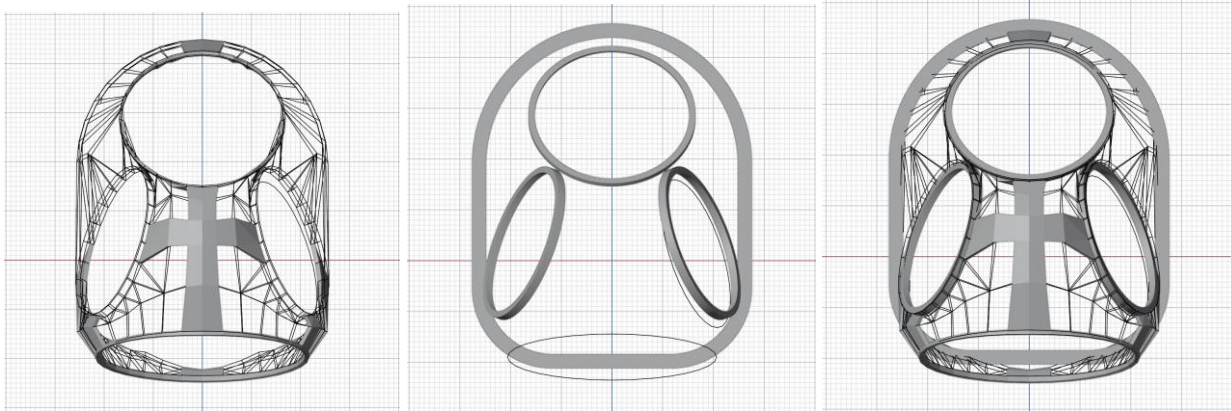


Figure 2.5.1-2. HUT Interstitial and Interface Geometry Morphing Example. [Left] *Skeletonized Interstitial HUT Geometry* [Middle] *HUT Interface Geometry* [Right] *Combined Interstitial and Interface Geometry*

The helmet and EVA, since they were standard sized for all HUTs.

2.5.2. Torso Shape to HUT Shape Model

Once the morphing HUT model was created, there was a need to design a model that would relate torso shapes to optimally fitting HUT shapes. This was accomplished through the creation of a multi-output linear regression model. This model's inputs are the torso PCs of an individual or location in the PC space, and the outputs are the estimated interface locations of the HUT.

A multi-output linear regression model was chosen for use in the model. A multi-output linear regression model is a statistical technique used for predicting multiple dependent variables based on a set of independent variables. It extends the concept of simple linear regression, which predicts a single output variable, to situations where there are multiple outputs of interest. In this case the inputs were a set of torso PCs and the output was the corresponding HUT interface location, orientation, and sizes of what is predicted to be the optimal HUT for that torso shape.

2.5.3. Clustering Analysis

In order to train the multi-output linear regression model, a representative selection of torsos needed to be created so that HUTs could be shaped to fit them; this representative torso

population was created through an affinity clustering analysis of the CAESAR database's torsos (Frey & Dueck, 2007), see Figure 2.5.3.-1. Affinity clustering, also known as affinity propagation, is a clustering algorithm used in machine learning and data analysis. It is a clustering technique that, unlike other clustering methods, does not require the specification of the number of clusters in advance. Instead, affinity clustering automatically groups data points into clusters based on their similarities. It operates by iteratively propagating "affinities" between data points to determine the most representative "exemplars" within the dataset. An exemplar is a data point that serves as the representative or center of a cluster.

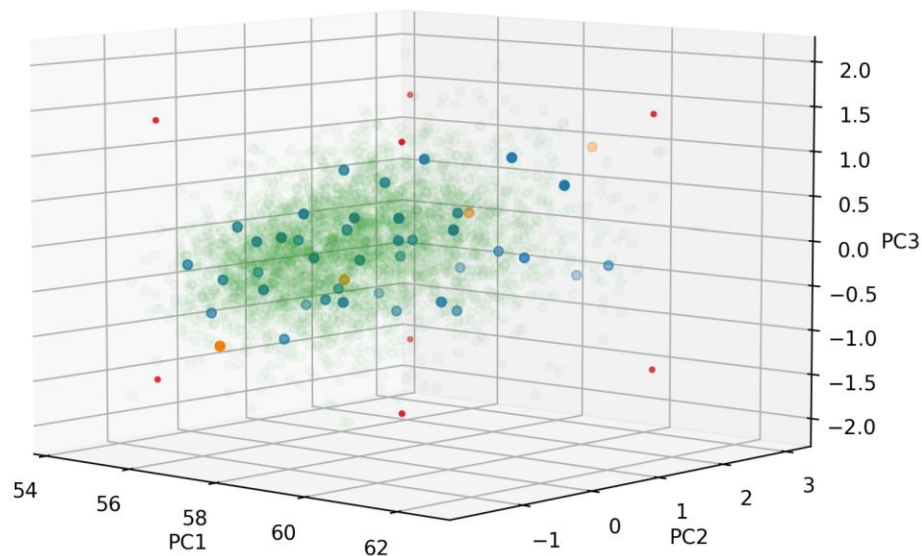


Figure 2.5.3.-1. Torso Shape Principal Component Space. *Green: Caesar Database Subjects, Blue: Affinity Cluster Exemplars, Red: Boundary Mannequin Datapoints, Orange: Torsos Used to Generate Standard HUT Sizes*

Affinity clustering has several parameters that can be tuned to customize the algorithm's output. The preference factor was set to -15 to create a set of 39 individual clusters. Thirty-nine clusters were sufficient to replicate the distribution of the entire CAESAR dataset in PC space while still being low enough for manual sizing of HUTs to each exemplar torso mannikin.

2.5.4. HUT Shape Dataset

The exemplar data points represent a series of torso PCs. These PCs can be transformed into torso mannequins through an inverse PCA transformation. The resulting torsos are synthetic in that they do not represent an actual scan subject but a specific location in the torso PC space of the entire dataset.

These torso mannequins were then visualized along with the morphing HUT model. The morphing HUT model was then adjusted to fit each exemplar mannequin. Three independent

spacesuit sizing experts repeated this process. The result was a dataset of 117 HUT shape/Torso PC combinations.

2.5.5. Historical HUT Fit Rules

To inform the HUT customization process, a summary of historical HUT sizing rules was provided to each of the spacesuit sizing experts. Therefore, a summary of the sizing rules will be given here.

Because all current integrated spacesuit systems used in flight or developmental research have used standardized HUT sizing systems, the rules were written to accommodate marginal fit cases. An example is with the EMU, where the scye bearing is recommended to be at least 1" from the top of the wearer's shoulder. However, when the placement of the head is discussed, it simply states that the head should be placed well in the helmet. This makes sense in a system where the vertical distance between the helmet and scye bearing is either constant or available in several discrete sizes at most. If sizing technicians were given strict sizing rules for shoulder and head placement, satisfying both requirements with a standardized system would be impossible.

The Scye bearings should be located on the wearer's shoulder joint center. This allows the rotational component of the shoulder joint's range of motion to mimic the rotation achieved with the suit's shoulder through the scye bearing. If the scye bearings are too close together, there could be issues donning and doffing the suit, as well as limited mobility due to poor alignment of the shoulder bearing. If the scye bearings are too far apart, the wearer will likely align their torso asymmetrically in the suit to correctly position one of the arms in the HUT and favor working with that side, reducing overall mobility and comfort of the spacesuit.

The correct tightness of the fit of the spacesuit is subjective and, therefore, hard to quantify and describe in a set of rules. However, in general, there should be several inches between the torso of the subject and the HUT, allowing for repositioning of the body in the HUT and the ability for deep breaths. Since this aspect of the fit of the HUT would be in part dictated by the padding thickness selected by the crew, the fit rules just stated to leave several inches between the HUT and the test subject in all areas except the shoulder bearings and immediately surrounding geometry.

There are two schools of thought on HUT-torso contact. One school believes that all contact with the HUT should be minimized, see Figure 2.5.5.-1. The other school of thought believes there should be significant contact between the front of the HUT and the front of the torso of the wearer. Therefore, during the virtual sizing of the HUTs, it was up to the sizing expert to subjectively place the interface locations in such a way as to create what they believed was the optimal overlap between the HUT and the torso.

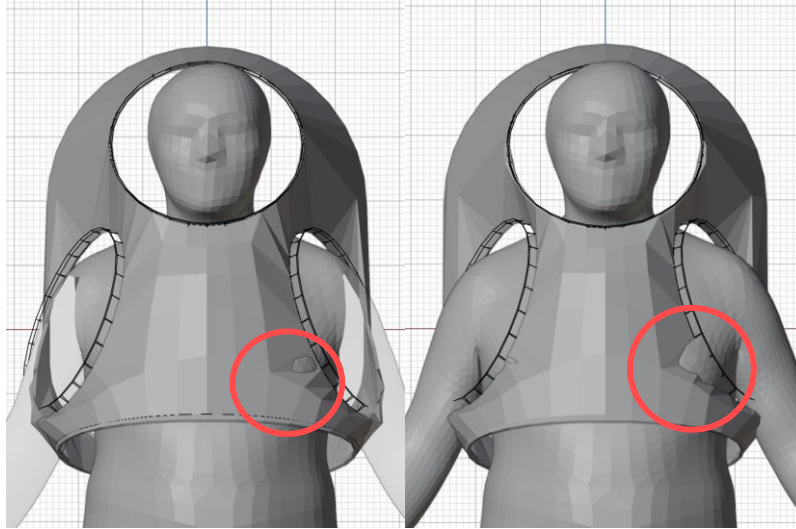


Figure 2.5.5.-1. Examples of different opinions of optimal chest/HUT contact A: Minimal contact, B: significant contact

2.5.6. HUT Space Model

The dataset of 117 exemplar torsos and sized HUTs was used to train a multi-output linear regression model. The locations of the HUT interfaces were collected along with the exemplar torso's PCs and used to train a multi-output linear regression model that predicts the HUT interface locations for any given torso PC combination. Model inputs are the 4 PCs of a selected torso. Model outputs are the various HUT interfaces' location, shape, and orientation. This Torso to HUT shape model is the center of the standard and custom HUT design frameworks.

2.5.7. Standard HUT Design Framework

The goal of the standard HUT design framework is to create a discreet HUT sizing system that can accommodate as much of the general population as possible with as few standard sizes as possible. Previous HUT systems and current developmental suits feature five or fewer available sizes. Therefore, a target of 4 sizes for the standard HUT design framework was chosen to represent the high end of size selections of a suit system used for an extended time.

Table 2.5.7.-1. The number of discreet sizes included in historical standardized HUT sizing systems.

Spacesuit System	Number of HUT Sizes
Shuttle EMU Original Sizing System	5
Current EMU Sizing System	3
Orlan	1
Mark III	2
xEMU	2 (4 with shoulder spacing adjustment)

The use of a standard HUT system offers many logistical benefits. Numerous crew members can use a small number of HUTs, reducing the total number of manufactured components and operation complexity needed to provide each EVA astronaut with their HUT for the mission. Additionally, manufacturing the suit components is simplified and can be carried out well before the actual use of the parts.

2.5.8. Optimization of a Standard HUT System Size Distribution

The distribution of the discreet HUT sizes was optimized to accommodate as many individuals of the general population as possible, using four standard sizes. To accomplish this, the CAESAR dataset’s torsos were segmented into different groups that would fit into each HUT size. Different segmentation techniques were investigated with very different distributions of the standard sizes.

One of the methods of attempting to segment the torso dataset was using a K-means clustering algorithm. A K-means algorithm is an unsupervised machine-learning algorithm that segments a dataset into a selected number of clusters (Frey & Dueck, 2007). These clusters have equal variance. While the CAESAR dataset has a wide distribution of torso shapes, there is also a high concentration of scan subjects with torsos located at the center of the distribution. Therefore, when the data is clustered to minimize the cluster variance, these cluster centers will be located near the center of the entire distribution, far away from outlier torso shapes. This discreet sizing distribution could maximize the level of fit the system could provide for a good portion of the population while sacrificing the ability to accommodate individuals with torsos further away from the average torso shape of the entire population.

Table 2.5.8.-1. HUT sizes, percentiles, and Z scores.

	Small	Medium	Large	Extra Large
PC1	12.5 (-1.5)	37.5 (-0.3)	62.5 (0.9)	87.5 (2.1)
PC2	12.5 (-1.6)	37.5 (0.1)	62.5 (1.4)	87.5 (2.8)
PC3	12.5 (-2.0)	37.5 (-0.7)	62.5 (0.6)	87.5 (1.9)
PC4	12.5 (-2.0)	37.5 (-0.7)	62.5 (0.6)	87.5 (2.0)

Instead, the torso PC space was segmented geometrically along an axis running from the stacked 0.5th percentile location to the stacked .99.5th percentile location. The torsos used to generate the HUTs were the stacked 12.5th percentile, 37.5th percentile, 62.5th percentile, and 87.5th percentile locations, see Table 2.5.8.-1. This was chosen to ensure that even the extremely small and large stacking conditions would be accommodated with the standard HUT system, see Figure 2.5.8.-1.

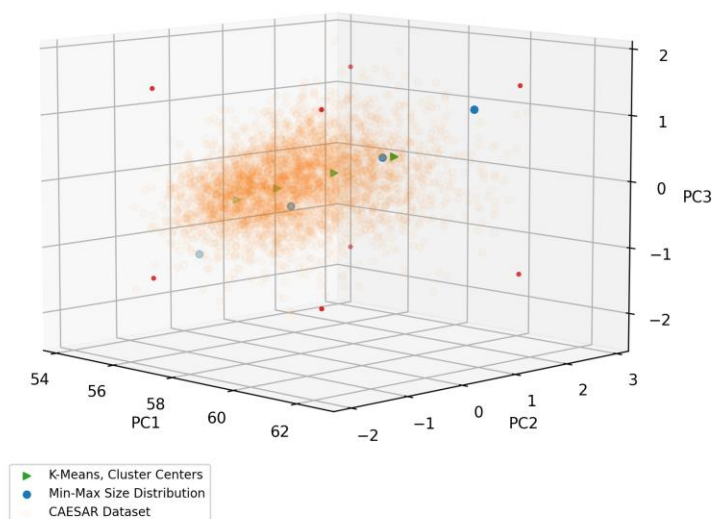


Figure 2.5.8.-1. Standard HUT Size Selection Process, K-means vs. geometric segmentation

2.5.9. Method for Generating Standard HUTs

The Standard HUTs were generated using specific torso PC combinations from the geometric segmentation of the PC space. The PC combinations were used to generate four synthetic torso shapes through an inverse transformation operation. Then, HUTs were generated to fit these torsos, becoming the four standard HUT sizes for the standardized design framework. HUT recommendations can be made by determining how far away any given individual's torso shape is from the synthetic torsos used to generate the HUTs in the PC space. Further, fit checks are needed to ensure that the individual fits in the HUT, as the closest HUT in the PC space may be too small.

2.5.10. Custom HUT Design Framework

The Custom HUT design framework utilized a 3D scan of an individual. From this scan, the torso vertices were segmented out and transformed into a PC combination. This combination was used to predict the optimal interface locations through the HUT shape model. Further minor adjustments were made if needed to ensure proper shoulder bearing clearance.

Subjects were scanned using a hand scanner while posed in a standard A-pose. The scanner was a COTS LIDAR scanner with a resolution of up to 0.2mm. During the scan, subjects wore non-synthetic fiber scan-wear. The raw scan data was processed through the same vertex homologation process detailed above, resulting in an individualized scan in the standard vertex layout.

During the vertex homologation process, the vertices of the torso were grouped. The torso PCA performed previously was then used to translate the torso vertex's locations into a set of torso PCs. These PCs describe the subject's torso shape in terms of the CAESAR dataset's torso PC

space. The subjects PCs were then used as input for the torso shape to HUT shape model, predicting the ideal HUT for the subject.

The HUT was then overlaid with the homologated scan of the subject, with the subject's head placed correctly in the helmet interface of the HUT. The vertical position of the scye bearings was then adjusted to ensure a 1" gap between the top of the shoulder and the interior of the scye-bearing interface of the HUT.

2.6. Results

2.6.1. Implementation of the Standard and Custom Design Frameworks

To implement both design frameworks, the torso shape of the test subject needs to be analyzed and located in the CAESAR database's torso PC space. This was done by scanning the test subject. 3D scans of test subjects were taken using an Arctec Leo handheld 3D scanner. The Arctec Leo works by flashing structured light onto the scanned test subject and taking images. The scanner's location is recorded for each image, allowing the images to be used to triangulate landmarks on the object resulting in a point cloud outline of the object. This data set can then be processed using Arctec Studio 6, resulting in a 3D scan of the test subject in a standard file format.

Subjects were posed in a neutral posture to replicate the posture used for the CAESAR database. In addition, posing aids were used to help support the subjects' arms throughout the scan.

The ho-model used to convert the CAESAR database was then deformed to match the raw scan data through a non-rigid ICP algorithm. This process accomplished several things. First, it filled any gaps there may have been in the 3D scans. Second, it converted the scan to a structured vertex layout, including segmenting the torso's vertices for further analysis. Lastly, the process reduced the resolution of the scan, de-identifying the test subject, see Figure 2.6.1.-1.

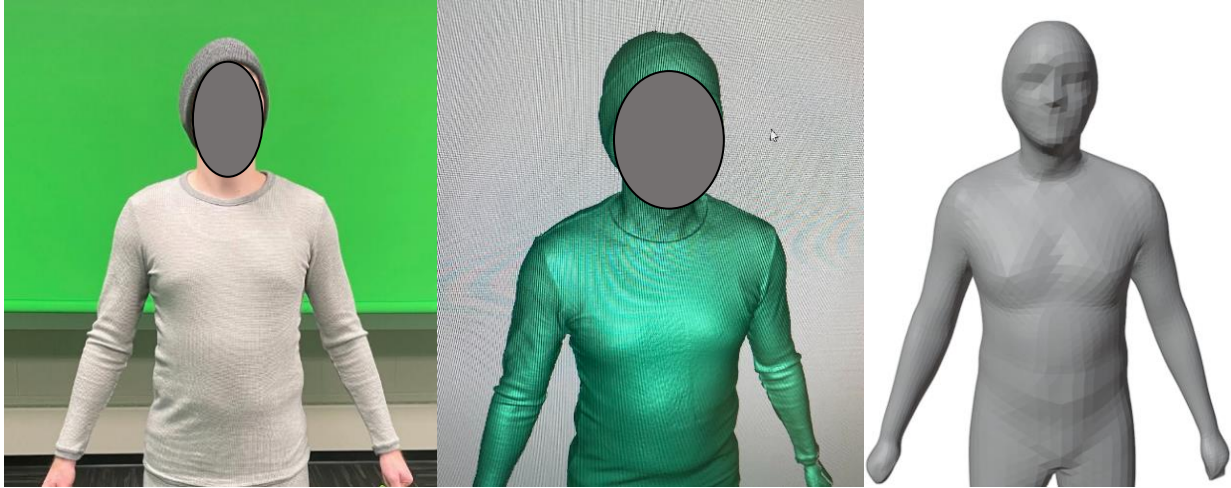


Figure 2.6.1-1. Scan Processing. A: Test subject, B: 3D scan data, C: Ho-model deformed to fit 3D scan data.

The scan's torso vertex layout can then be used to calculate the test subjects' torso principal components, relating their anthropometry to the entire CAESAR dataset population. These principal components can then be used in the custom and standardized design frameworks detailed above.

2.6.2. Design Framework Limitations

While this was the first attempt to utilize this type of torso shape analysis in developing custom and standardized HUT design frameworks, there are many shortcomings and room for further development. First, the CAESAR scan database had the scan subjects hold an "A" pose for scanning. While this is a good standard pose and easily repeatable, it does not replicate the body's posture when in a suit. Often the bulk of the suit's HUT forces the arms away from the torso. A pose that holds the arms up higher such as a "T" pose or arms forward pose may better replicate the postures frequently seen in a spacesuit which could improve the HUT design frameworks.

Second, the torso to HUT shape model was entirely based on the opinion of 3 spacesuit sizing experts, and not HITL. If time and resources were not a concern, the model could be improved by integrating user feedback on specific torso and HUT combinations so that the model could be fine-tuned to better predict the actual ideal HUT shape for any given individual.

Design Evaluation 1: Subject Fit Survey

“I knew I was alone in a way that no earthling has ever been before.”

– Michael Collins

3.1. Study Goals

Poor spacesuit fit also can lead to other problems decreasing suit fit, comfort, and mobility. For example, the poor fit of spacesuits can lead to a reduced range of motion in the suit. This restricted range of motion can limit the usability of a suit and result in the wearer employing different methodologies for moving spacesuit limbs, such as the asymmetric placing of their body in the suit or generating counterforces with other parts of their body to actuate a limb. To determine the effect of HUT shape in spacesuit fit, subjects were given a subjective fit survey after each HUT evaluation. The subject survey asked subjects to evaluate the HUT's feature alignment, discomfort, and indexing. This survey will give insight to the subject aspects of HUT fit.

3.2. State of the Art: Spacesuit Fit Assessment

Suit fit is the combination of a number of different factors. These include how well the functional components of the suit align with the body of the wearer, whether or not the suit causes any discomfort during use, and how much space there is between the suit and the body of the wearer. The various HUTs tested by the subjects were evaluated on the basis of these subjective metrics.

3.2.1. Feature Alignment

Feature alignment refers to how well-placed the spacesuit's features are relative to the wearer's body. The alignment of these features is critical to the spacesuit's fit, comfort, mobility, and safety. Critical features that should be well aligned are the scye bearings, helmet, and waist interface.

When the HUT is optimally shaped, the scye bearings of the HUT should be centered on the center of the wearer's shoulder joint. This allows for the spacesuit arm to rotate with the wearer's arm. There also should be a gap of at least 1" from the top of the shoulder and the inside of the scye bearing. This is to accommodate the rotation of the scapulothoracic joint when the arms are raised. Lack of this gap will cause hard contact between the shoulder and the scye bearing when the arm is raised above a horizontal position.

The lateral placement of the scye bearings relative to the subject is also essential. When the scye bearings are placed too close together, donning the HUT can be impossible, as the shoulders need to fit between the bearings to enter the HUT. Conversely, if the scye bearings

are spaced too far apart, the scye bearings can limit the range of motion of the shoulder joint. As discussed, the wearer may attempt to correct this issue through the asymmetric placement of the torso in the HUT.

The orientation of the scye bearing can be used to improve the fit and mobility of the spacesuit. The scye bearing is typically tilted relative to the sagittal and transverse plane. The tilting of the front of the bearing towards the sagittal plane improves the internal transverse shoulder range of motion as the distance between the front of the bearings is reduced. This tilting also increases the distance between the back of the bearings, allowing for the arms and shoulders of the suit to be donned easier. The bearings are also tilted relative to the transverse plane for similar reasons. This tilting increases the overhead reach mobility of the suit and allows for the suit to be doffed through a waist disconnect if needed, see Figure 3.2.1.-1.

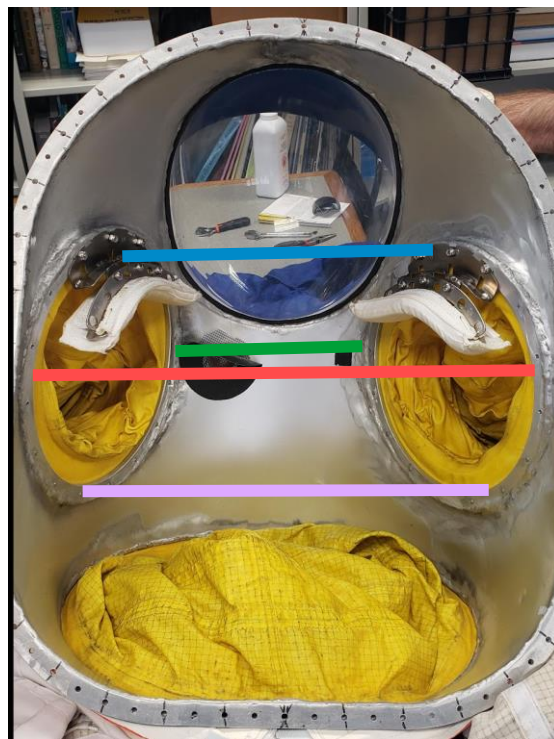


Figure 3.2.1.-1. Demonstration of typical scye bearing orientation for rear entry hatch spacesuits.

Proper placement and orientation of the head in the helmet are essential for the wearer to have an adequate field of view. The ability to see their surroundings and work area is critical for situational awareness, safety, and mission effectiveness. The helmet view area comprises a section of a spherical or elliptical bubble. This view area extends below the transverse plane of the helmet. This is important as it allows the wearer to look down at the DCU and, ideally, view their feet. The head must be centered in the helmet so that the total view area can be utilized and the space inside the helmet for head movement can be maximized.

If the proper location of the head in the helmet of the spacesuit and the shoulder inside the scye bearings is essential, it follows that the proper location of the helmet relative to the scye bearings is also essential for proper spacesuit fit. If there is a significant mismatch between the vertical and fore-aft position of the spacesuit components and the wearer's body, the suit will fit poorly. If the body's position is optimized for the head or shoulder positioning in the suit, the other element will be poorly located in the spacesuit.

In an integrated suit system, the waist geometry would be dictated by the design of the brief section of the suit. Generally, the waist interface would have an elliptical cross-section and be tilted relative to the coronal plane. Ideally, this interface would be as high as possible, accounting for the hatch and scye-bearing interfaces, see Figure 3.2.1.-2.



Figure 3.2.1.-2. Location of waist interface on a rear entry suit.

3.2.2. Discomfort

Discomfort refers to either hard contact with the spacesuit or the discomfort resulting from the suit forcing the body into an unnatural posture. Typically, minor suit-related discomfort can be self-mitigated by adjusting posture inside of the suit. However, long-lasting or high-level discomfort or pain over time can indicate dangerous suit fit issues. Ensuring a good suit fit minimizes the discomfort felt while in the suit and prevents developing acute or chronic suit-related injuries.

3.2.3. Indexing

The space inside the HUT allows the wearer to breathe normally, shift inside the suit, and comfortably operate the suit. If there is not enough space, the suit can be uncomfortable and hard to don. Conversely, too much room limits suit mobility and can likewise be uncomfortable. The ideal indexing for a suit varies from person to person. Some will prefer to feel tightly

enclosed in the suit; others like to have lots of space in the suit so that they can re-adjust their in-suit posture throughout the EVA. Even with this variability, suit indexing extremes should be avoided, such as having the HUT so small that it is difficult to don or being so large as to complicate moving the suit with the wearer's body.

3.3. Assessment Methods

Twelve subjects (10 males and two females) participated in physical fit and evaluation tests. The subjects' stature was 185-156cm, corresponding to the 96th to 14th percentile of the US Army-defined ANSUR population¹⁴. Before testing, the subject signed the consent form approved by the Institutional Review Board of the University of North Dakota. Each test subject tested at least 2 HUTs, including their custom and standard-sized HUT. Standard HUTs were selected based on the closest neighbor search, namely the standard HUT, which is the distance between the test subject's torso in the PC space and the torsos used to generate the standard HUTs. If, for some reason, the closest HUT was not suitable, for example, in case the HUT was too small for the subject to fit, the next closest HUT was chosen to be their closest suitable HUT, and the third closest was chosen to be their second closest suitable HUT. The criteria for being too small was the inability to don the HUT. If the subject noted excessive room in the previous smaller HUT that would only be increased by increasing HUT size, the HUT was considered too large and not included in the HUT evaluations.

For subject testing, the HUTs were mounted onto a static test stand, which was done to simulate a HUT held in place relative to the torso. It also allowed for the repeatable placement of the test subject within the HUT. The test subject's torso midline was first aligned with the mid-sagittal plane of the HUT, and then the HUT position was adjusted in the up-down axis such that the test subject's head was centered in the helmet. The head location was chosen as a design reference point to show the effects of vertical and horizontal helmet/scye distances. In addition, a single neck ring and helmet size were chosen, as including multiple helmet sizes would have made the variable design space too large. The HUT testing order was randomized across the subjects, and approximately half of the subjects started with the custom HUT.

Motion capture was used to record the movements of the test subjects in each HUT condition. The subjects were also asked to repeat the same type of motions in a shirtsleeve environment, and the corresponding motions were recorded. Each subject was asked to perform the following motion tasks: single-handed and double-handed reach envelope (Figure 3.3.-1. A). Retro-reflective markers were attached to plates attached to the test subject's torso and upper extremities to trace the joint center positions at 50 frames per second (Figure 3.3.-1. B).

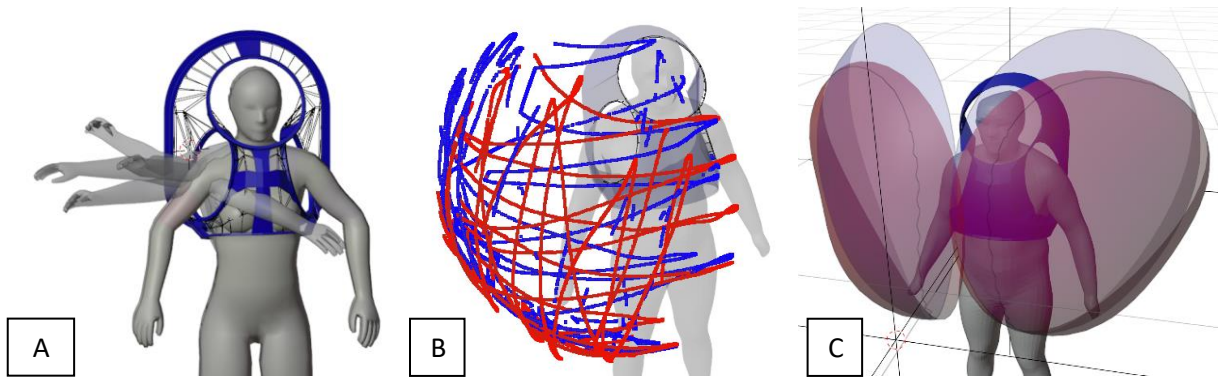


Figure 3.3.-1. A: Illustration of sweeping arm motions for reach envelope estimations, including side-to-side and up-down extremes, B: Right arm reach envelope hand traces, with the red trace representing standard HUT condition and blue trace custom HUT condition. C: Reach envelopes abstracted from the hand motion traces. Red envelope: standard HUT condition. Blue envelope: custom HUT condition.

After each HUT was tested, test subjects were asked to complete a fit survey (Figure 3.3.-2.). This survey was designed to record the subjective perception of the feature alignment of the HUT and any discomfort felt on different body regions caused by contact with suit components. The survey specifically asked subjects to report the perception gained throughout the testing and indexing of the HUT. Each question was answered on a five or 7-point scale. This survey was based on a previous study by NASA (Jarvis, Norcross, & Abercromby, 2017) (see Appendix 2). The 5-point scales (feature alignment) go from 1-5, with one corresponding with the best case. The 7-point scales (indexing) go from -3 to 3, with 0 corresponding with the best case.

A	Discomfort					Feature Alignment					B	
	None	▶	▶▶	▶▶▶	Severe	Ideal	▶	▶▶	▶▶▶	Worst Case		
Head	<input type="radio"/>											
Neck	<input type="radio"/>											
Upper Torso	<input type="radio"/>											
Lower Torso	<input type="radio"/>											
R-Shoulder	<input type="radio"/>											
L-Shoulder	<input type="radio"/>											
						Indexing					C	
						Too Small	▶	▶▶	▶▶▶	Too Large		
						<input type="radio"/>						
						<input type="radio"/>						
						<input type="radio"/>						
						<input type="radio"/>						

Figure 3.3.-2. Subjective spacesuit fit survey, A: Discomfort survey field, B: Feature alignment survey field, C: Indexing survey field

3.4. Results

The hand traces from a subject measured for reach envelope estimations are illustrated in Figure 3.3.-1. B. The standard and custom HUT condition is represented with the red and blue lines, respectively. The trace was first cleaned for missing markers, then fitted with the half-sphere template, of which the shape and size were parametrically adjusted using the radial basis function to best match with the 3D coordinates of the traces. Once the envelope for the

right hand was estimated, the envelope geometry was mirrored to create the left-hand reach envelope (Figure 3.3.-1. C) virtually. As a result, the size of the right-hand reach envelope is 77 cm height, 164 cm width, and 107 cm depth for the standard HUT condition and 87 cm height, 157 cm width, and 119 cm depth for the custom HUT condition. Thus, the overall size of the envelope is substantially increased, especially in the up-down and front-back direction, by 10 cm and 12 cm, respectively.

For the survey fields related to discomfort (Figure 3.3.-2. A), the data was converted into a binary discomfort/no discomfort level, divided at the threshold level 1.0, and calculated for a discomfort rating proportion (i.e., discomfort response count divided by total response count). The summary is listed in Table 1. It was observed that the discomfort was reported from about 27% (43 out of 159) of all ratings for both custom and standard HUT combined. However, the proportion of discomfort was smaller for the custom compared to standard HUT trials (2% vs. 25%). The shoulders (0% vs. 65%) and head (8% vs. 50%) show the most pronounced differences in discomfort ratings for the custom HUT.

To determine the statistical significance, the odds ratio was calculated for observing a discomfort report in different body regions. 95% confidence intervals were also calculated. With the definition of odd ratio, the standard HUT was determined to induce significantly more discomfort ratings than the custom HUT at $p < 0.05$. This was determined by checking if the corresponding 95% confidence interval does not include 1.0 within. The head, upper torso, and shoulder all indicated a significant increase in discomfort ratings in the standard HUT trials vs. the custom HUT trials. However, neck and midsection regions did not reach statistical significance.

Table 3.4.-1. Comfort rating statistics by standard and custom HUTs; CI: Confidence Interval

	Head		Neck		Upper Torso		Midsection		Shoulders	
	Custom	Standard	Custom	Standard	Custom	Standard	Custom	Standard	Custom	Standard
No Discomfort	11	10	10	14	12	15	11	14	12	7
Discomfort	1	10	2	6	0	5	0	6	0	13
Discomfort Rating Proportion (%)	8%	50%	17%	30%	0%	25%	8%	30%	0%	65%
Odd Ratio (95% CI)	9.31 (1.36, 260.63)		2.02 (0.36, 17.78)		34.87 (7.56, 820.96)		4.12 (0.55, 118.36)		192 (42.23, 4509.51)	

Table 3.4.-2. Mean (standard deviation) of feature alignment and indexing survey responses.

	Feature Alignment (Scye Bearing)	Feature Alignment (Waist)	Feature Alignment (Helmet)	Front-to-Back Spacing in HUT	Side to Side Spacing in HUT	Shoulder Volume Spacing in HUT	Space for Deep Breathing
Standard HUT	1.45 (1.12)	0.70 (0.84)	0.85 (0.96)	0.15 (1.11)	0.10 (1.18)	0.10 (1.18)	-0.10 (0.62)
Custom HUT	0.45 (0.67)*	0.65 (0.91)	0.25 (0.43)*	0.10 (0.94)	-0.10 (0.70)	-0.15 (0.48)	0.00 (0.00)

“*” Star indicates a statistically significant difference between custom and standard HUT at $p < 0.05$.

The survey responses for feature alignment and spacing (Figure 3.3.-2. B & C) were coded in a way that the median rating was coded as 0 and the leftmost and rightmost ratings as -3 and 3, respectively. Positive ratings indicate “too large,” and unfavorable ratings are “too small.” The descriptive statistics were summarized in Table 2, and the statistical significance was determined using a paired t-test. For feature alignment, a single-tailed t-test was used as the goal was to detect an increase or decrease in the ratings, whereas, for spacing, a two-tailed t-test was used, which can detect the change regardless of the direction. Overall, ratings converge to 0 (“neither too large nor small”) with custom compared to standard HUT, indicating improved feature alignment and spacing with the custom HUT. However, other ratings did not show significant differences.

Table 3.4.-3. Table 3. Summary of discomfort ratings by body regions and statistical significance testing

		Shoulder	Midsection	Head
Mean (Standard Dev.)	Custom HUT	0.00 (0.00)	0.14 (0.38)	0.00 (0.00)
	Closest Standard HUT	1.14 (1.46)	0.71 (1.25)	1.00 (0.82)
	Second Closest Standard HUT	1.29 (1.38)	0.57 (0.56)	0.57 (0.54)
Chi-Square Value		6.10	2.92	8.59
P-Value		0.05*	0.23	0.01*

*: The difference between custom and standard test cases reached statistical significance at $p < 0.5$.

Each subject was given up to two standard HUTs. The second HUT was the second closest standard HUT to their PC scores. The distance in PC space was calculated by calculating the linear distance between the PC score coordinates representing the subject and the standard torso shapes (i.e., torso shape used for standard HUT generation). The subjects’ ratings were separately evaluated and statistically tested. Figure 3.4.-1. summarizes the responses from the discomfort survey (Table 3) for the closest and second closest HUT, along with the custom HUT. The responses were coded so that 0 represents no discomfort and 4 represents maximal discomfort. Overall, the histograms show that custom HUT tends to be associated with less discomfort (i.e., more survey scores distributed close to 0) compared to standard HUTs, both closest fitting standard sized HUT (determined by torso PC distance) and second closest fitting standard sized HUT. In addition, the distribution shows that the overall trend in responses showed a clear benefit in discomfort in the custom HUT trial condition. The statistical significance was determined using a Friedman test, which shows a significant improvement in HUT comfort in the shoulder and head.

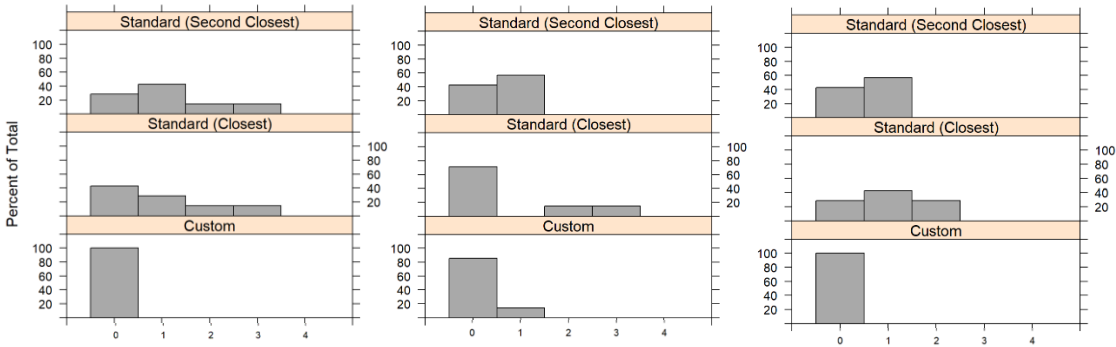


Figure 3.4-1. Percent of subject responses for scye bearing-shoulder feature alignment, helmet-head feature alignment, and shoulder discomfort.

3.5. Discussion

Analysis of the fit survey shows that discomfort was reduced in the head, upper torso, and shoulder regions when a customized HUT system was used. In addition, the feature alignment of the scye bearings and the helmet were significantly improved through a customized HUT system. Although this outcome should be interpreted with caution due to the short duration of testing completed (less than 15 minutes spent in any one HUT), there was a noticeable impact of HUT shape on the fit and comfort of the HUT.

The placement of the helmet relative to the scye bearings, if misaligned with the subject's body, can cause discomfort. For example, if the vertical distance between the interfaces is too small, either the head or shoulder placement in the HUT will be compromised, resulting in the head contacting the top of the helmet (Figure 3.5.-1. A) or the arm pit contacting the bottom of the scye bearing, creating a sense of discomfort. Conversely, if the vertical distance between the interfaces is too large, either the head or shoulder placement in the HUT will be compromised, resulting in the head being placed too low in the helmet or the scye bearing, limiting vertical movement of the arm, and creating hard shoulder contact due to scapular motion (Figure 3.5.-1. B).

The fore-aft alignment of the scye and helmet interfaces is also essential for HUT fit. If the distance is too small, the head or face can have uncomfortable contact with the inner surface of the helmet, forcing the subject into an unnatural posture or shoulder motion can be limited (Figure 3.5.-1. C). Conversely, if the distance is too large, the head can contact the back of the helmet or force the subject into an unnatural posture (Figure 3.5.-1. D).

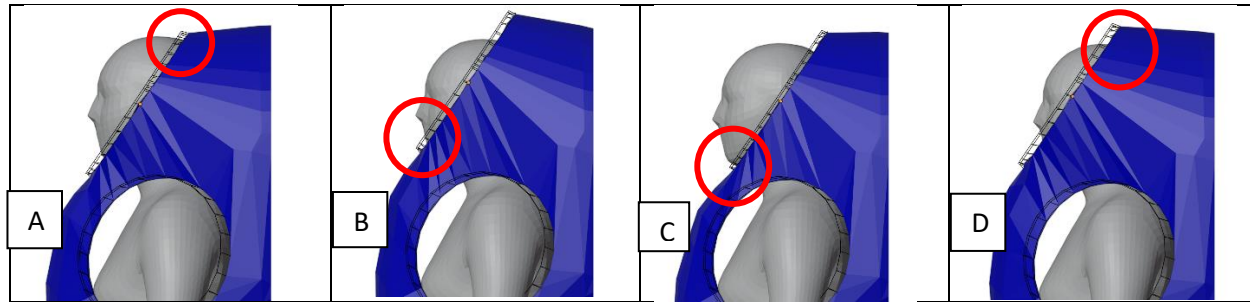


Figure 3.5.-1. Common HUT sizing issues. A: head contacting with the top of the helmet due to poor vertical helmet-scye distancing. B: chin contacting with the neck ring due to poor vertical helmet-scye distancing. C: chin contacting with the neck ring due to poor horizontal helmet-scye distancing. D: head contact with the top of the helmet due to poor horizontal helmet-scye distancing.

Interestingly the survey results indicated that perceived spacing was not significantly different between custom and standard HUT trials, regardless of the specific body regions. This may be due to the body primarily interacting with the scye bearing and the spacesuit helmet when mounted to a test stand. An integrated suit system may use padding, the thickness of which would be chosen by the crewmember to match their preference. The ideal spacing in the suit is subjective, with some crewmembers preferring a tighter or looser fit of the suit.

There are limitations to this study. One assumption is that the standard HUT system was designed to maximize accommodation across the population at a minimal cost. The result is that the standard HUT system was distributed in the torso PC space to fit extreme and more frequently seen torso shapes using a finite number of HUT sizes. Intuitively, the mobility and comfort metric would impair as the wearer's body size and shape are more different from the body each standard HUT was targeted in design. However, the specific patterns and trends of the degradation have not been identified in the previous studies, and it was also outside of the scope of this work. This issue probably needs to be addressed in the future once more sensitive and specific test tools and metrics are identified.

Additionally, this study looked at the HUT in isolation to determine the specific effect of the HUT shape; in reality, there will be compounding effects of the HUT shape in an integrated suit system. The mobility characteristics, such as the range of motion data presented in this study, can be different depending on the specific shoulder joint configuration and mechanisms for example. The HUT shape may be even more important in a complete suit as the colocation of the shoulder bearing may be critical for the proper function of the spacesuit arm.

In this study, only one pose, namely neutral standing, was considered for body shape analysis and HUT design variables. The intent was to replicate the pose available in the CAESAR database, but the shape of the shoulders and other body regions can likely change significantly with different poses; thus, the primary metrics of this study, such as indexing, comfort, and mobility, can vary accordingly. This issue needs to be addressed in future studies with a body shape database with more different poses. In addition, given the short duration of the test, the interpretation of the outcome, for example, comfort or discomfort, might be limited. This study

was intended to compare the comfort/discomfort between the standard and custom HUT, and for this goal, the test conditions and metrics were kept consistent across the two HUT types, such as test duration, procedures, and metrics. Although none of the subjects had experience wearing a pressurized spacesuit, the repeated measurement design of this study is believed to provide a valid comparison between the HUT types. A standard helmet and scye-bearing diameter were used for all the HUTs. This was done to enable the use of available hardware. However, to make the custom HUT genuinely customized for the individual body shape of the crewmember, these components also need to be individually customized.

3.6. Conclusion

The torso of the spacesuit is a critical component in determining the suit's fit, comfort, and mobility. Current suit systems, namely a discrete sizing scheme as with the standard HUTs in this study, benefit from the logistical advantages of modular spacesuits, such as the accommodation of many individuals with a finite set of suit components. However, with the use of a modular system, there is inevitably a difference between the individual wearer from the “nominal” body shape each of the modular size designs was aimed to fit. This gap ultimately results in a suboptimal fit of the suit for many individual wearers, and the overall fit of the crewmember population may not be at a desirable level.

The next era of space exploration and the growth of commercial space travel will see the adoption of new advanced spacesuit systems. As launch costs decrease, mission complexity and duration increase, and the diversity of astronauts grows, custom spacesuits could become attractive for optimizing spacesuit fit, comfort, and mobility. As seen here, the customization of spacesuit HUTs affects the comfort of the spacesuit. This study also demonstrated mobility improvements with custom HUTs, although population-wide fit and accommodation still need to be proven in the future. Additive manufacturing enables custom spacesuits to offer some of the logistical benefits of modular suit systems, including rapid production and sizing of suits to individuals and cost savings compared to conventional manufacturing techniques. Additional work needs to be done to develop the spacesuit sizing system as in this study and to examine potential benefits for future missions.

Design Evaluation 2: Mobility Testing

“By the way, I dislike the term "spacewalk." To me, "walk" is something you do on the ground using your legs. "Float" or even "swim" would be closer, but a new verb is needed. Even NASA's phrase "EVA" (for Extra-Vehicular Activity) is not very satisfactory, and they use it both for "spacewalks" and activities on the Moon.”

-Michael Collins.

4.1. Study Goals

Spacesuit mobility is critical for the completion of EVAs. The final mobility of the spacesuit results from a complex interaction between individual flexibility, suit design, suit fit, and pressurization. The evaluation of spacesuit mobility has evolved with the field of suit design and has always been a critical component of suit testing. In this study, spacesuit mobility was evaluated by measuring the motion characteristics of the HUTs, including range of motion and reach envelopes. The measured patterns will be compared between the custom and standard design HUTs to define the respective mobility performance.

4.2. Methods

The same HUT and subject conditions were used as described in Chapter 3.

4.2.1. Motion Capture System

Human-in-the-loop testing was done at the University of North Dakota's BiPED Laboratory (the Bi-PED Lab), see Figure 4.2.1.-1. This lab has a motion capture volume outfitted with a Vicon system using 10 IR cameras. The cameras were configured to capture the full range of movements from the test subjects and to track the trackers mounted on the subject's chest.

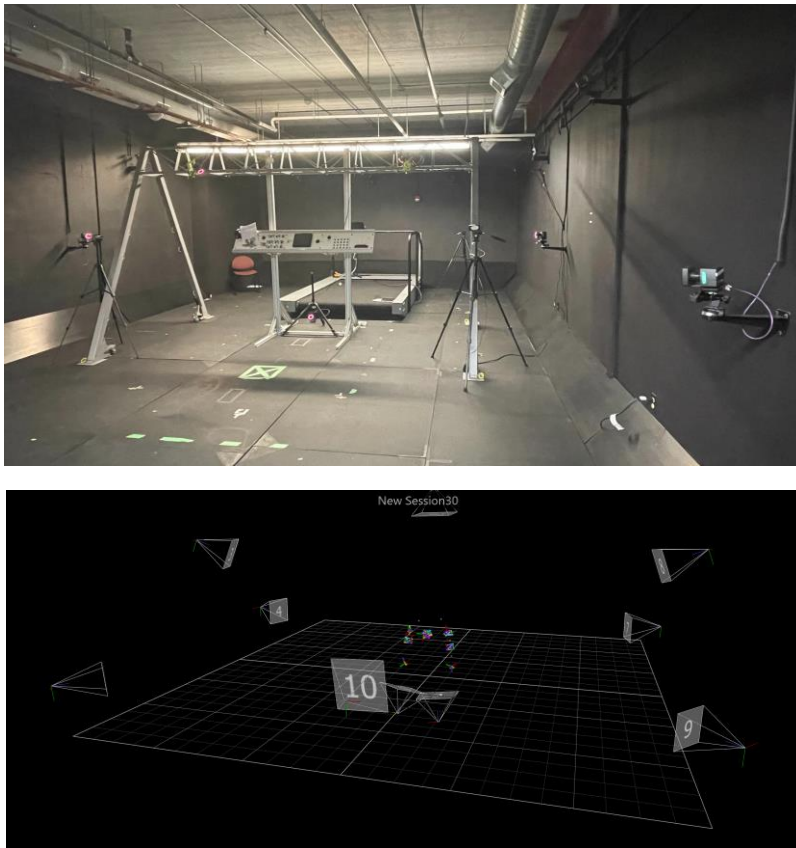


Figure 4.2.1.-1. BiPED Laboratory VICON Motion Capture Volume

Vicon motion capture systems are used in various applications, including biomechanics research, animation, and sports performance analysis. The system consists of several key components, including the cameras, the marker tracking software, and the computer processing hardware. The markers used in the Vicon system are small, reflective spheres that reflect light back to the cameras.

For this study, the markers were magnetically placed on several plates fixed onto the subject's body with Velcro. Each upper and lower arm segment of the subject had a plate attached with 6 markers. Each hand had a plate with 4 markers. The torso had a plate with 8 markers, see Figure 4.2.1.-2. The number of markers allowed for tracking of plate location and orientation even in the instance of a number of trackers missing due to occlusion or other issues. This system was initially developed for use with pressurized suit testing. In this case, no trackers were placed on the HUT.



Figure 4.2.1.-2. IR Motion Capture Tracker Plates. [Left] suited tracker system [Right] shirt sleeve tracker system.

The Vicon system records the location of each tracker at a rate of 50 frames per second. The raw motion capture data is then processed using several labeling pipelines that identify the various limb segments and calculate the associated joint centers. Gaps in the data were filled using rigid body, cyclical, and pattern gap-filling techniques. Using these joint centers, the angle between limb segments projected onto the planes of the body can be calculated.

4.2.2. Protocol 1: Range of Motion

To test the subject's range of motion in the different HUT conditions, subjects were asked to perform several movements, each for 3 repetitions, in a shirtsleeve environment and wearing the HUT mockups.

Table 4.2.2.-1. Shoulder Movements Used to Determine Range of Motion

Pose	Description		Pose	Description	
Flexion	The arm is raised as high as possible to the front of the body.		Adduction	The arm is lowered on the coronal plane and moved inward to the maximum extent.	

Extension	The arm is lowered and moved backward as far as possible.		Internal Transverse Rotation	The arm is raised parallel to the ground and rotated inward across the body.	
Abduction	The arm is raised laterally to the side on the coronal plane as high as possible.		External Transverse Rotation	The arm is raised parallel to the ground and rotated outward from the body.	

*Note: Shoulder Convoluters were not used during mobility testing

The subjects were instructed to perform each motion listed in Table 4.2.2.-1. and to move their limb as far as comfortably. Movements were paired to create complete ranges of motion. For example, the flexion and extension motions were paired to examine the rotational range of motion along the sagittal plane. Abduction and adduction movements were paired to look like the rotational range of motion along the frontal plane. Finally, internal, and external transverse rotation movements were paired to examine the rotation range of motion along the transverse plane. Each motion was performed 3 times.

Raw motion capture data was processed using Vicon Nexus software to label trackers and fill any data gaps. Next, additional Nexus data pipelines was used to calculate joint centers. Cleaned and processed data was then analyzed using Vicon ProCalc. Finally, the joint angles were calculated based on the relative locations of the body's joint centers.

4.2.3. Protocol 2: Reach Envelop

Reach envelope testing is a method used to assess the mobility of a spacesuit and its impact on an astronaut's ability to perform tasks. This type of testing involves measuring the maximum reach of a person while wearing the suit and is used to evaluate the total extent of the volume reachable by the individual, see Figure 4.2.3.-1.

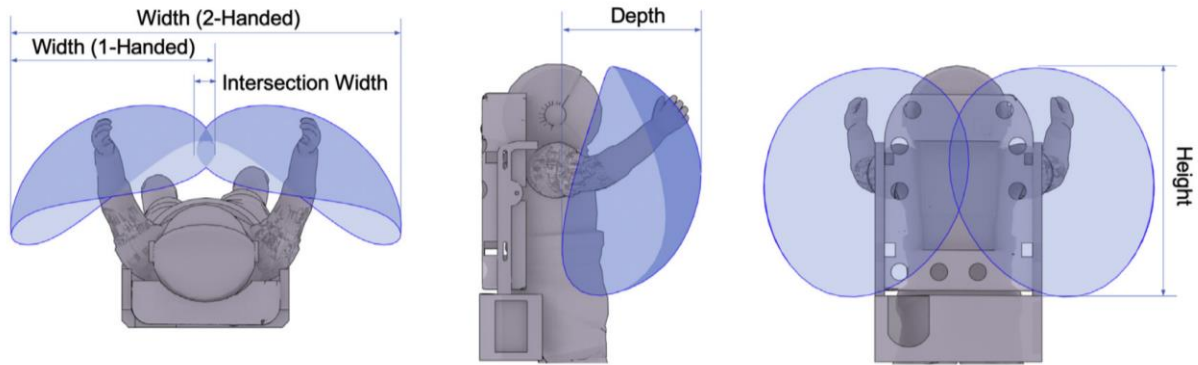


Figure 4.2.3.-1. Single Hand Reach Envelope Visualization

Previously, the reach envelope was qualitatively measured through HITL testing of test subjects in simulated/mockup environments. However, in recent years, advanced motion capture systems have led to quantitative reach envelope evaluation methods (Abercromby, Thaxton, Onady, & Rajulu, 2006). These systems use markers placed on the joints to track movement and precisely measure joint angles.

Reach envelope testing has become an essential aspect of spacesuit design and evaluation. The ability of an astronaut to move freely and perform tasks while wearing a suit is critical to the success of any mission. By evaluating the reach envelope of a suit, designers can ensure that it provides the necessary range of motion for astronauts to complete their objectives safely and effectively.

Different types of reach envelopes can represent different aspects of suit mobility. The most evident case is single-handed reach envelopes, where the area available to a single arm is mapped. Reach envelope calculation can be done with both arms simultaneously; the overlapping area indicates areas both hands can reach. A similar metric can be found through dual-hand reach envelopes, where a subject holds both hands together, performing the sweeps. The size and shape of upper body reach envelopes can change depending on the position of the rest of the body. For example, when seated in a rover, the body's position in the suit is changed, reducing the total reach envelope size and changing the shape. Reach envelope analysis can also be used to analyze the mobility of other joints, including leg limb segments. Situation-specific reach envelopes can be created to cater to actual use cases. For example, NASA performed a study looking at the upper body reach envelope of the EMU, accounting for the ability of the total body mobility of the suit while attached to the leg restrain system of the Canada Arm used for EVAs on the ISS (Kim, et al., 2019), see Figure 4.2.3.-2.

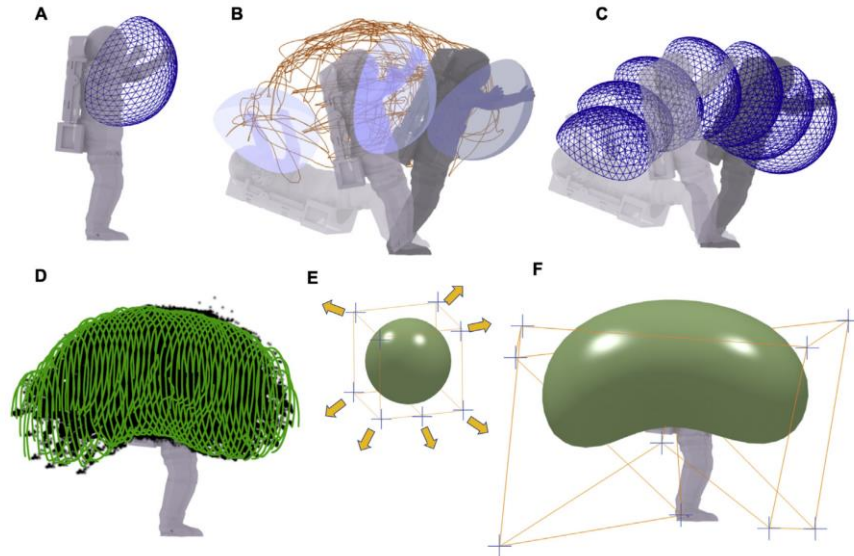


Figure 4.2.3.-2. Full Body Reach Envelope Visualization of the EMU, While Using ISS Foot Restraint (Kim, et al., 2019)

For this study, both single-hand and double-hand reach envelopes were measured. For single-hand envelopes, subjects were instructed to keep their arm as straight as possible throughout the range of motion. For the right-handed reach envelopes, the location of the top right tracker on the hand tracker plate was used to generate the movement traces. For the left-handed reach envelopes, the top left tracker of the hand tracker plate was used to generate the movement traces. Finally, the top right tracker on the right-hand tracker plate generated the movement traces for dual-handed reach envelopes. The system records tracker location at a rate of 50 frames per second, with a resolution of # mm.

There have been several different methodologies for calculating reach envelopes. One method entails having the test subject do a series of arm sweeps in vertical and horizontal motions covering the total extent of their reach envelope. Subjects first started with horizontal sweeps, told to move their outstretched hand left and right up to the extent of their reach, starting with their hand by their side. Each sweep they were instructed to move their hand upwards covering new areas of the reach envelope, once the subject reached the top of their range of motion, they were instructed to repeat the process but running from the top of their range of motion of the original position. Subjects were then instructed to perform similar sweeps, starting with their hand as aft as possible and then moving their hand forward and across their body to map their reach envelope (Figure 4.2.3.-3).

The process was also completed with both hands held together, mapping the area reachable by both hands at the same time.

By tracking the location of the hand in a global coordinate system, the sweeps can be converted into trace lines, showing the shape and extent of the reach envelope. A base template can then be matched to the shape of the trace.

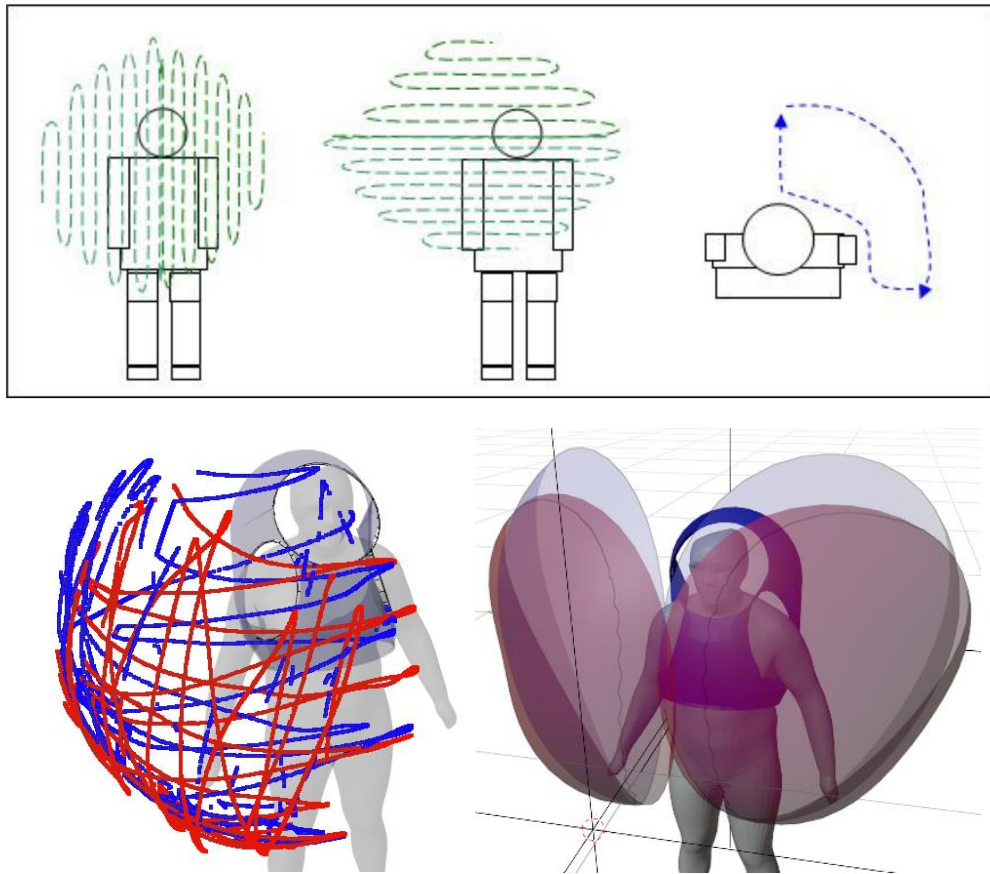


Figure 4.2.3-3. Reach Envelope Mapping Technique. [Top] vertical and horizontal sweeping motions used to generate reach envelopes, (Abercromby, Thaxton, Onady, & Rajulu, 2006) [Bottom Left] recorded hand sweeps [Bottom Right] resultant reach envelopes

This 3D surface can be used to quantify the size and shape of the reach envelope. The total width, height, and depth of the reach envelope was recorded relative to the cartesian coordinate system of the 3D visualization environment, see Figure 4.2.3-4.

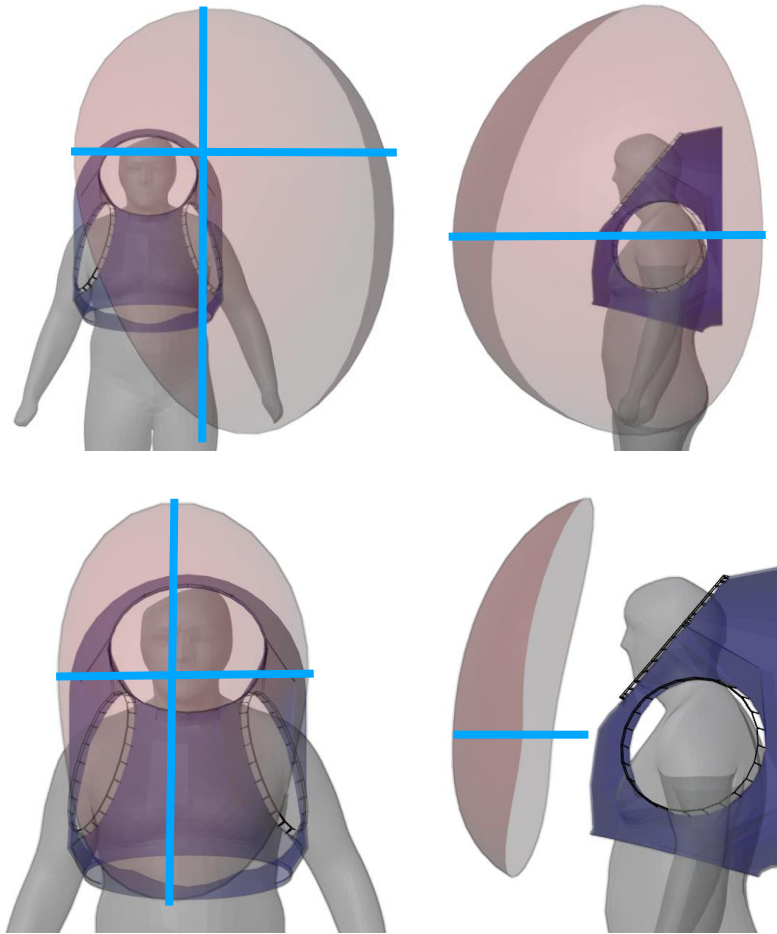


Figure 4.2.3-4. Reach Envelope Measuring Technique. [Top Left] Single hand reach envelope width and height, [Top Right] Single hand reach envelope depth definition, [Bottom Left] Double hand reach envelope width and height definition [Bottom Right] Double hand reach envelope depth definition

4.3. Results

4.3.1. Results 1: Range of Motion Results

The ranges of motion were recorded and analyzed to determine the effect of HUT sizing systems on total mobility.

Table 4.3.1.-1. Range of Motion Descriptive Statistics

		Flex-Ext (R)	Flex-Ext (L)	Ab-Ad (R)	Ab-Ad (L)	Int-Ext (R)	Int-Ext (L)
Custom HUT	STDDEV	20	28	20	22	11	13
	Mean	223	220	96	99	120	121
	Mean Diff	9	7	5	1	6	2
Closest Standard HUT	STDDEV	22	20	19	22	9	19
	Mean	214	213	91	99	114	119
Second Closest Standard HUT	STDDEV	16	20	21	20	7	11
	Mean	206	220	92	99	118	117

Note: All measurements are in degrees

The ROM data was used to calculate the average and standard deviation of each range and HUT condition combination, see Table 4.3.1.-1.

Table 4.3.1.-2. Custom vs. Closest Standard-Sized HUT Ranges of Motion

		Flex-Ext (R)	Ab-Ad (R)	Int-Ext (R)	Flex-Ext (L)	Ab-Ad (L)	Int-Ext (L)
Custom vs. Closest Standard HUT vs. Closest Standard HUT	Ave. Diff.	14	9	8	14	4	5
	P-Value	0.05*	0.01*	0.01*	0.03*	0.41	0.36
Custom vs. Second Closest Standard HUT	Ave. Diff.	15	6	3	1	2	5
	P-Value	0.08**	0.07**	0.52	0.92	0.72	0.22
Closest vs. Second Closest Standard HUT	Ave. Diff.	3	-2	-4	-11	-0	-0
	P-Value	0.81	0.72	0.20	0.07**	0.93	0.98

Note: All measurements are in degrees

*: The difference between custom and standard test cases reached statistical significance at $p < 0.5$.

** : The difference between custom and standard test cases reached practical significance at $p < 0.01$.

The ranges of motion with the different HUT conditions were then run through a paired two-tailed student's T-test to determine the statistical significance and average pairwise difference in mobility between the various HUT conditions.

When wearing the custom-sized HUT, the subjects' range of motion was larger than the closest and second closest-sized standard-sized HUT. The statistical significance of this change varied. Compared to the custom HUT the closest standard HUT condition showed significant differences in mobility in the flexion-extension and abduction-adduction ranges of motion for both the right and left sides (p-values of 0.05, 0.01, 0.01, and 0.03, respectively).

The increase in mobility for the second closest HUT was not as significant, with only the right and left flexion extension ranges showing practically significant improvements, with p-values of 0.08 and 0.07, respectively.

Comparing the two standard-sized HUT conditions, only the left abduction-adduction range showed practically significant improvement with a p-value of 0.07.

4.3.2. Results 2: Reach Envelop Results

The dimensions of the reach envelopes were recorded and analyzed to determine the effect of HUT sizing systems on total mobility. The mean and standard deviations were calculated using every HUT evaluation that used the specified condition.

Table 4.3.2.-1. Reach Envelope Descriptive Statistics

		Left-Hand Reach Envelope			Right Hand Reach Envelope			Dual Hand Reach Envelope		
		Width	Depth	Height	Width	Depth	Height	Width	Depth	Height
Shirt Sleeve	STD DEV	0.22	0.13	0.09	0.19	0.10	0.10	0.23	0.17	0.21
	Mean (meters)	1.10	1.09	1.34	1.13	1.06	1.34	0.85	0.47	1.06
Custom HUT	STD DEV	0.23	0.09	0.09	0.18	0.12	0.10	0.06	0.09	0.10
	Mean	0.83	0.91	1.21	0.88	0.93	1.21	0.57	0.27	0.87
Closest Standard HUT	STD DEV	0.16	0.10	0.08	0.17	0.10	0.08	0.06	0.08	0.12
	Mean	0.74	0.94	1.19	0.79	0.91	1.18	0.51	0.25	0.85
Second Closest Standard HUT	STD DEV	0.24	0.10	0.09	0.18	0.04	0.10	0.08	0.11	0.07
	Mean	0.73	0.85	1.18	0.81	0.89	1.11	0.46	0.24	0.75

Note: All means and standard deviations are in meters

The average and standard deviation of each dimension and HUT condition were calculated and tabulated, see Table 4.3.2.-1.

Table 4.3.2.-2. Analysis of Reach Envelope Data

		Left-Hand Reach Envelope			Right Hand Reach Envelope			Dual Hand Reach Envelope		
		Width	Depth	Height	Width	Depth	Height	Width	Depth	Height
Custom vs. Closest Standard HUT	Ave. Diff.	0.12	0.02	0.03	0.04	0.02	0.03	0.06	0.02	0.31
	P-Value	0.09**	0.45	0.21	0.08**	0.56	0.22	0.01*	0.13	0.02*
Custom vs. Second Closest Standard HUT	Ave. Diff.	0.10	0.04	0.03	0.08	0.03	0.07	0.08	0.01	0.09
	P-Value	0.08**	0.33	0.20	0.09**	0.60	0.23	0.02*	0.62	0.03*
Closest vs. Second Closest Standard HUT	Ave. Diff.	-0.03	0.06	-0.02	0.00	0.00	0.043	0.03	0.00	0.06
	P-Value	0.56	0.17	0.48	0.93	0.90	0.16	0.35	0.77	0.02*

Note: All means and standard deviations are in meters

*: The difference between custom and standard test cases reached statistical significance at $p < 0.5$.

** : The difference between custom and standard test cases reached practical significance at $p < 0.01$.

The different HUT conditions were then run through a paired two-tailed student’s T-test to determine the statistical significance and pairwise average difference in reach envelope size between the various HUT conditions.

The average reach envelope of the subjects when wearing the custom-sized HUT was larger than the closest and second closest-sized standard-sized HUT. The statistical significance of this change varied.

For the dual hand reach envelope, custom sizing of the HUT resulted in a statistically significant increase in the envelope’s width and height when compared to the closest standard-sized HUT, with p-values of 0.01 and 0.02, respectively. There was also a practically significant increase in the single-hand reach envelopes width on both the left and right sides, with p-values of 0.09 and 0.08, respectively.

For the dual hand reach envelope, custom sizing of the HUT resulted in a statistically significant increase in the envelope’s width and height when compared to the closest standard-sized HUT, with p-values of 0.01 and 0.02, respectively. There was also a practically significant increase in the single-hand reach envelopes width on both the left and right sides, with p-values of 0.09 and 0.08, respectively.

When comparing the envelope dimensions of the closest standard-sized HUT with the second closest HUT, the only statistically significant difference was in the height of the dual-hand reach envelope.

4.4. Discussion

4.4.1. Ranges of Motion

The data suggests a benefit of custom sizing of the HUT on spacesuit mobility. The size and nature of the effect is not apparent. When the custom HUT was compared to the closest standard-sized HUT, there was a consistent benefit to both the left and right sides. Compared to the second closest HUT condition, the results were not as clear. This may be due to the additional size of the second closest HUT (often larger than the closest HUT), permitting the subject to place their torso asymmetrically in the HUT. This could explain why there was an asymmetric benefit on the right-side ranges of motion and no benefit on the left.

When the standard HUT conditions were compared to each other, there was only practically significant difference on a single range of motion, suggesting that within the standard size range, there is no significant difference in mobility between the discreet sizes. The significant to practically significant benefits in mobility from the custom HUT to both of the standard sizes suggest that the bulk sizing of the HUT is not where the improvement in mobility is coming from. However, instead fine-tuning both the interface locations' orientation and position to fit the wearer increases the mobility of the spacesuit.

4.4.2. Reach Envelops

The custom HUT showed significant improvement in dual hand reach envelop size. This is in line with the expectation of better alignment of the HUT features with specific body locations. The benefit was not seen in all conditions at the same significance level. The single-hand reach envelope widths saw a practically significant increase with HUT customization but no significant increase in envelope depth and height. This suggests that using a customizable HUT design framework can maximize the reach envelope and, therefore, the mobility of a spacesuit.

While there was a significant difference in several envelope dimensions between custom and the two standard HUT conditions, there was only one metric that was statistically significantly better when the closest standard HUT was compared to the second closest HUT. This suggests that the additional benefit seen with the custom HUT was not only due to the overall size of the HUT better matching the subjects' body, but the additional improvement in interface orientation and relative location meaningfully improved mobility.

A couple of unaccounted-for factors could limit the power of this analysis. First, in an integrated suit system, the wearer's torso is held in position in the HUT through shape features on the interior of the HUT, optional crew-preference padding, straps, and additional contact with the rest of the suit. While torso movement is still possible in a complete suit, the lack of indexing features, padding, and strapping in the suspended HUT mockup allows the subject to move within the HUT throughout testing. This was somewhat mitigated by placing the subject in the HUT as described above but did little to limit the subject drifting in the HUT throughout testing.

Second, the custom sizing framework was designed to center the scye bearing on the center of the shoulder joint. This allows for the rotation of the shoulder joint and the spacesuit arm to rotate equally. By not including the shoulder assembly of the spacesuit in the testing, the effect of HUT shape on mobility could be isolated but it did not consider the compounding effects of the shoulder joint. Improved shoulder position in the scye bearing will likely have a significantly positive effect on suited shoulder mobility.

Design Evaluation 3: Stress Analysis by Finite Element Modeling

“Even more basic, any EVA puts man just one thin, glued-together, rubber membrane away from near-instant death.”

– Michael Collins

5.1. Goals of this Study

In order to determine the feasibility of 3D printed spacesuits, the state of the art of 3D printed spacesuits was reviewed. Since this study focused on the design and implementation of a 3D printed HUT, there was a knowledge gap on how a 3D printed spacesuit HUT would handle pressurization. To address this Finite Element Analysis was completed on a HUT CAD model. Included in the analysis were three candidate materials, including two 3D printable polymers. Three suit pressures and three HUT shell thicknesses were analyzed to evaluate the suitability of different material, pressure, and thickness combinations for use in an actualized HUT. This work is an initial study and doesn't address the impact of human generated loads experienced by used hardware.

5.2. State of the Art

3D printing, also known as additive manufacturing, creates physical objects from a digital model by adding material layer by layer. 3D printers create parts using a computer-controlled process that deposits material, such as plastic, metal, or ceramic, layer by layer until the desired part is complete.

3D printing typically begins with a 3D model created using computer-aided design (CAD) software. The CAD design loads into software that generates the model's layer-by-layer patterns through a process called “slicing.” The 3D printer uses this digital information to deposit the material layer by layer to build the object. Depending on the type of printer and material used, the printer can use various techniques to deposit the material, such as extrusion, powder bed fusion, or vat photopolymerization.

For this study a COTS 3D printer was used to manufacture the HUT mockups from PLA plastic, see Figure 5.2.-1.



Figure 5.2.-1. 3D Printed Mockup Process. [Left] CAD geometry of skeletonized HUT mockup [Right] 3D Printers used to fabricate HUT mockups.

3D printing has numerous applications, including prototyping, product development, tooling, and production of end-use parts. It allows for creating complex geometry that would be difficult or impossible to produce using traditional manufacturing techniques. Additionally, 3D printing is a relatively fast and cost-effective way to produce small quantities of custom parts, which can be helpful for research and development or create unique, one-of-a-kind objects.

5.2.1. Fused Filament Fabrication

FFF (Fused Filament Fabrication) is a 3D printing process that works by extruding a continuous filament of a thermoplastic material, such as ABS or PLA, through a heated nozzle, which melts the material and then deposits it layer by layer to create a three-dimensional object.

FFF 3D printing is one of the most popular and widely used 3D printing technologies because it is relatively simple, affordable, and accessible. It can be used to create a wide range of objects, from simple prototypes to complex parts and models, and is often used in engineering, architecture, product design, and education.

5.2.2. Multi-Material Printing

Dual extrusion is a feature of some desktop FFF 3D printers that enables the printer to use two different materials or colors in a single print. This feature allows for greater design flexibility and can enhance the functionality and appearance of printed objects.

A dual extrusion 3D printer typically has two or more extruders, each of which can be loaded with a different material or color. The extruders are mounted on a single carriage that moves back and forth along the X or Y axis, allowing them to deposit material in different areas of the print bed.

When using a dual extrusion 3D printer, the user can choose which extruder to use for each print part. For example, one extruder can be used for the main body of the object, while the other can be used for small details or accents. The user can also specify which extruder to use for support material, which is used to support overhanging parts of the print.

Dual extrusion can be used to manufacture multi-material spacesuit components, such as joining flexible segments directly to rigid joining elements. Further, there is the possibility of printing entire assemblies in one process resulting in ready-to-use suit components with minimal to no post-processing (5.2.2.-1.).



Figure 5.2.2.-1. Dual material 3D printed component, demonstrating the mating of flexible and rigid thermopolymers.

5.2.3. Selective Laser Sintering

Selective Laser Sintering (SLS) is a 3D printing technology that uses a high-powered laser to fuse powdered material into a three-dimensional object. SLS is an additive manufacturing process that, similarly to FFF, builds up a part layer by layer. As a result, the process is ideal for creating complex geometry and structures that cannot be produced with traditional manufacturing methods. In addition, the sintering process can be applied to a more extensive range of materials vs. the FFF extrusion process. SLS materials can range from thermoplastics and ceramics to metals.

The SLS process starts with a bed of powdered material. A laser then scans the surface of the powder bed, selectively melting and fusing the material in the shape of the first layer of the desired object. Once the first layer is complete, a new layer of powder is added, and the process is repeated until the entire object is formed.

One of the main advantages of SLS is that it does not require support structures like other 3D printing technologies because the surrounding powder bed supports the printing process. Advanced 3D printing manufacturing methods allow for more complex and intricate designs and reduce the amount of post-processing work required.

SLS is commonly used in aerospace, automotive, and medical device manufacturing, requiring high-strength and heat-resistant materials. It can also be used for rapid prototyping and low-volume production of end-use parts.

5.2.4. In-situ materials sourcing

In-Situ Resource Utilization (ISRU) uses available resources on-site rather than transporting all necessary resources from Earth. This approach will reduce the cost and complexity of space missions and enable longer-duration missions with greater self-sufficiency in the future once these systems and processes are fully developed.

One of the most promising areas for ISRU in space is the production of metals. These materials are essential for constructing habitats, structures, vehicles, equipment, and infrastructure. The Moon, Mars, asteroids, and celestial objects contain valuable metals such as iron, nickel, and titanium. These can be extracted using mining and refining processes similar to those used on Earth. The resulting metals can be used for construction, 3D printing, and other applications.

Previously used systems will become a rich source of resources, such as derelict spacecraft and rovers that have reached the end of their planned life. Metals and plastics will be able to be gleaned from these systems and reused in new products. Recycling space systems will reduce the need to transport new materials from Earth and can save resources and money.

Work has been done to synthesize polymers, in part, from the Martian atmosphere. As this field of research matures, it may be possible to recreate many of the thermopolymer used in 3D printing using local in-situ resources (Rosenberg & Makel, 2000).

Harvesting and processing lunar regolith: The lunar regolith, or soil on the moon's surface, contains many valuable materials such as aluminum, silicon, and titanium. These materials can be extracted and used for manufacturing using technologies such as smelting and electrolysis.

Overall, the potential for ISRU in space for metals and polymers is significant. By using local resources, space missions can be more sustainable and cost-effective, enabling more ambitious exploration and long-term settlements.

5.2.5. Metal 3D Printing

While FFF printing is commonly associated with 3D printing and was the first system deployed on the ISS, other alternative systems are being developed to be deployed soon (Figure 5.2.5.-

1.). These systems will demonstrate the feasibility of manufacturing metal components in a space mission context.

Creating metal components in space offers significant advantages. The harsh conditions of space require materials that can withstand extreme temperatures, radiation, vacuum conditions, and impacts from micrometeorites. Metals, such as titanium or steel, have properties that can meet these demands. Additionally, manufacturing parts in space reduces the cost and risk of launching heavy components from Earth. Instead, raw materials like metal powder could be launched and components manufactured as needed. This on-demand production capability could facilitate repairs, enable the construction of large structures, and even contribute to establishing extraterrestrial bases. The elimination of gravity also allows for the creation of structures that would be impossible or more difficult to manufacture on Earth due to gravity-induced sag or deformation.

A titanium disconnect ring was printed using Redwire's high fidelity prototype 3D printer. This printer is housed in flight like hardware and is being developed for deployment on the ISS (Figure 5.2.5.-1).

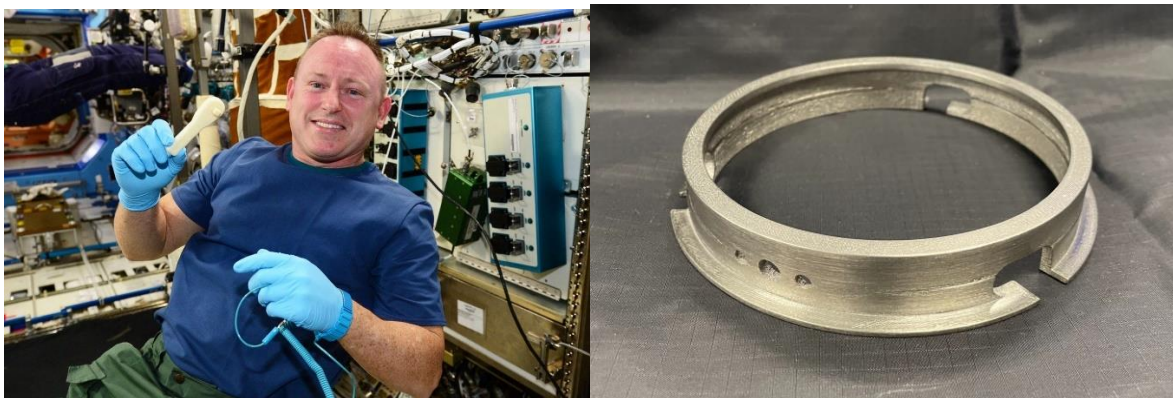


Figure 5.2.5.-1. 3D Printing in Space Capabilities. *[Left] first object 3D printed in space, a small ratchet tool [Right] 3D printed titanium glove disconnect part*

5.2.6. Spacesuit Structures

The spacesuit's structural components can be split into three different categories. These are connecting, shape, and mobility elements. Connecting elements include donning/doffing features and quick disconnects. Shape elements are portions of the suit that conform to the wearer's body but are primarily meant to remain rigid. These include the HUT and the rigid brief section in modern planetary suits. Finally, mobility elements are parts of the spacesuit that allow the suit to move along with the body. Mobility elements can further be separated into two categories: bearings allowing for rotation of body segments and bending joints. 3D printing can be used to produce all of these elements.

5.2.7. Design of 3D Printed Bending Elements

Numerous types of bending elements have been designed for use in spacesuits. FFF printing machines have specific capabilities that must be considered when designing parts. A flexible polymer must be used when designing bending elements. A standard flexible polymer for 3D printing is TPU; due to the best practices for printing TPU, a bellows joint design was chosen. The benefit of the bellows design was that it could be printed using a near-continuous extrusion, minimizing the starting and stopping of the polymer flow. The topology of the joint is also advantageous as the material does not overlap with itself.

The work needed to actuate an idealistic spacesuit joint can be calculated through Equation 5.2.7.-1.

$$\text{Actuation Work} = \text{Pressure} * \Delta \text{Volume}$$

Equation 5.2.7.-1.

This equation points to two ways to reduce the effort needed to move a joint. The first is to minimize the pressure of the suit. Reducing the operating pressure of the suit has been done successfully but brings operational challenges of pre-breaths and fitting into other pressurized systems of the mission. The other way of reducing the work required is minimizing the change in volume over the range of motion. All spacesuit joints are designed to minimize this. Minimizing the change in volume of the joint is accomplished in most joint designs by having an “expanding” and “contracting” side of the joint (Figure 5.2.7.-1.). These sides can be asymmetrical or symmetrical, depending on the joint design. As volume is created by the expansion of one side of the joint, the contracting side’s volume shrinks. This balance reduces the total volume change of the joint.



Figure 5.2.7.-1. 3D Printed Flexible Bellows Assembly Mobility Demonstration, Pressurized to 4.3 PSI

Bellows joints are comprised of several components. First is the flexible TPU bellows. The Bellows are printed as a single component and are kept thin enough to provide flexibility but thick enough to be durable for cyclical use. The mobility of the joint design is related to the overhang angle of the bellows profile and the diameter of the bellows. The overhang angle of the bellows and the diameter should be kept as small as practicable to maximize the joint's mobility. The bellows' shape is maintained when pressurized through restraint rings. These rings are semi-rigid rings that resist the ballooning of the flexible components. When the joint is pressurized, the bellows will tend to maximize the volume of the pressurized element. If this is not mitigated, the joint will become a rigid cylinder. A restraint cable keeps the joint at the designed length to counter this (Figure 5.2.7.-2.).



Figure 5.2.7.-2. Bellows Assembly [Left] flexible bellows component as [Right] assembled bellows assembly.

5.2.8. Design of a 3D Printed Glove Quick Disconnect

Spacesuit components are joined together through disconnects. High-cycle connections are made through quick disconnects that can be actuated quickly. Disconnects must be able to create an air-tight seal while acting against the pneumatic and incidental forces. Air-tight seals are created by compressing a gasket with a sealing surface. Pneumatic forces include plug loads and hoop loads. The plug load acts axially on the disconnect and is a crucial consideration for designing the locking feature of the disconnect. Hoop loads were a concern but were not as problematic in the disconnect design.

Initial designs utilized a bayonet locking mechanism. The air-tight seal was created by pressing a knife-edge surface into a silicon gasket. More recent designs featured a more robust seal design, with the sealing surface parallel to the central axis of the disconnect. In addition, the

bayonet system was replaced with a locking ring, with a series of keyed surfaces that allow the halves to be joined and locked into place (Figure 5.2.2.-1.).



Figure 5.2.2.-1. 3D Printed Glove Disconnects. *[Left] updated glove disconnect [Right] original bayonet type glove disconnect*

While developed for glove disconnects, the disconnect geometry was modeled as a parametric model that generates the connection geometry based on a given inner diameter. Therefore, larger diameter disconnects of this design could be used for boot or helmet disconnects.

5.2.9. Design of a 3D Printed Spacesuit Arm Assembly

The arm is a sub-assembly of the spacesuit that incorporates all three types of spacesuit components. First, a bending element accommodates the flexion of the elbow. Next, the wrist and shoulder rotation are made possible with bearings. The glove is attached with a quick disconnect. The connecting shape components hold the various elements in place and create the final shape of the arm.

The bending element is connected to the wrist and bicep cuffs at an angle. The canted angle maximizes the joint's range of motion by allowing the bending of the bellows in both directions to contribute to the total range of motion of the joint.

Initial SSAA prototypes lacked bearings and had rigid connections to the wrist and bicep. Later iterations include sealed bearings for the wrist and biceps. The additional bearings would allow more complete ranges of motion in an integrated suit (Figure 5.2.4.-1.).



Figure 5.2.4.-1. Spacesuit Arm Assembly Design Evolution. [Left] 1st generation 3D printed spacesuit arm assembly [Right] 2nd generation 3D printed spacesuit arm assembly.

Further developments would be needed to mature the design of the SSAA for an actualized suit system. For example, spacesuit arm assemblies typically include some length adjustment through a cable winch or a belt wrapped around a capstan. In addition, the pressurized assembly can be modified by varying the length of the restraint cable.

5.2.10. Design and construction of the NDX-3 and NDX-4

The HSFL has constructed two 3D-printed prototype spacesuits. The first suit was the NDX-3. The construction of the NDX-3 was based on the bellows bending element, bayonet disconnect, a threaded disconnect, and dual planar HUT design. The NDX-1 inspired the NDX-3's general architecture. The NDX-1 is a Martian prototype spacesuit developed at the HSFL. The NDX-3 was an initial prototype that proved that disconnects, significant rigid and flexible components, and bending elements could be 3D printed and assembled into a suit prototype, see Figure 5.2.7.-1. This prototype, while successful, revealed many of the ongoing challenges of 3D-printed spacesuits.



Figure 5.2.7.-1. NDX-3 3D Printed Spacesuit Prototype

The NDX-3 succeeded the NDX-4, which featured a redesigned HUT, shoulder assembly, and glove disconnects. One of the issues with the NDX-3 was the shoulder bearing location and sizing. Therefore, larger bearings were incorporated into the NDX-4. The NDX-4 HUT was designed using the sizing system described above, predicting the optimal scye bearing placement based on the anthropometry of Professor de Leon. In addition, the shoulder joints were redesigned to work better with the 3D printing process. To this end, an annular ring shoulder design was chosen. The NDX-4 also features a rear entry hatch design, more in line with current governmental and contractor developmental planetary spacesuits.



Figure 5.3.1.-1. 3D Printed HUTs. [Left] custom sized NDX-4 HUT, featuring a rear entry hatch [Right] NDX-3 HUT, featuring a dual planar entry method

5.3. Methods

The HUT of the spacesuit experiences a large number of stresses through use. These include impact, human-induced loads, and pressurization loads. While essential to consider, impact loads may not be the primary design consideration for a HUT. In a micro-gravity environment, the astronaut is often attached to a robotic arm or floating in space. The suit rarely moves fast enough to generate large forces that could compromise the suit. In a Lunar environment, there is reduced gravity, roughly $1/6^{\text{th}}$ of that seen on Earth. The reduced lunar gravity causes things to fall at $1/6^{\text{th}}$ the speed. For the Apollo missions, while falls were common, they were seldom uncontrolled and often were intentional to allow access to the lunar surface. The uncontrolled falls tended to be backwards. If these falls were replicated in a modern planetary suit, the primary impact location would be the waist-brief-hip and PLSS of the suit. Impact loads should still be considered but may be addressed through new technologies such as crumple pads or shock-absorbing bumpers.

The human-induced loads on a spacesuit are complex and highly dependent on the suit's fit and the operating environment and, therefore, outside the scope of this work.

The pneumatic loads on a spacesuit HUT are essential to consider as the torso of the spacesuit is the largest diameter component of the suit and therefore encounters the highest loads. By performing a Finite Element Analysis simulation of a pressurized HUT, it is possible to see how different candidate materials can withstand various pressurization levels. Further, with a complete understanding of the load distribution on a HUT, paths to design optimization can be made, including topology optimization and other generative design tools that could minimize the weight of the HUT without compromising the suit's structural integrity.

Finite element Analysis is a simulation tool that can simulate any number of physical phenomena.

5.3.1. HUT Construction

The Shuttle EMU utilizes a fiberglass HUT (Barrera & Tello, 1992). Fiberglass is a composite material, where glass fibers, often woven, are embedded into an epoxy matrix. The composite material benefits from the high tensile strength of the glass fibers, but these fibers alone would be flexible and only able to hold tensile loads. The epoxy matrix gives the composite material rigidity and compressive strength. As a result, composites often offer comparable strength to conventional engineering materials while reducing the overall weight of a component.

The use of composite materials also has significant drawbacks. The manufacturing process of composite parts is very complex. The order and orientation of the fiber reinforcements are carefully planned and require skilled workers to manufacture them correctly. In addition, the basis for the fiber reinforcement is typically a woven fabric. The material's structure complicates the design and manufacturing process by introducing micro and mesoscale

structures that can dramatically affect the final material properties. Due to this material and manufacturing complexity, the manufacturing process of flight hardware must be analyzed and certified in addition to the actual hardware.

As a result, developmental suits such as the Mark III and xEMU have featured machined aluminum HUTs. Aluminum has the benefit of being relatively lightweight, robust, and easy to manufacture. Additionally, using an isotropic material such as a metal billet simplifies the analysis of material performance.

Future HUT designs may use additive manufacturing or 3D printing (de Leon, Tomovic, & Green, *New Methods of Manufacturing Spacesuits for Deep Space*, 2021), (Green & de Leon, 2021). Historically, manufacturing has focused on removing material from bulk, such as metal or plastic billets. Conversely, additively manufactured parts are formed by accreting material, building up a final part. There are also hybrid manufacturing processes where a base part is 3D printed and finished through traditional machining methods.

There are numerous types of 3D printing with a wide range of materials. However, the most common consumer-grade 3D printers use Fused Filament Fabrication. FFF builds up parts by extruding thermo-polymer filament through a hot nozzle and drawing parts layer by layer. A 3D axis gantry moves the nozzle along pre-programmed paths extruding plastic to create the part layer by layer. Direct Energy Deposition (DED) is similar to FFF. However, the DED process creates parts with a metal welding bead rather than extruded plastic.

Selective Laser Sintering (SLS) is a common industrial 3D printing technique. SLS systems use lasers to sinter powder granules together. Once the machine finishes sintering a single layer, additional powder covers the sintered part and the sintered to the previous layer. The final part is formed layer by layer through this process. SLS is a versatile manufacturing method and can use many different materials, including high-impact resistant nylons and types of metals.

Traditional subtractive manufacturing has several drawbacks. First, significant waste is associated with milling large parts from solid metal blocks. Second, the manufacturing process has limitations due to the machine and tooling design. As a result, designing and manufacturing using these methods require great care and skill from engineers and machinists.

Additive manufacturing reduces waste by using only the material needed for the parts and, in some cases, support material. Support material can also typically be recycled and used as feedstock for printing. Additive manufacturing does not require specific tooling or fixtures to make complex parts. Additionally, the number of axes of a milling machine or the available tooling does not constrain the geometry of additively manufactured parts. The design freedom afforded by additive manufacturing makes the creation of precise, complex curvatures easily achievable, particularly enabling the employment of topology optimization and generative design in part design. Provided the machines do not need repair, their use is relatively hands-off and not labor-intensive.

5.3.2. Material Selection

Polycarbonate (PC), Polyethylene (PE), Polypropylene (PP), Acrylonitrile Butadiene Styrene (ABS), Ultra-High-Molecular-Weight Polyethylene (UHMWPE), Polyether Ether Ketone (PEEK), and Polylactic Acid (PLA) are a diverse range of plastics, each with unique properties. PC is a thermally stable and impact-resistant material used for bulletproof windows and eyewear, while PE is a standard, flexible plastic used in packaging and construction. PP is robust and lightweight, known for its chemical resistance, making it useful in packaging and automotive components. ABS is a strong, rigid plastic with high impact resistance and excellent mechanical properties, and UHMWPE offers outstanding toughness, chemical resistance, and low moisture absorption. PEEK is a high-performance plastic known for its exceptional resistance to extreme temperatures, chemicals, and radiation, which makes it an ideal choice for space applications. Lastly, PLA is a biodegradable plastic derived from renewable resources, boasting properties like a high Young's Modulus and low to moderate outgassing tendency, making it a more environmentally friendly choice.

Outgassing is a process where a material releases volatile substances into the surrounding environment. This typically occurs when a material is exposed to certain conditions, such as elevated temperatures or reduced pressure. The volatile substances that outgas from a material can be a variety of compounds, often including solvents or additives used in the material's production or residual unreacted components from the material's synthesis. In some instances, outgassing can be harmless or even go unnoticed, but in other cases, it can present health risks or technical challenges. For instance, in the confined environment of a spacecraft, material outgassing can contaminate the spacecraft's atmosphere or deposit on sensitive equipment, potentially causing malfunctions. Therefore, materials intended for such applications are often required to pass stringent outgassing criteria to ensure their safety and suitability.

Table 5.3.2.-1. Polymer Material Characteristics (Material Property Database, 2023), (Outgassing Data for Selecting Spacecraft Materials, n.d.)

Plastic	Density (g/cm ³)	Young's Modulus (GPa)	Yield Strength (MPa)	Outgassing	Melting Temperature (C)
Polycarbonate	1.2	20.-2.4	55-70	Moderate	155-165
Polypropylene	0.9	1.5-2.0	20-40	Moderate	16-170
ABS	1.04-1.06	2.0-2.3	40-50	Moderate	190-270
UHMWPE	0.93-0.94	0.7-1.0	17-20	High	130-136
PEEK	1.3	3.6	80-100	Low	343
PLA	1.24	3.5	55	Low	150-160
Aluminum 6061	2.7	68.9	275*	None	582

PEEK stands out as the most suitable for use in space. PEEK is a high-performance thermoplastic with a high melting point and exceptional resistance to chemicals, radiation, and extreme temperatures. In addition, its superior mechanical properties, including high tensile strength and impact resistance, make it suitable for high-impact components. Moreover, its low outgassing properties make it suitable for vacuum and near-vacuum conditions found in space, thus reducing potential harm to sensitive instruments onboard the spacecraft.

PLA, while typically thought of as a consumer grade printing material, is interesting for use in space due to its low outgassing properties.

5.3.3. Stress Requirements

The pneumatic pressures experienced by the HUT are the direct result of the positive pressurization of the spacesuit. Various pressures have been used in spacesuits and are decided through complex trade studies and consideration of the overall mission architecture.

A certain level of Oxygen is needed for humans to survive. However, this level is well below what one would first expect. The standard air pressure at sea level on Earth is 14.7 PSI. This air is majorly nitrogen, with lower oxygen and trace gas components. The oxygen component is only 3.2 PSI, meaning that if a suit is operating at the same oxygen concentration as sea level, the suit could be pressurized to just 3.2 PSI.

Other considerations prevent designing and operating spacesuits at that low pressure. A pure oxygen environment, at specific pressures, is hazardous. An example of this was the Apollo 1 vehicle mockup in which astronauts were training. Faulty wiring caused a spark, creating a runaway burn of anything flammable in the capsule. All of the astronauts died, unable to escape. Because of this, NASA no longer allows spacecraft to be designed for operating with 100% oxygen. Spacesuits are an exception to this rule, made possible by careful consideration of in-suit systems (Thomas & McMann, 2012). Therefore, spacesuits are conventionally used at a lower pressure than the habitat, rover, station, or capsule.

This pressure differential can be problematic. Since additional gases must be used in the higher-pressure components of the mission architecture, significant nitrogen pressures are needed to make up the rest of the gas mixture. When a human breathes in nitrogen, some of that nitrogen dissolves into the bloodstream. The amount of dissolved nitrogen is proportional to the nitrogen pressure in the breathing air gas mix. As the nitrogen level is lowered, this nitrogen condenses and is released from the bloodstream. If this occurs too quickly, nitrogen bubbles can appear in the bloodstream, potentially causing extreme pain and injury.

When depressurizing a spacesuit, the nitrogen level is slowly lowered over time to prevent the generation of nitrogen bubbles in the bloodstream. This process is called a pre-breath and adds significant time and operational complexity to performing an EVA.

Table 5.3.3.-1. Historical and Current Suit and Vehicle Pressures

Program	Suit Pressure (PSI)	Vehicle Pressure (PSI)
Apollo (Ayrey, 2020)	3.5	4.8
Shuttle/ISS (Harris, 2001)	4.3	14.7
Artemis (Coan, 2020)	8.2-4.3	14.7-Not yet defined

Because of this, there is a tradeoff between suit mobility, pre-breath duration, and other mission constraints. A summary of historical mission vehicle and suit pressures is given in Table 5.3.3.-1.

The Apollo capsule operated at a pressure less than standard pressure. The lower capsule pressure allowed the suits to operate at an even lower pressure. More recent systems, such as the shuttle, forced suit designers to consider other factors in determining the suit pressure. The concept of operations for the shuttle was to be able to lift off from Earth, perform missions, and rapidly return to Earth. Because of this, the shuttle was designed to operate at standard pressure. The operating pressure of the shuttle EMU was, therefore, higher than the Apollo suits. This legacy vehicle and suit pressures have been carried into the ISS program.

Studies have examined the optimal suit/vehicle pressure combination that maximizes suit mobility, minimizes pre-breath time, and maximizes mission safety. One study proposed a 6.1 PSI (suit) 12 PSI (vehicle) pressure combination (Wilde, 1981). As suit design improves, higher-pressure suits can be used without sacrificing mobility. The current developmental suit concept of operations includes in-EVA pre-breathing capability. The current operation concept has the astronaut begin the EVA with a higher suit pressure. The suit pressure is then safely lowered over time while the crew member continues to work during the EVA. The xEMU requirements document called for an 8.2 PSI operating pressure (Coan, 2020).

5.3.4. SolidWorks FEA

SolidWorks is a 3D solid modeling program frequently used for mechanical design and analysis. SolidWorks has a simulation package with Finite Element Analysis (FEA) capabilities (Dassault Systemes, 2022). FEA is a process where the mechanical properties of a part or assembly are simulated. The loads experienced by the system are explicitly defined in terms of the FEA environment. Assumptions can be made, such as part symmetry. Assuming symmetry allows for the mechanical reaction to applied loads of whole parts to be inferred by only simulating a portion of the whole part.

A surface model of the NDX-4 HUT (Figure 5.2.7.-1.) was exported from the 3D surface modeling environment, with the hatch, helmet, scye rings, and waist interface holes filled in. This model was imported into SolidWorks as a surface object. In an actualized suit, the interfaces would be approximately rigid. However, suit pressurization would still create loads on these cross-sections that would be transferred to the surface structure of the HUT. These

forces are called “plug loads.” To simulate the rigidity of a suit interface while also allowing the HUT to deform freely, the helmet, scye rings, and waist geometry were simulated as if they were 5cm thick plates. The plug loads are simulated by applying the same suit operating pressure across the surfaces filling the gaps in the HUT. Half of a HUT was simulated, reducing the time and power needed to run the simulations. A pressure load was applied to all of the faces of the model, simulating the effect of suit pressurization and the plug loads on the HUT interfaces (Figure 5.3.4.-1.).

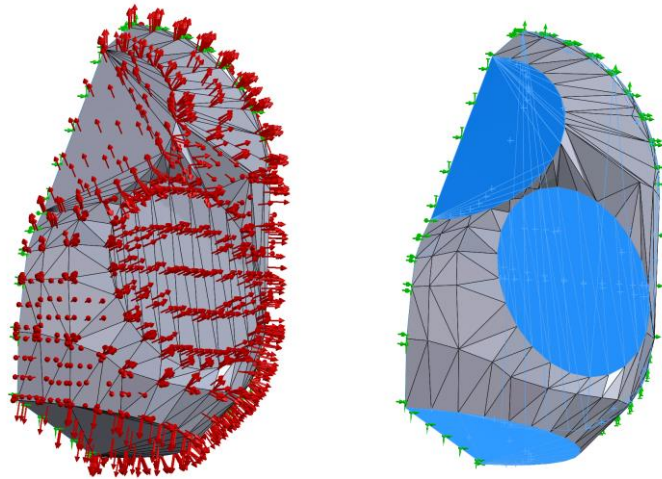


Figure 5.3.4.-1. HUT FEA Visualization. *[Left] FEA boundary conditions, red arrows show pressure load [Right] blue geometry shows rigid plate geometry integrated into the HUT to replicate the plug loads experienced on HUT interfaces*

The material properties of the HUT, the thickness of the non-interface HUT shell, and the pressure were varied to investigate the feasibility of using various conventional and 3D printed materials for manufacturing this HUT design.

5.4. Results

The material structure resulting from additive manufacturing is rarely homogeneous and often has micro and mesoscale structures that can affect the bulk properties of the “as-manufactured” material. Specifically, 3D printed parts often have relatively weak inter-layer bonds leading to less strength in specific directions. In some cases, the part can be designed with this in mind, such that all the significant loads on the part are applied parallel to the plane of the layers. However, the HUT is a complex 3-dimensional object subjected to various loads applied in various directions. As such, the structural effects of 3D printing must be considered when estimating the strength of 3D-printed parts. This printing effect can be seen as a roughly 50% decrease in yield strength (Perez, Celik, & Karkkainen, 2021), (Li & Lou, 2020).

When designing aerospace components, safety factors play a crucial role in ensuring the reliability and safety of a component or system. When determining yield strength

requirements, a safety factor is often applied to account for uncertainties and variabilities that may arise in real-world conditions. These can include discrepancies in material properties, manufacturing defects, unforeseen loading conditions, degradation over time, and limitations in the accuracy of the analytical or numerical models used in the design process. By dividing the material's yield strength by a safety factor (usually greater than one), engineers can determine a reduced "allowable stress" for the design, providing a buffer against these uncertainties. The higher the safety factor, the larger this buffer, and thus the lower the risk of failure. However, a higher safety factor can also result in over-engineering, with increased weight and cost. Therefore, the choice of safety factor is a balance between safety, performance, and cost. As a common practice in the HSFL, A safety factor of 3 was used.

Considering the yield strength of the bulk material, the degradation of strength caused by imperfect layer bonding, and a safety factor, failure criteria can be calculated if the simulation shows that strength exceeds this criterion for any given material, thickness, and pressure combination that shows that that combination would not be suitable for use.

$$Failure\ Criteria = \frac{Yield\ Strength}{Safety\ Factor} * Layer\ Bonding\ Effect$$

Equation 5.4.-2.

Given the yield strengths found in Table 5.3.2.-1., the failure criteria for PEEK and PLA are calculated using Equation 5.4.-1. and given in Table 5.4.-1. The failure criteria for aluminum are also given in Table 5.4.-1.; however, since conventional aluminum components would not be 3D printed, the failure criteria do not consider any degradation due to poor layer bonding.

Table 5.4.-1. Polymer Material Characteristics

Material	Yield Strength (MPa)	Failure Criteria (MPa)
PEEK	100	16.7
PLA	55	9.2
Aluminum 6061	275	91.7

The simulation was run using PLA, PEEK, and Aluminum 6061 materials. The thickness of the HUT shell varied, including 4mm, 6mm, and 8mm thicknesses. 3 Different pressures were considered, 4.3 PSI, 6.2 PSI, and 8.2 PSI. The simulation output included a stress heatmap where the stresses were concentrated on the surface of the HUT.

PLA, the weakest material considered, was not suitable for lower thickness and higher-pressure combinations. With a failure criterion of 9.2 MPa, at 4mm, PLA was only acceptable for use at 4.3 PSI, see Figure 5.4.-2. Still, given that PLA is typically used for consumer 3D printing, it is surprising that it can handle the full operating pressure of the current spacesuit.

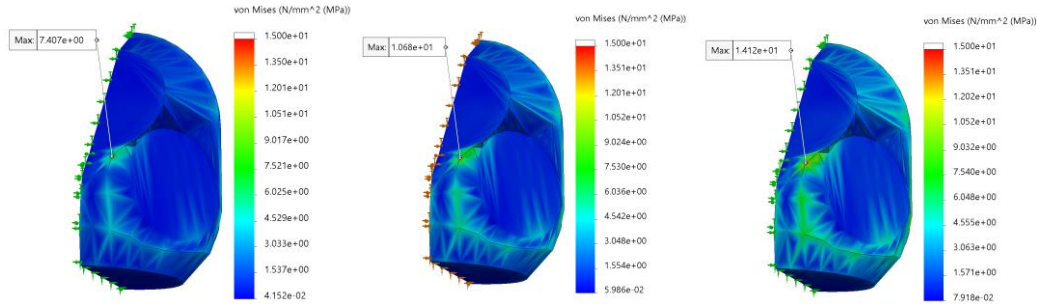


Figure 5.4.-2. 4mm Thick PLA HUT FEA Results. [Left] 4.3 PSI [Middle] 6.2 PSI [Right] 8.2 PSI

When the thickness of the PLA HUT was increased to 6mm, even when pressurized to 8.2, the failure criterion was not surpassed.

With a failure criterion of 16.7 MPa, PEEK could withstand the loads at all pressure and thickness combinations; the highest stresses were seen at 4mm thickness and 8.3 PSI, resulting in a max stress of 14.7 MPa, see Figure 5.4.-3. On the other hand, aluminum 6061, with a failure criterion of 91.7 MPa, could withstand the loads at all pressure and thickness combinations; the highest stresses were seen at 4mm thickness and 8.3 PSI, resulting in the max stress of 14.1 MPa, see Figure 5.4.-3.

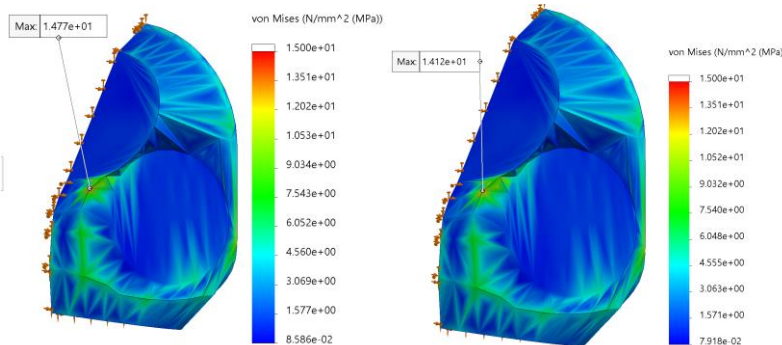


Figure 5.4.-3. Highest Stress Cases for PEEK and Aluminum HUTs. [Left] PEEK 4mm HUT at 8.23 [Right] Aluminum 4mm HUT at 8.23 PSI

Table 5.4.-2. Polymer Material Characteristics (Material Property Database, 2023)

	4mm	6mm	8mm
Volume	1800 mm ³	2700 mm ³	3600 mm ³
PLA	2.23 kg	3.35 kg	4.46 kg
PEEK	2.34 kg	3.51 kg	4.68 kg
Aluminum 6061	4.86 kg	7.29 kg	9.72 kg

Aluminum, with a density of 2.7 g/cm³, is significantly heavier than PLA and PEEK, with densities of 1.24 and 1.3 g/cm³, respectively. However, this density comes with superior strength, especially when considering the degrading effect of poor layer adhesion of the

strength of 3D printed parts. That being said, it appears that PLA and PEEK HUTs with 4mm-8mm thicknesses may be suitable for use. The total weight of the HUT model, not including the interface plugs, is shown in Table 5.4.-2. for each thickness considered.

5.5. Discussion

HUTs are highly integrated components of the spacesuit and experience a variety of forces ranging from pressure-induced loads, impact loads from bumps and falls, interface loads resulting from plug loads, and forces caused by and transferred from the human inside the suit. This preliminary study investigates the feasibility of implementing HUTs using common and state-of-the-art 3D printing materials. Even considering common consumer materials, a HUT shape pressure vessel can be manufactured and subjected to pressurization and plug loads without failure. Further in-depth analysis should include additional modes of loading the HUT, but this preliminary analysis shows that high thicknesses of PLA and moderate to low thicknesses of PEEK may be suitable for HUT manufacturing.

5.5.1. Future Optimization

Once the total stresses that a HUT is expected to encounter, the design of the HUT can be optimized. The stress maps of the HUTs indicated a significant variation in local stresses. Therefore, the material thickness can be varied to provide extra strength in high-stress areas and removed from high curvature areas that encounter lower stresses. Additionally, load paths can be created to deal with the additional impact of human-induced loads. This optimization could be done through topology optimization. Topology optimization is a powerful tool that can be utilized to design parts optimized for strength, performance, and weight.

5.5.2. Sizing of 3D Printed Spacesuits

Digital sizing of conventional sewing patterns is still an active area of research. Translating between two-dimensional patterns and three-dimensional garments is complex and complicated by the unique deformation modes of anisotropic fabrics. 3D printed components, on the other hand, are inherently three-dimensional objects, meaning that changes in final shape can more directly be translated into the as-manufactured part.

The traditional manufacturing of mechanical components requires highly skilled craftsmen and specialized tooling. In addition, much of the work needed to manufacture a part is spent setting up machines to perform specific processes. As such, many mechanical components are made in batches allowing the cost of tool setup to be spread over an entire batch of parts. 3D printing removes the need for extensive machine setup, meaning that a batch of unique parts can be made using the same amount of time, energy, and labor as a set of identical parts. Therefore, a customized 3D-printed spacesuit would require the same effort to manufacture as a standard-sized suit.

Additive manufacturing combined with advanced suit sizing systems can enable the rapid sizing and manufacturing of custom-size spacesuit systems.

5.5.3. Barriers to 3D printing Spacesuits

3D-printed spacesuits are a promising technology for long-term outer space exploration and settlement. However, this technology currently has significant headwinds preventing immediate use. This includes the high cost of rocket launches. Each kilogram mass launched into space costs thousands of dollars to launch. With custom/3D printed spacesuits, the fit, comfort, and mobility benefits of such a system would come with the additional launch costs of sending up a new spacesuit for each crew member. Whereas, with the current modular system, a single spacesuit component array can be launched and used by a more significant number of individual crewmembers.

3D printing technology rapidly matures with apparent space exploration and settlement missions' applications. The ability to rapidly produce new tools, equipment, and replacement parts in situ will be vital for the next push into deep space. That being said, 3D printers generally use highly processed homogeneous material feedstock. This material feedstock is currently manufactured in large factories here on Earth. For this technology to offer the most benefits, work needs to be done to develop ways of manufacturing thermopolymer from in-situ resources. Until this is achieved, any potential benefits of 3D printing suit components would rely on the re-cyclability of the materials and the stowage benefit of launching bulk materials rather than manufactured suit components. ISRU is an active area of research, and with the push to return to the moon, much work is being done to look at how various materials can be made from what will be found there.

The final barrier to adopting 3D-printed spacesuits is the lack of an intensive 3D-printed design and testing program. However, work done at the HSFL has shown that it is possible to 3D Print many, if not most, of the components needed to make a spacesuit. Additionally, materials testing has shown that the thermopolymer is compatible with the Martian environment. Still, performing an EVA in a microgravity environment exposes the suit and the crewmember to a wide variety of risks that must be addressed. For example, additional work needs to be done to understand how 3D-printed spacesuits would withstand trips and falls in reduced gravity environments and how the performance of joints changes with cyclical bending and numerous pressurization cycles. In addition, the thermal environment of the sub-EPG spacesuit needs to be understood entirely if a thermopolymer pressure garment is to be used, as excessive heat could deform parts or cause ruptures.

Conclusion

“We are off! And do we know it, not just because the world is yelling ‘Liftoff’ in our ears, but because the seats of our pants tell us so!” –Michael Collins

6.1. The Next Generation of Spacesuit Torsos

The torso of the spacesuit is a critical component of the spacesuit. The design and shape of the HUT defines the overall architecture of the larger suit system on a fundamental level. Over time the design of spacesuit torsos has shifted from soft fabric and zipper construction methods to rigid or semi-rigid structures housing rotary bearings and hard mounting points for various other suit components, often including a rear entry hatch. In the near term, we can expect the next-generation planetary spacesuits to feature rigid, hard upper torsos with a rear entry hatch. This architecture will help future astronauts contend with the enduring issue of lunar dust contamination. Micro-gravity and Martian suits may feature other, as-yet unflown, torso architectures such as the dual planar type of HUT, see Figure 6.1.-1.



Figure 6.1.-1. Conceptual Design of a Dual Planar 3D Printed Spacesuit

The design of the next generation of spacesuits will need to address the ongoing problems of HUT-induced shoulder injuries while allowing astronauts to complete novel and increasingly complex EVAs. These suits will need to offer improvements in fit, comfort, and mobility compared to current and legacy suit systems.

The torso of the spacesuit interfaces with many crucial components of the suit, including the helmet, shoulder, waist, PLSS, and entry method of the suit. By optimizing the location of these interfaces, the fit, comfort, and mobility of the spacesuit can be improved. Conventionally, the location of these interfaces has been defined by selecting a HUT from a discreet-sized HUT picked from a range of several standard-sized torso components. This framework was adopted

during the shuttle era to address the need for infrequent EVAs by a growing number of EVA-capable astronauts. Future planetary missions will require much more frequent EVAs, often by a small selection of astronauts, potentially opening the door for the customization of spacesuits.

To mitigate some of the operational shortcomings of custom suit systems, additive manufacturing can be used to manufacture custom suit components rapidly. Work is being done at UND's HSFL to develop 3D-printed spacesuits.

6.2. HUT Design Frameworks

Custom and standardized design frameworks have been used previously for spacesuits. This work demonstrated how these frameworks could be improved upon through the torso shape analysis of 3D scan databases. By having a deeper understanding of how torso shape varies across the general population, the distribution of discreet HUT sizes was tailored to accommodate as much of the population as possible. The torso shape analysis also identified representative torso shapes that were used to summarize the infinite number of possible torsos. These representative torsos were then used to build a torso shape to HUT shape model that can estimate the optimal HUT for any given torso shape. This model can then be implemented directly as a custom HUT design framework or incorporated into a standardized discreet sizing framework.

6.3. Subject Fit Survey

The benefits of HUT customization were investigated through a mixed-method analysis that included subject fit surveys and objective mobility metrics. Using a subjective fit survey, how well the HUTs interface aligns with the wearer, any discomfort, and how much space there is in the HUT can be recorded and compared across HUT conditions. Survey results demonstrated the benefit of a custom HUT in aligning suit features with that of the wearer while also reducing reported head and shoulder discomfort.

6.4. Mobility Testing

The testing methods for spacesuit mobility have evolved. Early attempts at defining suit mobility have focused on measuring joint angles. More recently, more comprehensive mobility testing methods have been developed, including defining the complete reach envelope of the suit system. Both shoulder joint ranges of motion and reach envelope analysis were employed to investigate the difference between standardized and custom HUT design frameworks. Range of motion analysis suggests a benefit in using a customized HUT vs. a standard sized HUT. Likewise, reach envelope analysis showed increased reach envelope size when a custom HUT is worn.

6.5. 3D Printed Spacesuits

The design, sizing, and manufacturing of spacesuits is an incredibly labor-intensive process. Through digital design frameworks, such as those outlined here, combined with additive manufacturing techniques, custom sized spacesuits can be produced, offering fit, comfort, and mobility benefits while offering many of the logistical benefits previously associated with modular suit systems.

UND's HSFL has developed functional spacesuit mobility, disconnect, and shape components, demonstrating the feasibility of future integrated suits comprised of 3D printed parts. Further commercial and specialty thermos-polymers have good material properties for use in the construction of HUTS at all potential suit operating pressures.

6.6. Next steps in Spacesuit HUT Design

The current HUT design framework acted as a proof of concept for the design of a majorly digital HUT design framework but did not represent the true potential of such a system. Future frameworks could be built around 3D scan databases of more relevant poses. The current framework consists of an open-loop design cycle; future frameworks can integrate user feedback on the predicted HUT shapes to improve and modify the torso shape to the HUT shape model.

6.7. Next Steps in 3D Printed Spacesuits

Traditional manufacturing processes are not suitable for in-situ manufacturing and repair. On the other hand, 3D printing enables the rapid and unskilled manufacturing of complex parts and has excellent potential for use with in-situ manufacturing. Excitingly, there are many ways to utilize the resources we will find in space through different manufacturing methods.

Spacesuits will always be a critical component of living and working in space. In addition, 3D-printed spacesuits will be critical as our space missions turn toward the settlement of outer space. These technologies should be developed to prepare for this and improve the suits made here on earth.

In the near term, 3D printing can enable new suit-sizing concepts. In addition, the rapid and low-overhead manufacturing processes can mitigate some critical problems with customized spacesuit systems. 3D printed parts are already integrated into high-fidelity developmental EVA and flown launch and entry suits. As 3D printing technology matures, additive manufacturing will likely make more flight-suit components.

New types of spacesuits may be adopted in the future, including Mechanical Counter Pressure spacesuits. These suits are skintight garments that provide the pressure needed to survive in space through mechanically pressing on the skin rather than pneumatic pressure. The need for

critical fit over every cm of the wearer's body will require new materials and manufacturing techniques, which may be directly applied to the astronaut through a 3D printing process.

One thing is for sure; future spacesuits will be custom sized, and 3D printed.

Bibliography

- Abercromby, A., Thaxton, S., Onady, E., & Rajulu, S. (2006). *Reach Envelope and Field of Vision Quantification in Mark III Space Suit using Delaunay Triangulation*. Houston, TX: NASA.
- Abramov, I., & Skoog, I. (2003). *Russian Spacesuits*. Springer Praxis Books.
- Aitchison, L. (2012). A Comparison of Methods for Assessing Space Suit Joint Ranges of Motion. *International Conference on Environmental Systems*. San Diego, CA.
- Amberg, B., Romdhani, S., & Vetter, T. (2007). Optimal Step Nonrigid ICP Algorithms for Surface Registration. *IEEE Conference on Computer Vision and Pattern Recognition*. Minneapolis: IEEE.
- Anderson, A. (2014). *Understanding Human-Space Suit Interaction to Prevent Injury During Extravehicular Activity*. Boston: MIT.
- Annid, J., & Webb, P. (1971). *Development of a Space Activity Suit*. Yellow Springs, OH.
- Ashdown, S. (2007). *Sizing in Clothing*. Woodhead Publishing.
- Ayrey, B. (2020). *Lunar Outfitters*. Gainesville: University Press of Florida.
- Barrera, E. V., & Tello, H. M. (1992). *COMPOSITE MATERIALS FOR THE EXTRAVEHICULAR MOBILITY UNIT*. Houston: NASA Summer Faculty Fellowship Program.
- Bernal, Y., Gordon, A., Gupta, G., Kim, H., & Sudhakar, R. (2021). *Spacesuit Padding Design for Mobility and Comfort*. Online: 12th International Conference on Applied Human Factors and Ergonomics.
- Blender Foundation. (2018). *Blender - a 3D modelling and rendering package*. Amsterdam: Blender Foundation.
- Brown, H., Boyd, A., Denevi, B., Henriksen, M., Manheim, M., Robinson, M., . . . Wagner, R. (2022). Resource potential of lunar permanently shadowed regions. *Icarus*.
- Buzzi, F. (2017). *All Too Human, A Critique on the Modulor*. Retrieved from Failed Architecture: <https://failedarchitecture.com/human-all-too-human-a-critique-on-the-modulor/>
- Byrne, B. (2023). *How NASA Is Selecting the Next Astronauts to Walk on the Moon*. Retrieved from Smithsonian Magazine: <https://www.smithsonianmag.com/science-nature/how-nasa-is-selecting-the-next-astronauts-to-walk-on-the-moon-180981511/>
- CAESAR 3-D Anthropometric Database . (2012). Society of Automotive Engineers International.
- Casting Light on Permanently Shadowed Regions*. (2018). Retrieved from LROC SESE ASE: <http://lroc.sese.asu.edu/posts/979>

- Centers for Disease Control and Prevention. (2023). *Unfit to Serve*. Retrieved from Centers for Disease Control and Prevention: <https://www.cdc.gov/physicalactivity/resources/unfit-to-serve/index.html>
- Christoffersen, R., Lindsay, J. F., Noble, S. K., Meador, M. A., Kosmo, J. J., Lawrence, J. A., . . . McCue, T. (2008). *Lunar Dust Effects on Spacesuit Systems*. NASA.
- Coan, D. (2020). EVA-EXP-0075. *EVA Exploration Workshop*. Houston.
- Cohen, M. (1989). *United States of America Patent No. US4842224A*.
- Dassault Systemes. (2022). SolidWorks.
- Davis, K., Rhodes, R., Kim, H., Benson, E., Hernandez, Y., Vu, L., & Rajulu, S. (2020). xEMU Lower Torso Assembly (LTA) Brief Fleet Sizing Study. *39th International Conference on Environmental Systems*. Online: Texas Digital Library.
- Davis, K., Rhodes, R., Sudhakar, R., Hernandez, Y., Benson, E., Jarvis, S., . . . Kim, H. (2021). Integrative Fit Assessments for. *50th International Conference on Environmental Systems*. Online: Texas Digital Library.
- de Leon, P., & Harris, G. (2009). NDX-2: Development of an Advanced Planetary Space Suit Demonstrator System for the Lunar Environment. *International Conference on Environmental Systems*.
- de Leon, P., Tomovic, S., & Green, W. (2021). New Methods of Manufacturing Spacesuits for Deep Space. *50th International Conference on Environmental Systems*. Online: Texas Digital Library.
- Dodd, T. (2019). A tour of SpaceX's spacesuit! Every Day Astronaut.
- Dombrowski, R., Hobbs, E., Jacobs, S., Wagner, N., Katarova, M., & Rhodes, R. (2022). Advanced Nanocomposites for Exploration Extravehicular Mobility Unit (xEMU) Suits using STF-Armor™ for Lunar Regolith Dust Mitigation. *International Conference on Environmental Systems*.
- Exploration Extravehicular Activity Services (xEVAS)*. (2022, Jun 14). Retrieved from SAM.gov: <https://sam.gov/opp/2acfdeae77644a3285f1701a2392d5f3/view>
- Foundation, B. (2023). Blender - a 3D modelling and rendering package. Amsterdam.
- Frey, B. J., & Dueck, D. (2007). Clustering by Passing Messages Between Data Points. *Science*.
- Gast, M., & Moore, S. (2011). A Glimpse from the Inside of a Space Suit: What it is Really Like to Train for an EVA. *Acta Astronautica*.

- GORDON, C. C., CHURCHILL, T., CLAUSER, C. E., BRADTMILLER, B., McCONVILLE, J. T., TEBBETTS, I., & WALKER, R. A. (1989). *1988 ANTHROPOMETRIC SURVEY OF U.S. ARMY PERSONNEL: METHODS AND SUMMARY STATISTICS*. Yellow Springs.
- Gordon, C. C., L., B. C., Bradtmiller, B., Parham, J. L., Barrientos, P., Paquette, S. P., . . . Kristensen, S. (2014). *2012 ANTHROPOMETRIC SURVEY OF U.S. ARMY PERSONNEL: METHODS AND SUMMARY STATISTICS* . Natick: U.S. Army Natick Soldier Research, Development and Engineering Center.
- Graziosi, D., Jones, B., Ferl, J., Scarborough, S., Hewes, L., Ross, A., & Rhodes, R. (2016). Z-2 Architecture Description and Requirements Verification . *International Conference on Environmental Systems*.
- Green, W., & de Leon, P. (2021). Use of a Robotic Testing Device to Investigate the Effects of Sizing on Space Suit Joints. *50th International Conference on Environmental Systems*. Online: Texas Digital Library.
- Griffin, B., Howard, R., Rajulu, S., & Smitherman, D. (2009). Creating a Lunar EVA Work Envelope. *39th International Conference on Environmental Systems*. Savannah, GA.
- Harris, G. L. (2001). *The Origins and Technology of the Advanced Extravehicular Space Suit*. San Diego, CA: American Astronautical Society.
- Historical Evolution of Astronaut Selection*. (2016). Retrieved from Space Safety Magazine: <https://www.spacesafetymagazine.com/space-exploration/astronaut-cosmonaut/historical-evolution-astronaut-selection/>
- Hotzman, J., Gordon, C., Bradtmiller, B., Corner, B., Mucher, M., Kristen, S., . . . Blackwell, C. (2011). *MEASURER'S HANDBOOK: US ARMY AND MARINE* . Natick, Massachusetts: U.S. Army Natick Soldier Research, Development and Engineering Center.
- ILC Dover. (1975). *FINAL REPORT ON DEVELOPMENT OF A SEALED BEARING FOR SPACE SUITS*.
- Jarvis, S., Norcross, J., & Abercromby, A. (2017). Subjective Suit Fit Assessment . *Subjective Suit Fit Assessment* . Galveston, TX: NASA.
- Kim, H., Benson, E., Jarvis, S., Hernandez, Y., & Sudhakar, R. (2019). Human modeling tools for spacesuit and. In S. Scataglini, & G. Paul, *DHM and Posturography*. Elsevier.
- Kim, H., Hernandez, Y., Benson, E., Jarvis, S., Meginnis, I., & Rajulu, S. (2019). Underwater space suit performance assessments part 2: Reach envelopes as a comparative performance metric. *International Journal of Industrial Ergonomics*.
- Kim, H., Vu, L., Benson, E., Rhodes, R., & Rajulu, S. (2020). Predictive Assessments of Spacesuit Fit: Monte-Carlo Modeling and Analysis. *Applied Human Factors and Ergonomics Conference*. Washington, D.C: NASA.

- Kim, H., Young, K., & Jarvis, S. (2016). *Virtual Suit Fit Assessment Using Body Shape Model*. NASA Technology Poster Day Presentation.
- Kim, H., Young, K., Bernal, Y., Boppana, A., Vu, L., Benson, E., . . . Rajulu, S. (2016). A Parametric Model of Shoulder Articulation for Virtual Assessment of Space Suit Fit. *3D Body Scanning Technologies Conference*. Lugano.
- Li, Y., & Lou, Y. (2020). Tensile and Bending Strength Improvements in PEEK Parts Using Fused Deposition Modelling 3D Printing Considering Multi-Factor Coupling. *Polymers*.
- Manyapu, K. (2017). *Spacesuit Integrated Carbon Nanotube Dust Mitigation System For Lunar Exploration*. Grand Forks: UND.
- Material Property Database*. (2023). Retrieved from MatWeb: <https://www.matweb.com/>
- McMann, H., & McBarron, J. (1983). *CHALLENGES IN THE DEVELOPMENT OF THE SHUTTLE EXTRAVEHICULAR MOBILITY UNIT*. Houston, TX: NASA.
- Meginnis, I. M., Rhodes, R. A., & Kim, D. J. (2022). NASA Advanced Space Suit xEMU Development Report – Hard Upper Torso Assembly. *International Conference on Environmental Systems*.
- Microsoft Corporation. (2018). Microsoft Excel. <https://office.microsoft.com/excel>.
- Miller, S., & Hargrove, S. (2022). xPLSS Structural Backplate Design, Manufacture, and Test Overview. *International Conference on Environmental Systems*.
- Mitchel, K. (2012, August 1). CTSD-ADV-590, Rev. C. *Hazard Analysis for the Mark III Space Suit Assembly (SSA) Used in One-g Operations*. Houston, TX: NASA.
- Muller, G., & Graziosi, D. (2015). Design and Testing of Advanced Space Suit Hybrid Upper Torso. *International Conference on Environmental Systems*.
- Newman, D. (2002). *ASTRONAUT BIO-SUIT SYSTEM FOR EXPLORATION CLASS MISSIONS*. USRA. *Outgassing Data for Selecting Spacecraft Materials*. (n.d.). Retrieved from NASA.gov: <https://outgassing.nasa.gov/>
- Perez, D., Celik, E., & Karkkainen, R. (2021). Investigation of Interlayer Interface Strength and Print Morphology Effects in Fused Deposition Modeling 3D-Printed PLA. *3D Printing and Additive Manufacturing*.
- Pishchulin, L., Wuhrer, S., Helten, T., Theobaltd, C., & Schiele, B. (2017). Building Statistical Shape Spaces for 3D Human Modeling. *Pattern Recognition*.
- Polaris Program. (2023, 7 2). *Polaris Dawn*. Retrieved from <https://polarisprogram.com/dawn/>

- Reid, C., Harvill, L., England, S., Young, K., Norcross, J., & Rajulu, S. (2014). An Ergonomic Evaluation of the Extravehicular Mobility Unit (EMU) Space Suit Hard Upper Torso (HUT) Size Effect on Metabolic, Mobility, and Strength Performance. *Human Factors and Ergonomics Society's International Annual Meeting*. Chicago, IL.
- Rhoades, R., MacFarland, S., & Campbell, D. (2022). NASA Advanced Space Suit xEMU Development Report. *International Conference for Environmental Systems*.
- Rosenberg, S., & Makel, D. (2000). Synthesis of Ethylene and Other Useful Products on Spacecraft and Planetary Bases. *International Conference On Environmental Systems*.
- Scheuring, A., McCulloch, P., Van Baalen, M., Charles, M., Watson, R., & Blatt, T. (2011). Shoulder Injuries in US Astronauts Related to EVA Suit Design. *83rd Annual Aerospace Medical Association Meeting*. Atlanta, GA.
- Scheuring, R. (2012). *Shoulder Injuries in US Astronauts Related to EVA Suit Design*. Atlanta, GA: Aerospace Medical Association.
- Ta, J. B., & Treviño, R. C. (2016). *WALKING TO OLYMPUS, Volume II*. NASA.
- The "Vitruvian Man" Da Vinci – Why Was the "Vitruvian Man" Created?* (2022). Retrieved from Art in Context: <https://artincontext.org/the-vitruvian-man-da-vinci/>
- Thomas, K. S., & McMann, H. J. (2012). *U.S. Spacesuits*. New York: Springer-Praxis.
- Thornton, W., Hoffler, G., & Rummel, J. (1974). ANTHROPOMETRIC CHANGES AND FLUID SHIFTS. *Skylab Life Science Symposium, Vol.2*. Houston, TX.
- Van Cise, E., Kelly, B., Radigan, J., & Cranmer, C. (2016). Experiences with Extra-Vehicular Activities in Response to Critical ISS Contingencies. *The International Conference on Space Operations*. Daeheon.
- Van Rossum, G., & Drake, F. L. (2009). *Python 3 Reference Manual*. Scotts Valley: CreateSpace.
- Vu, L., Benson, E., Kim, H., & Rajulu, S. (2018). *Assessing Torso Shape and Posture Variations with Flexible Strain Sensors*. Teleconference: NASA/ University of Minnisota.
- Vu, L., Kim, H., & Rajulu, S. (2019). Posture Transfer Method on Pre-Scanned Full-body Geometry for Space Architecture Design. *International Conference on Applied Human Factors and Ergonomics*. Washington, DC.
- Vykukal, H. (1986). *USA Patent No. 4593415*.
- Wilde, R. (1981). *EXTRAVEHICULAR CREWMAN WORK SYSTEM (ECWS) STUDY PROGRAM, PREBREATHE ELIMINATION STUDY FINAL REPORT*. Houston.
- Williams, D., & Johnson, B. (2003). *EMU Shoulder Injury Tiger Team Report*. NASA.

Young, A., & Avino, M. (2009). *Spacesuits: The Smithsonian National Air and Space Museum Collection*. PowerHouse Books.

Appendix 1: Hard Upper Torso Fit Rules

Hard Upper Torso Fit Rules	
1	The subject's body is oriented in the HUT such that the back of the head and the back of the shoulders are approximately 3 inches from the hatch.
2	The top of the scye bearings is at least 1" above the top of the shoulder joint.
3	The subject's shoulders are as far forward into the scye bearings as possible.
4	The central axis of the helmet bubble should be in line with the subject tragion
5	The waist disconnect ring should align with the bottom of the subject's ribcage.
6	There should be a 2" on all sides between the subject and the waist disconnect.

Appendix 2: Subjective Fit Survey Basis

DISCOMFORT							
			None \longrightarrow Severe				
Affected Region			0	1	2	3	4
Torso	Head	L-Side	<input type="radio"/>	<input type="radio"/>	<input type="radio"/>	<input type="radio"/>	<input type="radio"/>
	Neck	Top	<input type="radio"/>	<input type="radio"/>	<input type="radio"/>	<input type="radio"/>	<input type="radio"/>
	Upper Torso	None	<input type="radio"/>	<input type="radio"/>	<input type="radio"/>	<input type="radio"/>	<input type="radio"/>
	Lower Torso	None	<input type="radio"/>	<input type="radio"/>	<input type="radio"/>	<input type="radio"/>	<input type="radio"/>
Arms	R-Shoulder	None	<input type="radio"/>	<input type="radio"/>	<input type="radio"/>	<input type="radio"/>	<input type="radio"/>
	L-Shoulder	None	<input type="radio"/>	<input type="radio"/>	<input type="radio"/>	<input type="radio"/>	<input type="radio"/>
	R-Lower Arm	None	<input type="radio"/>	<input type="radio"/>	<input type="radio"/>	<input type="radio"/>	<input type="radio"/>
	L-Lower Arm	None	<input type="radio"/>	<input type="radio"/>	<input type="radio"/>	<input type="radio"/>	<input type="radio"/>
	R-Hand	None	<input type="radio"/>	<input type="radio"/>	<input type="radio"/>	<input type="radio"/>	<input type="radio"/>
	L-Hand	None	<input type="radio"/>	<input type="radio"/>	<input type="radio"/>	<input type="radio"/>	<input type="radio"/>
Legs	R-Upper Leg	None	<input type="radio"/>	<input type="radio"/>	<input type="radio"/>	<input type="radio"/>	<input type="radio"/>
	L-Upper Leg	None	<input type="radio"/>	<input type="radio"/>	<input type="radio"/>	<input type="radio"/>	<input type="radio"/>
	R-Lower Leg	None	<input type="radio"/>	<input type="radio"/>	<input type="radio"/>	<input type="radio"/>	<input type="radio"/>
	L-Lower Leg	None	<input type="radio"/>	<input type="radio"/>	<input type="radio"/>	<input type="radio"/>	<input type="radio"/>
	R-Foot	None	<input type="radio"/>	<input type="radio"/>	<input type="radio"/>	<input type="radio"/>	<input type="radio"/>
	L-Foot	None	<input type="radio"/>	<input type="radio"/>	<input type="radio"/>	<input type="radio"/>	<input type="radio"/>

INDEXING									
				Ideal \longrightarrow Worst Case					
HUT Indexing		Worst Position	Tight/Loose	0	1	2	3	4	
PART 1	Front to Back spacing	Bending over	Neither	<input type="radio"/>	<input type="radio"/>	<input type="radio"/>	<input checked="" type="radio"/>	<input type="radio"/>	
	Side to Side spacing	On hands and knees		<input type="radio"/>	<input checked="" type="radio"/>	<input type="radio"/>	<input type="radio"/>	<input type="radio"/>	
	Shoulder volume spacing		Neither	<input type="radio"/>	<input checked="" type="radio"/>	<input type="radio"/>	<input type="radio"/>	<input type="radio"/>	
	Spacing for deep breaths		Loose	<input type="radio"/>	<input type="radio"/>	<input checked="" type="radio"/>	<input type="radio"/>	<input type="radio"/>	
	Brief Indexing								
	Front to Back spacing	Sitting		<input type="radio"/>	<input checked="" type="radio"/>	<input type="radio"/>	<input type="radio"/>	<input type="radio"/>	
	Side to Side spacing	Bending over		<input type="radio"/>	<input checked="" type="radio"/>	<input type="radio"/>	<input type="radio"/>	<input type="radio"/>	
	Vertical (crotch) spacing			<input type="radio"/>	<input type="radio"/>	<input checked="" type="radio"/>	<input type="radio"/>	<input type="radio"/>	
	Glove Indexing								
	Fingertip spacing			<input type="radio"/>	<input type="radio"/>	<input type="radio"/>	<input checked="" type="radio"/>	<input type="radio"/>	
	Finger crotch spacing			<input checked="" type="radio"/>	<input type="radio"/>	<input type="radio"/>	<input type="radio"/>	<input type="radio"/>	
	Hand circumference spacing			<input type="radio"/>	<input type="radio"/>	<input checked="" type="radio"/>	<input type="radio"/>	<input type="radio"/>	
	Overall Indexing								
	Shoulder-to-crotch length			<input type="radio"/>	<input type="radio"/>	<input checked="" type="radio"/>	<input type="radio"/>	<input type="radio"/>	
Shoulder-to-heel length			<input type="radio"/>	<input type="radio"/>	<input type="radio"/>	<input checked="" type="radio"/>	<input type="radio"/>		
Heel-to-toe length			<input type="radio"/>	<input type="radio"/>	<input type="radio"/>	<input type="radio"/>	<input checked="" type="radio"/>		
				Ideal \longrightarrow Highly Obstructed					
PART 2	Field of View	Worst Position	Obstruction	0	1	2	3	4	
	Side-to-side			<input type="radio"/>	<input type="radio"/>	<input type="radio"/>	<input checked="" type="radio"/>	<input type="radio"/>	
	Up and down			<input type="radio"/>	<input type="radio"/>	<input type="radio"/>	<input type="radio"/>	<input checked="" type="radio"/>	
	Vertical eye placement		NA	<input type="radio"/>	<input type="radio"/>	<input checked="" type="radio"/>	<input type="radio"/>	<input type="radio"/>	
Ability to see feet			<input type="radio"/>	<input type="radio"/>	<input checked="" type="radio"/>	<input type="radio"/>	<input type="radio"/>		

FEATURE ALIGNMENT						
*Planetary suits only		Ideal \longrightarrow Worst Case				
Soft Goods Breakpoints	Break Point Location	0	1	2	3	4
Elbow Break Location	Bicep	<input checked="" type="radio"/>	<input type="radio"/>	<input type="radio"/>	<input type="radio"/>	<input type="radio"/>
Knee Break Location*	Thigh	<input type="radio"/>	<input checked="" type="radio"/>	<input type="radio"/>	<input type="radio"/>	<input type="radio"/>
Joint-Bearing Alignment	Alignment Location					
Shoulder Bearing	Shoulder centered	<input type="radio"/>	<input type="radio"/>	<input checked="" type="radio"/>	<input type="radio"/>	<input type="radio"/>
Hip Bearing*		<input type="radio"/>	<input checked="" type="radio"/>	<input type="radio"/>	<input type="radio"/>	<input type="radio"/>
Thigh Bearing*		<input type="radio"/>	<input type="radio"/>	<input checked="" type="radio"/>	<input type="radio"/>	<input type="radio"/>

MOBILITY					
	Ideal \longrightarrow Worst Case				
Tasks	0	1	2	3	4
Bending over	<input checked="" type="radio"/>	<input type="radio"/>	<input type="radio"/>	<input type="radio"/>	<input type="radio"/>
Reaching in front	<input checked="" type="radio"/>	<input type="radio"/>	<input type="radio"/>	<input type="radio"/>	<input type="radio"/>
Reaching overhead	<input type="radio"/>	<input checked="" type="radio"/>	<input type="radio"/>	<input type="radio"/>	<input type="radio"/>
Kneeling	<input checked="" type="radio"/>	<input type="radio"/>	<input type="radio"/>	<input type="radio"/>	<input type="radio"/>
Squatting	<input checked="" type="radio"/>	<input type="radio"/>	<input type="radio"/>	<input type="radio"/>	<input type="radio"/>
Sitting	<input type="radio"/>	<input checked="" type="radio"/>	<input type="radio"/>	<input type="radio"/>	<input type="radio"/>

TEST DAY INFORMATION

Survey Administrator

Name of Test

Test Date

Test Point Type - Select One -

Suit Type - Select One -

Offload Environment - Select One -

Gravity Level - Select One -

Test Subject Number

Spacesuit Experience - Select One -

Experience in today's suit - Select One -

STE Name

STE Experience - Select One -

If "other", please explain

Is experimental hardware being used inside the suit? Yes No

If "yes", please explain (type, location, rigid/soft, dimensions, etc)

Are there any other general comments or unique things about the suit sizing today?

Preliminary Fit Questions (for those with prior suit fit check)

	Subject	Suit Engineer
Is anything about the suit abnormally uncomfortable?	<input type="checkbox"/> Yes <input type="checkbox"/> No	<input type="checkbox"/> Yes <input type="checkbox"/> No
Is the suit tighter or looser anywhere than usual (indexing issues)?	<input type="checkbox"/> Yes <input type="checkbox"/> No	<input type="checkbox"/> Yes <input type="checkbox"/> No
Are there obstructions to field of view that you haven't had before?	<input type="checkbox"/> Yes <input type="checkbox"/> No	<input type="checkbox"/> Yes <input type="checkbox"/> No
Do any of the suit breakpoints/bearings feel abnormally positioned?	<input type="checkbox"/> Yes <input type="checkbox"/> No	<input type="checkbox"/> Yes <input type="checkbox"/> No
Is there unusual difficulty maneuvering in the suit?	<input type="checkbox"/> Yes <input type="checkbox"/> No	<input type="checkbox"/> Yes <input type="checkbox"/> No
Are there any unusual stability problems in the suit?	<input type="checkbox"/> Yes <input type="checkbox"/> No	<input type="checkbox"/> Yes <input type="checkbox"/> No

Appendix 3: Subjective Fit Survey Used for HUT Evaluation

Subject ID Number:

Test Date:

HUT Size:

Test Type:

Ideal ▶▶▶▶▶ Worst	
Feature Alignment	Case
Shoulder Bearing	<input type="radio"/> <input type="radio"/> <input type="radio"/> <input type="radio"/> <input type="radio"/>
Waist Disconnect	<input type="radio"/> <input type="radio"/> <input type="radio"/> <input type="radio"/> <input type="radio"/>
Helmet	<input type="radio"/> <input type="radio"/> <input type="radio"/> <input type="radio"/> <input type="radio"/>

None ▶▶▶▶▶ Severe	
Discomfort	
Head	<input type="radio"/> <input type="radio"/> <input type="radio"/> <input type="radio"/> <input type="radio"/>
Neck	<input type="radio"/> <input type="radio"/> <input type="radio"/> <input type="radio"/> <input type="radio"/>
Upper Torso	<input type="radio"/> <input type="radio"/> <input type="radio"/> <input type="radio"/> <input type="radio"/>
Lower Torso	<input type="radio"/> <input type="radio"/> <input type="radio"/> <input type="radio"/> <input type="radio"/>
R-Shoulder	<input type="radio"/> <input type="radio"/> <input type="radio"/> <input type="radio"/> <input type="radio"/>
L-Shoulder	<input type="radio"/> <input type="radio"/> <input type="radio"/> <input type="radio"/> <input type="radio"/>

Too Small ▶▶▶▶▶ Too Large	
Indexing	
Front to Back Spacing	<input type="radio"/> <input type="radio"/> <input type="radio"/> o <input type="radio"/> <input type="radio"/> <input type="radio"/>
Side to Side Spacing	<input type="radio"/> <input type="radio"/> <input type="radio"/> o <input type="radio"/> <input type="radio"/> <input type="radio"/>
Shoulder Volume Spacing	<input type="radio"/> <input type="radio"/> <input type="radio"/> o <input type="radio"/> <input type="radio"/> <input type="radio"/>
Spacing for deep breaths	<input type="radio"/> <input type="radio"/> <input type="radio"/> o <input type="radio"/> <input type="radio"/> <input type="radio"/>

Ideal ▶▶▶▶▶ Obstructed	
Field of View	
Side-to-side	<input type="radio"/> <input type="radio"/> <input type="radio"/> <input type="radio"/> <input type="radio"/>
Up and down	<input type="radio"/> <input type="radio"/> <input type="radio"/> <input type="radio"/> <input type="radio"/>
Vertical eye placement	<input type="radio"/> <input type="radio"/> <input type="radio"/> <input type="radio"/> <input type="radio"/>
Ability to see feet	<input type="radio"/> <input type="radio"/> <input type="radio"/> <input type="radio"/> <input type="radio"/>

None ▶▶▶▶▶ Severe	
Ease of Donning	
	<input type="radio"/> <input type="radio"/> <input type="radio"/> <input type="radio"/> <input type="radio"/>

Notes:

Appendix 4: Range of Motion Raw Data

Table 6.7-1.1-1. Entry Method Trade Space (*Information approximated from Lunar Planetary Institute and NASA Apollo Mission pages*)

Subject Number	Flex-Ext (R)	Flex-Ext (L)	Ab-Ad (R)	Ab-Ad (L)	Int-Ext (R)	Int-Ext (L)
1	228.55	252.00	122.06	126.50	136.82	131.09
2	229.34	212.43	118.78	127.84		129.57
3	248.53	214.89	110.82	121.75	130.58	133.08
4						
5	215.70	228.59	91.55	99.04	117.36	126.71
6						
7	216.90	210.87	79.44	100.33	124.53	130.90
8	179.45	164.92	67.08	70.66	110.99	96.63
9	238.99	249.19	114.01	110.87	118.10	127.71
10	244.45	245.93	75.75	68.86	101.25	118.02
11	215.76		81.08	78.22		101.93
12	208.39	203.12	102.14	88.45	120.09	118.64

Table 6.7-2.1-1. Entry Method Trade Space (*Information approximated from Lunar Planetary Institute and NASA Apollo Mission pages*)

Subject Number	Flex-Ext (R) 1	Flex-Ext (T) 1	Ab-Ad (R) 1	Ab-Ad (L) 1	Int-Ext (R) 1	Int-Ext (L) 1
1	188.79	209.45	115.56	113.59	119.33	125.10
2	236.89	190.15	117.38	124.73	128.77	130.56
3	240.17	202.54	98.20	119.74	122.95	151.37
4						
5	179.82	231.26	85.49	73.05	114.04	106.77
6						
7	201.41	205.99	78.12	94.37	117.99	131.97
8						
9	210.78	229.32	89.26	106.66	107.75	117.52
10	243.09	245.93	65.08	65.70	102.64	83.50
11	212.67		66.76	78.15	111.60	110.08
12	211.31	190.88	101.42	112.12	104.80	115.91

Table 6.7-3.1-1. Entry Method Trade Space (*Information approximated from Lunar Planetary Institute and NASA Apollo Mission pages*)

Subject Number	Flex-Ext (R) 2	Flex-Ext (T) 2	Ab-Ad (R) 2	Ab-Ad (L) 2	Int-Ext (R) 2	Int-Ext (L) 2
1						
2	188.11	205.62	113.36	117.31	121.71	
3						
4						
5	197.94	247.58	83.20	88.84	125.92	124.75
6	N/D	N/D				
7	213.38	201.92	73.80	82.40	121.99	130.70
8						
9	230.05	235.15	118.80	122.11	109.52	111.06
10						
11	192.38	N/D	65.92	74.23	118.08	102.74
12	214.10	210.76	96.00	106.87	110.66	113.68

Appendix 5: Range of Motion Raw Data

Shirt Sleeve									
Test Subject Number	RE (X) (Left)	RE (Y) (Left)	RE (Z) (Left)	RE (X) (Right)	RE (Y) (Right)	RE (Z) (Right)	RE (X) (Dual)	RE (Y) (Dual)	RE (Z) (Dual)
1	0.61	1.21	1.26				0.48	0.25	0.80
2	0.94	1.19	1.26	0.75	1.18	1.27	0.55	0.17	0.74
3	1.16	0.99	1.45	1.00	0.98	1.41	0.89	0.56	1.24
5	1.33	1.20	1.33	1.33	1.05	1.28	1.03	0.48	1.13
7	1.32	1.01	1.36	1.31	0.89	1.38	1.12	0.64	1.30
8	1.22	1.20	1.35	1.22	1.04	1.41			
10	1.09	1.16	1.44	1.01	1.22	1.41	1.01	0.57	1.23
11	1.07	1.03	1.43	1.19	1.04	1.44	0.77	0.55	1.07
12	1.12	0.85	1.18	1.19	1.08	1.15	0.93	0.59	0.99

Custom									
Test Subject Number	RE (X) (Left)	RE (Y) (Left)	RE (Z) (Left)	RE (X) (Right)	RE (Y) (Right)	RE (Z) (Right)	RE (X) (Dual)	RE (Y) (Dual)	RE (Z) (Dual)
1	0.54	0.98	1.24				0.51	0.20	0.85
2	0.60	0.99	1.24	0.54	0.90	1.17	0.54	0.16	0.80
3				0.86	1.13	1.40	0.68	0.25	1.04
5	1.27	0.91	1.27	1.06	0.73	1.13	0.64	0.28	0.85
7	0.98	0.80	1.32	1.10	0.87	1.27	0.49	0.22	0.94
8	0.77	0.81	1.13	0.91	0.93	1.23	0.61	0.21	0.80
10	0.85	1.04	1.22	0.77	1.05	1.19	0.59	0.45	0.90
11	0.89	0.87	1.20	0.99	0.89	1.24	0.56	0.36	0.93
12	0.75	0.87	1.04	0.78	0.92	1.06	0.54	0.32	0.69

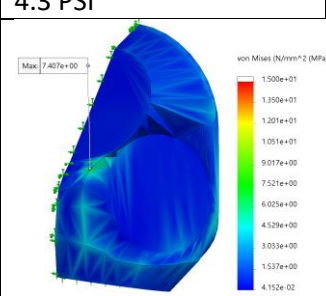
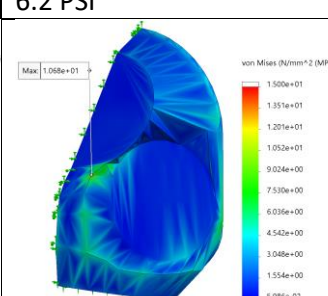
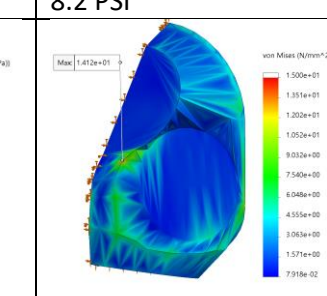
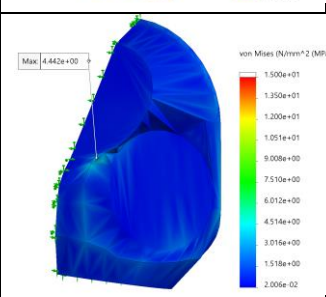
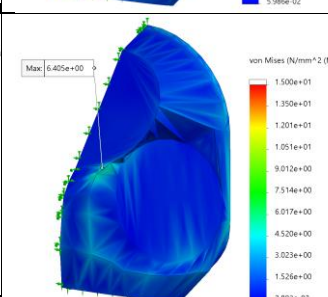
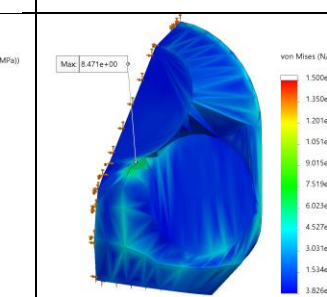
	Standard 1								
Test Subject Number	RE (X) (Left)	RE (Y) (Left)	RE (Z) (Left)	RE (X) (Right)	RE (Y) (Right)	RE (Z) (Right)	RE (X) (Dual)	RE (Y) (Dual)	RE (Z) (Dual)
1	0.54	0.98	1.19				0.43	0.21	0.77
2	0.54	0.98	1.19	0.61	0.83	1.09	0.48	0.16	0.69
3	0.93	1.01	1.31	0.83	1.04	1.31	0.61	0.27	1.07
5	0.76	0.96	1.15	1.03	0.89	1.17	0.50	0.29	0.89
7	1.01	0.99	1.24	1.04	0.90	1.26	0.56	0.21	0.95
8	0.75	0.83	1.10	0.80	0.75	1.18	0.55	0.15	0.76
10	0.69	1.10	1.31	0.65	1.05	1.22	0.48	0.43	0.90
11	0.80	0.78	1.16	0.75	0.89	1.12	0.53	0.31	0.84
12	0.61	0.84	1.07	0.63	0.91	1.10	0.45	0.24	0.73

	Standard 2								
Test Subject Number	RE (X) (Left)	RE (Y) (Left)	RE (Z) (Left)	RE (X) (Right)	RE (Y) (Right)	RE (Z) (Right)	RE (X) (Dual)	RE (Y) (Dual)	RE (Z) (Dual)
1	0.49	0.90	1.20				0.40	0.17	0.71
2	0.48	0.85	1.17	0.52	0.91	1.10	0.39	0.12	0.70
3									
5	0.96	1.01	1.27	0.95	0.93	1.15	0.60	0.38	0.83
7	0.99	0.80	1.29	0.98	0.83	1.24	0.51	0.19	0.84
8									
10									
11	0.88	0.72	1.08	0.79	0.85	0.99	0.46	0.35	0.75
12	0.60	0.86	1.08	0.80	0.91	1.05	0.41	0.25	0.69

Appendix 6: HUT Pressurization FEA Results

Material	Thickness	4.3 PSI	6.2 PSI	8.2 PSI
PLA	4mm	<p>von Mises (N/mm² (MPa))</p> <p>Max 7.407e+00</p> <p>Yield strength: 6.000e+01</p>	<p>von Mises (N/mm² (MPa))</p> <p>Max 1.068e+01</p>	<p>von Mises (N/mm² (MPa))</p> <p>Max 1.412e+01</p>
	6mm	<p>von Mises (N/mm² (MPa))</p> <p>Max 4.442e+00</p>	<p>von Mises (N/mm² (MPa))</p> <p>Max 6.405e+00</p>	<p>von Mises (N/mm² (MPa))</p> <p>Max 8.471e+00</p>
	8mm	<p>von Mises (N/mm² (MPa))</p> <p>Max 3.095e+00</p>	<p>von Mises (N/mm² (MPa))</p> <p>Max 4.462e+00</p>	<p>von Mises (N/mm² (MPa))</p> <p>Max 5.901e+00</p>

Material	Thickness	4.3 PSI	6.2 PSI	8.2 PSI
PEEK	4mm	<p>Max: 7.744e+00 von Mises (N/mm²)</p>	<p>Max: 1.117e+01 von Mises (N/mm² (MPa))</p>	<p>Max: 1.477e+01 von Mises (N/mm² (MPa))</p>
	6mm	<p>Max: 6.013e+00 von Mises (N/mm²)</p>	<p>Max: 6.013e+00 von Mises (N/mm² (MPa))</p>	<p>Max: 7.953e+00 von Mises (N/mm² (MPa))</p>
	8mm	<p>Max: 2.919e+00 von Mises (N/mm²)</p>	<p>Max: 4.209e+00 von Mises (N/mm² (MPa))</p>	<p>Max: 5.567e+00 von Mises (N/mm² (MPa))</p>

Material	Thickness	4.3 PSI	6.2 PSI	8.2 PSI
Aluminum 6061	4mm			
	6mm			
	8mm	